International Journal of Heat and Mass Transfer 208 (2023) 124065

Contents lists available at ScienceDirect

International Journal of Heat and Mass Transfer

journal homepage: www.elsevier.com/locate/hmt

# Bubble growth models in saturated pool boiling of water on a smooth metallic surface: Assessment and a new recommendation

M.M. Mahmoud [a], T.G. Karayiannis [b,*]

[a] Zagazig University, Faculty of Engineering, Zagazig 44519, Egypt
[b] Brunel University London, Department of Mechanical and Aerospace Engineering, Uxbridge, UB8 3PH, UK

ARTICLE INFO

*Article history:*
Received 23 December 2022
Revised 6 February 2023
Accepted 6 March 2023

*Keywords:*
Pool boiling
Metallic surfaces
Bubble growth mechanisms
Bubble growth models

ABSTRACT

Prediction of bubble growth rate is very important for the development of accurate models for bubble departure diameter and thus the heat transfer rates in nucleate boiling. This paper presents an evaluation study to the existing homogeneous and heterogeneous bubble growth models using our experimental data for bubble growth in saturated pool boiling of deionized water on a plain copper surface. The experiments were conducted at pressures 1, 0.5 and 0.15 bar and superheat in the range 5.1 – 19.5 K. To start with, the paper presents a critical review on bubble growth models in homogeneous and heterogeneous boiling. It was found that homogeneous growth models achieved some partial agreement with the experimental data at some conditions and thus they should be used carefully in heterogeneous boiling. There was a good agreement between some of the models that were suggested based on the assumption that bubble growth occurs due to evaporation from the superheated boundary layer around the bubble. The models based on microlayer evaporation only could not explain the experimental data, i.e. partial agreement at some conditions. The model that predicted the data very well at all conditions was the "relaxation boundary layer" model by Van Stralen [25]. This model was generalized in the current study by suggesting two new empirical models for the departure diameter and departure time.



## 1. Introduction

Boiling exists in many applications such as refrigeration and air conditioning, power generation including nuclear plants and cooling of high heat flux electronic devices. The performance of a boiling heat transfer surface is usually inferred from the classical boiling curve – a relation between wall heat flux $q_w$ and wall superheat ($\Delta T_w = T_w - T_{sat}$). A surface has a superior performance when $q_w$ increases rapidly with small changes in $\Delta T_w$, i.e. when the curve is nearly vertical. Thus, prediction of the boiling curve in nucleate boiling (from the onset of boiling to the onset of critical heat flux) is very crucial for the design of any boiling heat transfer equipment. Historically, the work conducted by Jakob and his research group, in the 1930s, may be the first attempt to suggest a phenomenological model for the prediction of heat transfer rates in nucleate boiling based on bubble-agitation mechanism (heat transfer is enhanced by turbulence in the liquid bulk and the wall thermal boundary layer). This work is summarized in chapter 29 in the textbook by Jakob [1]. Based on this mechanism, several models have since emerged, such as the models suggested by Rohsenow [2] and Forster and Zuber [3]. With the advent of 1960s, different heat transfer mechanisms were suggested based on one single bubble and thus several models have been emerged. Examples are the models proposed by Han and Griffith [4] and Mikic and Rohsenow [5], who assumed that the heat transfer mechanism, in the area of bubble influence, is periodic quenching of the surface by the cold liquid that rushes down towards the nucleation site after bubble departure. At locations outside the area of bubble influence, the heat transfer mechanism was assumed to be natural convection. In literature, this quenching mechanism was originally called by [4] "bulk-convection", while it was also referred to as transient conduction. This modelling approach was also called in literature "heat flux partitioning approach", i.e. the total heat flux is resulting from the summation of heat fluxes due to each separate mechanism. Other examples include the models by Yu and Cheng [6], Kim and Kim [7] and Zupančič et al. [8] who assumed natural convection, transient conduction and evaporation. Despite the large number of models in literature, there are still large discrepancies amongst these models. For example, Mahmoud and Karayiannis [9] plotted the boiling curve predicted using 26

* Corresponding author: Department of Mechanical and Aerospace Engineering, Brunel University London, Uxbridge, Middlesex, UB8 3PH, UK.
*E-mail address:* tassos.karayiannis@brunel.ac.uk (T.G. Karayiannis).

https://doi.org/10.1016/j.ijheatmasstransfer.2023.124065

**Nomenclature**

*Abbreviations*

| | |
|---|---|
| A | Asymptotic |
| I | Inertia |
| MAE | Mean Absolute Error |
| ONB | Onset of Nucleate Boiling |
| WTBL | Wall Thermal Boundary Layer |
| $A$ | factor in Eq. (13) and (42), $[J/kg]^{1/2}$ |
| $A_{bc}$ | bubble base contact area, $[m^2]$ |
| $A_P$ | projected area, $[m^2]$ |
| $Ar$ | Archimedes number, $Ar = (g/\nu_L^2)(\sigma/\rho_L g)^{3/2}$, [-] |
| $B$ | factor in Eq. (16) and (42), $[m/s^{0.5}]$ and constant in Eq. (21) |
| $Bo$ | Bond number, $\Delta\rho g R_c^2/\sigma$, [-] |
| $b$ | curvature factor in Eq. (30) and (46) and coefficient in Eq. (49), $[m/s^{0.5}]$ |
| $b^*$ | factor in Eq. (36), [-] |
| $c$ | bubble shape factor in Eq. (49) and (73), [-] |
| $c_b$ | empirical constant in Eq. (49), [-] |
| $C_1$ | bubble growth constant in $R = C_1 t^n$, $[m/s^n]$ |
| $C_2$ | constant in $\delta_0 = C_2\sqrt{\nu t}$, [-] |
| $c_{pL}$ | liquid specific heat, [J/kg K] |
| $c_{pv}$ | vapour specific heat, [J/kg K] |
| $D$ | bubble diameter, [m] |
| $D_s$ | diameter of heat transfer surface, [m] |
| $F$ | factor defined in Eq. (17), [-] |
| $f_{bd}$ | bubble departure frequency, [Hz] |
| $f_\rho$ | density factor, $(1 - \rho_v/\rho_L)$, [-] |
| $f_\theta$ | bubble shape factor, [-] |
| $g$ | gravitational acceleration, $[m/s^2]$ |
| $h$ | heat transfer coefficient, $[W/m^2\ K]$ |
| $h_b$ | boiling heat transfer coefficient, $[W/m^2\ K]$ |
| $h_v$ | vapour heat transfer coefficient, $[W/m^2\ K]$ |
| $h_{fg}$ | latent heat, [J/kg] |
| $Ja$ | Jakob number, $\rho_l c_{pl}\Delta T_{sL}/\rho_v h_{fg}$, [-] |
| $k_{cu}$ | thermal conductivity of copper, [W/m K] |
| $k_L$ | thermal conductivity of liquid, [W/m K] |
| $L$ | characteristic length for natural convection, [m] |
| $l_{ch}$ | length scale in Eq. (17) and (19), [m] |
| $m_v$ | vapour mass, [kg] |
| $N$ | Stephan number, $c_{pL}\Delta T_{sL}/h_{fg}$, [-] or number of experimental data points |
| $N_m$ | dimensionless factor in Eq. (77), [-] |
| $N_1$ | factor in Eq. (75), [-] |
| $N_2$ | factor in Eq. (75), [-] |
| $N_q$ | factor in Eq. (75), [m/s |
| $n$ | time exponent in the growth law, [-] |
| $Nu$ | Nusselt number, $Nu = hD_s/k_l$, [-] |
| $P$ | pressure, [Pa] |
| $P_C$ | critical pressure, [Pa] |
| $P_r$ | reduced pressure, [-] |
| $P_{sat}$ | saturation pressure, [Pa] |
| $P_v$ | vapour pressure, [Pa] |
| $P_{L\infty}$ | liquid pressure at infinity, [Pa] |
| $\Delta P$ | pressure difference, [Pa] |
| $Pr$ | Prandtl number, [-] |
| $Q_{mL}$ | heat transfer rate across the microlayer, [W] |
| $q$ | heat flux, $[W/m^2]$ |
| $q_{Lb}$ | heat flux towards the liquid bulk, $[W/m^2]$ |
| $q_{mL}$ | heat flux across the microlayer, $[W/m^2]$ |
| $q_{sL}$ | heat flux from superheat liquid, $[W/m^2]$ |
| $r$ | radial distance, [m] |
| $r_{cont}$ | bubble contact radius, [m] |
| $R_{Fritz}$ | bubble radius from Fritz-Ende model, [m] |
| $R_{av}$ | average bubble radius, [m] |
| $R_c$ | cavity mouth radius, m] |
| $R_0$ | radius of bubble embryo, [m] |
| $R$ | bubble radius, [m] |
| $\dot{R}$ | bubble growth velocity, [m/s] |
| $\ddot{R}$ | bubble growth acceleration, $[m/s^2]$ |
| $R_1$ | radius due to inertial growth, [m] |
| $R_2$ | radius due to asymptotic growth, [m] |
| $R_d$ | departure radius, [m] |
| $R_{exp}$ | measured radius, [m] |
| $Ra$ | Rayleigh number, $\beta_L g(T_w - T_l)D_s^3/\alpha\nu$, [-] |
| $R_{pred}$ | predicted radius, [m] |
| $R^+$ | dimensionless radius, see Eq. (42) |
| $R^2$ | correlation coefficient, [-] |
| $t$ | time, [s] |
| $t_{ch}$ | characteristic time scale in Eq. (19), [s] |
| $t_d$ | departure time, [s] |
| $t_0$ | characteristic time scale in Eq. (17), [s] |
| $t_{wt}$ | waiting time, [s] |
| $t_\delta$ | boundary layer penetration time, [s] |
| $T$ | temperature, [K] |
| $t^+$ | dimensionless time in Eq. (16) and (19), [-] |
| $T_{sat}$ | saturation temperature, [K] |
| $T_5$ | thermocouple no. 5 below the surface |
| $T_{Lb}$ | liquid bulk temperature, [K] |
| $T_w$ | boiling surface temperature, [K] |
| $T_{L\infty}$ | liquid temperature at infinity, [K] |
| $T_{sL}$ | superheated liquid temperature |
| $T_{max}$ | maximum temperature, [K] |
| $\Delta$T | temperature difference, [K] |
| $\Delta T_w$ | wall superheat, $(T_w - T_{sat})$, [K] |
| $\Delta T_{sL}$ | liquid superheat, $(T_L - T_{sat})$, [K] |
| $\Delta T_\infty$ | liquid subcooling, $(T_{sat} - T_L)$, [K] |
| $u_L$ | liquid velocity, [m/s] |
| $V_b$ | bubble volume, $[m^3]$ |
| $y$ | vertical distance, [m] |
| $\Delta y$ | distance between $T_5$ and the surface, [m] |

*Greek Symbols*

| | |
|---|---|
| $\alpha_L$ | liquid thermal diffusivity, $[m^2/s]$ |
| $\beta_L$ | thermal expansion coefficient [1/K] |
| $\beta_{1..5}$ | Empirical constants in Eqs. (59)-(63) |
| $\beta$ | bubble growth factor, [-] |
| $\gamma$ | coefficient in Eq. (23) and Eq. (75) |
| $\delta$ | transient boundary layer thickness, [m] |
| $\delta_{th}$ | thermal boundary layer thickness, [m] |
| $\delta_{eff}$ | effective boundary layer thickness, [m] |
| $\delta_0$ | initial microlayer thickness, [m] |
| $\delta_{Ls}$ | bubble boundary layer thickness, [m] |
| $\zeta$ | direction normal to the bubble, [m] |
| $\theta$ | contact angle, [deg] |
| $\kappa$ | density ratio $\rho_v/\rho_L$, [-] |
| $\mu_L$ | liquid viscosity, [Pa. s] |
| $\nu$ | kinematic viscosity $[m^2/s]$ |
| $\rho_L$ | liquid density, $[kg/m^3]$ |
| $\rho_v$ | vapour density, $[kg/m^3]$ |
| $\sigma$ | surface tension, [N/m] |
| $\psi$ | interface permeability factor, [-] |

models for water at atmospheric pressure and reported a wide scatter, e.g. for a fixed heat flux value of 250 $kW/m^2$, the wall superheat (or surface temperature) predicted by one model was 28 K while it was about 4 K by another model (about times 7 difference in the heat transfer coefficient). The large discrepancy amongst

the models may be attributed to the following: (i) lack of understanding of several fundamental aspects and the complex effects of several factors such as bubble dynamics (growth rate, departure diameter, departure frequency), fluid properties and surface microstructure that affect the active nucleation site density. (ii) all phenomenological heat transfer models depend on sub-models for the prediction of bubble departure diameter and frequency, which depend strongly on bubble growth rate. The problem is that there is a wide scatter amongst the existing bubble growth models as reported by Mahmoud and Karayiannis [10] and as will be presented and discussed later in the current study. This could be a reason for the discrepancy amongst nucleate boiling heat transfer models. Additionally, some researchers estimated bubble growth rate in nucleate boiling using models suggested for homogeneous boiling, which may not be valid.

Based on the above, there is a need for more experimental research with careful measurements of bubble growth rate, which can help evaluate the existing bubble growth models and thus understand the reasons of discrepancies. In the current study, bubble growth rate was measured in saturated pool boiling of deionized water on a smooth copper surface at three pressures 0.15, 0.5 and 1 bar and superheat 5.1 – 19.5 K. The measurements were conducted using a high-speed, high-resolution video camera integrated with a microscopic lens. The bubble growth characteristics, the forces acting on the bubble during its growth period, and the mechanisms of heat flow to the bubble were discussed in a separate publication, see Mahmoud and Karayiannis [9]. The current study focuses on discussing and evaluating the existing homogeneous and heterogeneous bubble growth models using our experimental data. This will help understand the differences amongst the models and the bubble growth mechanism(s). Additionally, a recommendation will be given at the end of the paper for the accurate prediction of bubble growth rate in saturated boiling of water. The paper is organised as follows: Section 2 presents the bubble growth fundamentals to help the reader track the differences amongst the models, Section 3 gives a description of the experimental system and validation and Section 4 presents the evaluation of the bubble growth models. Section 5 gives recommendation for predicting bubble growth rate while Section 6 gives the conclusions of the study.

## 2. Bubble growth fundamentals

It is well-known that bubble growth can be divided into two main categories: symmetric growth in *uniformly superheated liquid* (the whole bubble is surrounded by superheated liquid – homogeneous boiling) and asymmetric growth in *non-uniformly superheated liquid* (part of the bubble is surrounded by superheated liquid as is the case in growth on a heated surface – heterogeneous boiling). From now on, "homogeneous" will refer to uniform superheat while "heterogeneous" will refer to non-uniform superheat. It is important to start with a brief description to the bubble growth problem without going into the complex details of the equations. In homogeneous boiling, the bubble growth problem was usually formulated by applying the laws of mass, momentum and energy conservation. Applying the mass and momentum conservation for a spherical bubble results in Eq. (1), which was given by Scriven [11] and was also called the extended Rayleigh [12] equation. This equation was obtained based on the following simplifying assumptions: (i) spherical symmetry for a bubble growing in an infinite medium, (ii) Newtonian fluid with constant properties, (iii) compressibility effects, external and body forces are ignored, (iv) the pressure and temperature inside the bubble are uniform, (v) the liquid surrounding the bubble flows with a velocity $u_L = (1-\rho_v/\rho_L)(dR/dt)$, due to mass transfer across the interface (vi) the bubble grows without translational and rotational motion.

$$\frac{P_v - P_{L\infty}}{(1-\rho_v/\rho_L)\rho_L} = R\frac{d^2R}{dt^2} + \frac{3}{2}\left(\frac{dR}{dt}\right)^2 + \frac{2\sigma}{(1-\rho_v/\rho_L)\rho_L R} + \frac{4\mu_L R}{(1-\rho_v/\rho_L)\rho_L}\frac{dR}{dt} \quad (1)$$

The different stages of bubble growth can be understood from Eq. (1), with the help of the schematic drawing in Fig. 1, for inviscid liquids (ignoring the last term in the r.h.s. of Eq. (1)) and ignoring the vapour to liquid density ratio ($\rho_v/\rho_L \ll 1$ for most fluids). Bubble growth in stage 1 (left schematic) occurs isothermally ($T_v = T_{L\infty}$) at the beginning (time $t \approx 0$) when the bubble nucleus fluctuates around its initial equilibrium radius $R_0$. In this case the velocity and acceleration are very small and thus the liquid inertia terms (1st and 2nd terms in the r.h.s. of Eq. (1)) are negligible. Accordingly, the dynamic growth will be driven by the pressure difference $P_v - P_{L\infty} = 2\sigma/R$, which is called the "surface tension dominated stage". In stage 2 (mid schematic), the growth occurs isothermally similar to stage 1 but the bubble grew to a radius slightly larger than the initial radius $R_0$. Thus, the surface tension term (3rd term in the r.h.s.) becomes negligibly small and thus bubble growth will be dominated by the liquid inertia, which is called the "inertia-controlled growth". It is worth mentioning that the time scale in the first and second stages is very small, in the order of microseconds. For example, Sernas and Hooper [13] and Forster and Zuber [14] reported that dynamic effects diminish after 50 μs (based on experimental measurements) and after 100 μs (based on numerical analysis), respectively. In stage 3 (right schematic), when time increases further, evaporation occurs at the bubble surface and a thin thermal boundary layer develops around the bubble, which was called by Plesset and Zwick [15] "the cooling effect". Thus, the vapour temperature drops from its initial superheat to the saturation temperature and consequently the vapour pressure $P_v$ becomes equal to the liquid pressure $P_{L\infty}$ (system pressure). This makes the l.h.s. of Eq. (1) vanishes and the dynamic effects do not drive the bubble growth anymore. Accordingly, another mechanism must takeover, which is the "heat diffusion mechanism" driven by the temperature difference $T_{L\infty} - T_v$, which was commonly called "heat transfer-controlled growth" or "asymptotic growth". From now on, we shall use "asymptotic" to refer to the heat transfer-controlled growth. It is worth mentioning that there is no analytical solution to Eq. (1) but there are either approximate solutions for each separate stage of growth or a complete numerical solution. For example, Rayleigh [12] simplified the bubble growth problem by ignoring the surface tension stage, ignoring the vapour to liquid density ratio ($\rho_v/\rho_L$) and assuming that the bubble grows isothermally (no heat transfer), i.e. ($P_v - P_{L\infty}$) remains constant with time. This led to the well-known Rayleigh solution for the "inertia-controlled growth" given by Eq. (2), which indicates that the radius increases linearly with time $R \propto t$, i.e. bubble grows at a constant rate.

$$R = \sqrt{\frac{2}{3}\frac{P_v - P_{L\infty}}{\rho_L}}\,t \quad (2)$$

To generalize the bubble growth problem and include heat transfer at the bubble interface, the energy equation (see below) must be coupled with the dynamic equation (Eq. (1)). The coupling between the two equations was usually conducted through the pressure difference term ($P_v - P_{L\infty}$) in Eq. (1), which can be related to the degree of liquid superheat ($T_{L\infty} - T_v$) through some simplifying assumptions, e.g. Clausius–Clapeyron equation as defined in Eq. (3). The liquid temperature at the bubble interface, which equals the vapour temperature in thermodynamics equilibrium, can be obtained from the solution of the transient energy equation without heat generation (Eq. (4)) with the commonly

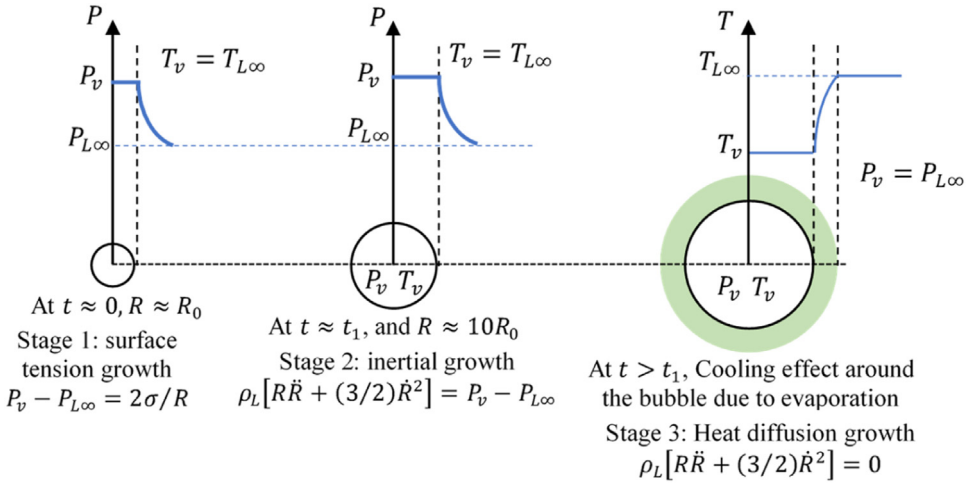


**Fig. 1.** Schematic drawing for the different stages of bubble growth in homogeneous boiling.

used boundary condition at the bubble interface defined in Eq. (5). Accordingly, the solution of Eq. (1) coupled with Eq. (4) with the appropriate initial and boundary conditions describe the full bubble growth problem including the whole stages of growth (surface tension, inertia and heat diffusion), which can be solved numerically. Because numerical solutions did not give an explicit expression for the bubble radius and because the dynamic effects are important only for very short time intervals at the beginning, many researchers ignored the complex initial growth stages (surface tension and inertia) and gave approximate analytical solutions for the asymptotic stage in which the bubble radius was found to be proportional to the square root of time ($t^{1/2}$). The asymptotic solution can be obtained simply from the energy balance at the interface (Eq. (5)) provided that the temperature gradient $(\partial T/\partial r)_{r=R}$ is known. In the following sub-sections, the bubble growth models in homogeneous and heterogeneous boiling will be reviewed and discussed.

$$\Delta P = P_v - P_{L\infty} = \frac{\rho_v h_{fg}}{T_{sat}}(T_{L\infty} - T_v) \tag{3}$$

$$\frac{\partial T}{\partial t} + \frac{(1-\rho_v/\rho_L)R^2}{r^2}\frac{dR}{dt}\frac{\partial T}{\partial r} = \frac{1}{\alpha_L}\frac{1}{r^2}\frac{\partial}{\partial r}\left(r^2\frac{\partial T}{\partial r}\right) \tag{4}$$

$$k_L\left(\frac{\partial T}{\partial r}\right)_{r=R} = \rho_v h_{fg}\frac{dR}{dt} \tag{5}$$

### 2.1. Bubble growth in homogeneous boiling

#### 2.1.1. Asymptotic growth models

Historically, Fritz and Ende [16] were the first to suggest a model for bubble growth in homogeneous boiling, which was based on energy balance at the bubble interface (see Eq. (5)), i.e. balance between conduction and evaporation heat fluxes. They assumed that the temperature drops across a thin boundary layer around the bubble (thin boundary layer approximation) and thus the effect of bubble curvature can be neglected. This allowed for the assumption that the temperature gradient at the bubble interface can be obtained from the well-known solution of the 1D transient heat conduction equation in a semi-infinite plate, i.e. $(\partial T/\partial r)_{r=R} = k_L \Delta T_{sL}/\sqrt{\pi \alpha_L t}$. In other words, the effect of liquid radial motion and bubble curvature on the temperature gradient were ignored. With this energy balance, the bubble radius was obtained as:

$$R_{Fritz} = \frac{2}{\sqrt{\pi}} Ja\sqrt{\alpha_L t} \tag{6}$$

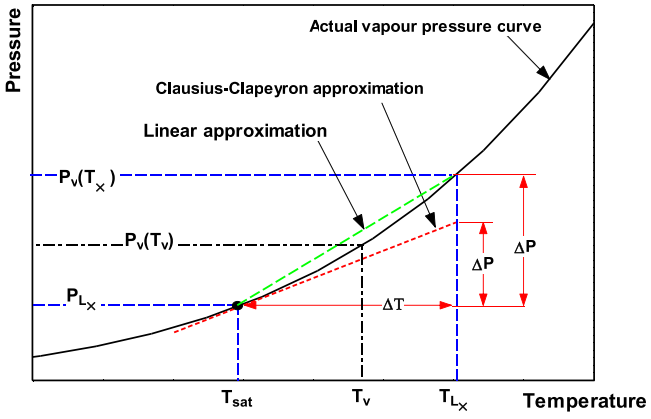


**Fig. 2.** Schematic drawing for the vapour pressure curve showing the linear approximation adopted by Plesset and Zwick [15] and the Clausius–Clapeyron approximation adopted by Forster and Zuber [14].

The Fritz and Ende [16] model may be considered as a benchmark because it ignored the effect of bubble curvature and liquid motion (convection) on temperature gradient and consequently on bubble growth. To consider these effects, Plesset and Zwick [15] and Forster and Zuber [14] independently solved the dynamic equation Eq. (1) coupled with the energy equation (Eq. (4)). Firstly, the two groups of researchers obtained the temperature at the interface by solving Eq. (4) for a spherical geometry with a moving boundary using two different mathematical approaches. To get a convergent solution, they simplified the problem by adopting the "thin boundary layer approximation", as was done by Fritz and End [16]. Secondly, the obtained interface temperature was used to achieve the coupling between the energy and the dynamic equations. The difference between the coupling method adopted by the two researchers was the assumption of the relation between the vapour pressure and temperature. Plesset and Zwick [15] assumed linear relationship between $\Delta P$ and $\Delta T$ while Forster and Zuber [14] used the linearized Clausius–Clapeyron equation. It is worth noting that the linearized Clausius–Clapeyron equation underpredicts the pressure difference especially as the superheat increases as seen in Fig. 2. Finally, the two groups of researchers ignored the inertia and surface tension stages of growth and gave an approximate solution to the asymptotic stage defined by Eq. (7) for the Plesset and Zwick [15] model and Eq. (8) for the Forster and Zuber [14] model. It is obvious from the two equations that the differ-

ence between the two models is 10%. Bankoff [17] followed the same approach and assumptions as [15] except that a temperature condition was imposed at the bubble interface rather than a heat flux condition. He adopted this approach to make the solution converge more rapidly. Although the boundary condition was different, he obtained exactly the same solution as [15]. Prisnyakov [18] considered the bubble as a thermodynamic system and applied the first law of thermodynamics, rather than the dynamic momentum equation, with the assumption that the vapour behaves as an ideal gas and the effect of bubble curvature was neglected. Thus, the conduction heat flux at the bubble interface was the same as that assumed by Fritz and Ende [16] and the difference was the expansion work included in the 1st law of thermodynamics. This energy balance resulted in Eq. (9), which was reported to be valid for $Ja$ up to 500. Comparing Eqs. (7), ((8) and (9) with the Fritz and Ende [16] model in Eq. (6) indicates that the difference is only a constant factor equals 2/3 in the Prisnyakov [18] model, $\sqrt{3}$ in the Plesset and Zwick [15] model and $\pi/2$ in the Forster and Zuber [14] model.

$$R = \sqrt{3}\frac{2}{\sqrt{\pi}} Ja\sqrt{\alpha_L t} = \sqrt{3} R_{Fritz} \tag{7}$$

$$R = \frac{\pi}{2}\frac{2}{\sqrt{\pi}} Ja\sqrt{\alpha_L t} = \frac{\pi}{2} R_{Fritz} \tag{8}$$

$$R = \frac{4}{3\sqrt{\pi}} Ja\sqrt{\alpha_L t} = \frac{2}{3} R_{Fritz} \tag{9}$$

Since the emergence of the above models, some researchers claimed that the "thin boundary layer approximation" may not be accurate, especially at small Jackob numbers. Scriven [11] solved the mass, energy and momentum conservation equations numerically without adopting the assumption of "thin boundary layer". Thus, a complete numerical solution was obtained rather than the above approximate solutions. The bubble interface was considered permeable, i.e. liquid and vapour can flow across the interface due to the difference in liquid and vapour density. Based on that he correlated the obtained numerical solution, for the asymptotic growth stage, in the form given by Eq. (10). The growth factor $\beta$ in Eq. (10) was plotted versus $c_{pL}\Delta T_{sL}/h_{fg}$ for different values of vapour to liquid density ratio ($\rho_v/\rho_L$) and specific heat ratio $(c_{pL} - c_{pv})/c_{pL}$. It is worth mentioning that the sensible heat of liquid and vapour was included in the energy balance, which was ignored by other researchers. He fitted the general numerical solution for $\beta$ with two separate equations, one for superheat $\Delta T_{sL} < 1K$ and one for $\Delta T_{sL} > 1K$. Because the wall superheat in nucleate boiling is always much larger than 1 K, the equation for the high superheat was commonly reported in literature as Eq. (11).

$$R = \beta\sqrt{\alpha_L t} \tag{10}$$

$$\beta = \begin{cases} \sqrt{\frac{12}{\pi}}\left[\frac{1}{\left[\frac{1}{Ja} + \frac{\rho_v}{\rho_L} - \frac{\rho_v}{\rho_l}\frac{c_{pv}}{c_{pL}}\right]}\right] \; general\ case \\ \sqrt{\frac{12}{\pi}} Ja \;\; when \;\; \rho_v/\rho_L \ll 1 \end{cases} \tag{11}$$

Eq. (11) indicates that the general numerical solution by Scriven [11] is exactly equivalent to the Plesset and Zwick [15] model when the density ratio is $\rho_v/\rho_L \ll 1$, which is the case for all fluids of interest such as water. He also concluded that the error in the Plesset and Zwick [15] model becomes very large only when the superheat is less than 1 K and when the density ratio is very large. Avdeev and Zudin [19] obtained an analytical solution to the general bubble growth problem (mass, energy and momentum conservation) assuming that the bubble interface is permeable, i.e. there is enhancement in heat transfer at the interface due to the liquid and vapour motion induced by the density difference. The effect of interface permeability was captured by a factor $\psi$ defined below, which was called by them "interface permeability factor". The obtained analytical solution for the bubble growth factor $\beta$ was given by Eq. (12). This equation is general and valid for all values of $Ja$ and density ratios. For example, when the density ratio is very small and negligible, the value of $N$ goes to zero and $\psi$ goes to 1. As the $Ja$ increases and $\psi = 1$ (ignore interface permeability effects), $\beta$ reduces to $\sqrt{12/\pi}$, which is similar to the Plesset and Zwick model [15]. They reported that their analytical solution deviates by 4% from the full numerical solution given by Scriven [11].

$$\beta = \sqrt{\frac{3}{\pi}} Ja\psi + \sqrt{\frac{3}{\pi}(Ja\psi)^2 + 2Ja},\ \psi = 1 + \sqrt{\frac{\pi}{2}\left(\frac{1}{\sqrt{1-N}} - 1\right)},$$
$$N = \frac{c_{pL}\Delta T_{sL}}{h_{fg}} = \frac{\rho_v}{\rho_L} Ja \tag{12}$$

### 2.1.2. Inertia-asymptotic growth models

In the above section, the solution of the bubble growth problem was only given for the asymptotic growth stage. At low system pressure and/or very large superheat, the bubble growth may be affected by the liquid inertia. Mikic et al. [20] were the first to suggest a method to combine the inertia and asymptotic stages into one model. With the help of the schematic shown in Fig. 2, there are two extremes for bubble growth. The first extreme occurs when $T_v$ equals $T_{L\infty}$ (isothermal growth), which results in the "inertia-controlled growth". The second extreme occurs when $T_v$ equals $T_{sat}$, which results in the "asymptotic growth". In the transition between the two extremes, the vapour temperature and pressure are in the range $T_{sat} \le T_v \le T_{L\infty}$ and $P_{L\infty} \le P_v \le P_v(T_{L\infty})$, respectively. Mikic et al. [20] used the Rayleigh [12] solution (Eq. (2)) for the inertia stage and the Plesset and Zwick [15] solution (Eq. (7)) for the asymptotic stage. In other words, they connected the Rayleigh bubble growth velocity (Eq. (13)) with the Plesset and Zwick [15] bubble growth velocity (Eq. (14)). They related the pressure difference $(P_v - P_{L\infty})$ in Eq. (13) with the temperature difference $(T_v - T_{sat})$ using the linearized Clausius–Clapeyron. The two solutions (inertial and asymptotic) were connected through the vapour temperature $T_v$ by substituting the term $\frac{(T_v - T_{sat})}{\Delta T_{sL}}$ from Eq. (13) into Eq. (14). On doing so, a quadratic equation, Eq. (15), was obtained, which satisfies the two extreme solutions. The solution of Eq. (15) resulted in the bubble growth radius written in a dimensionless form in Eq. (16).

$$\left(\frac{dR}{dt}\right)_{inertia} = \sqrt{\frac{2}{3}\frac{(P_v - P_{L\infty})}{\rho_L}} = \sqrt{\frac{2}{3}\frac{\rho_v h_{fg}(T_v - T_{sat})}{\rho_L T_{sat}}\frac{(T_{L\infty} - T_{sat})}{(T_{L\infty} - T_{sat})}}$$
$$= A\sqrt{\frac{(T_v - T_{sat})}{\Delta T_{sL}}}, A = \sqrt{\frac{2}{3}\frac{\rho_v h_{fg}(T_{L\infty} - T_{sat})}{\rho_L T_{sat}}} \tag{13}$$

$$\left(\frac{dR}{dt}\right)_{asymptotic} = \frac{1}{2}\sqrt{\frac{12}{\pi}} Ja\sqrt{\frac{\alpha_L}{t}}\frac{(T_{L\infty} - T_v)}{\Delta T_{sL}}$$
$$= \frac{1}{2}\sqrt{\frac{12}{\pi}} Ja\sqrt{\frac{\alpha_L}{t}}\left\{1 - \frac{(T_v - T_{sat})}{\Delta T_{sL}}\right\} \tag{14}$$

$$\frac{1}{A^2}\left(\frac{dR}{dt}\right)^2 + \frac{2\sqrt{t}}{\left(\sqrt{12\alpha_L/\pi}\right)Ja}\frac{dR}{dt} - 1 = 0 \tag{15}$$

$$R^+ = \frac{2}{3}\left[\left(t^+ + 1\right)^{3/2} - \left(t^+\right)^{3/2} - 1\right] \tag{16}$$

$$R^+ = \frac{AR}{B^2}, t^+ = \frac{A^2 t}{B^2}, B = \sqrt{\frac{12}{\pi}\alpha_L Ja}$$

Theofanou and Patel [21] adopted the same method as Mikic et al. [20] but with the following modifications: (i) the vapour density should not be assumed constant as was done by [20] who estimated the vapour density at the system pressure, which underestimates the value and consequently over-estimates the Jackob number and the growth rate in the asymptotic regime, see Eq. (14). Accordingly, they suggested considering the initial to final vapour density ratio, especially when this ratio is much larger than 1. The initial vapour density was defined based on $P_v(T_{L\infty})$, (see Fig. 2 for more clarity) while the final vapour density is the density defined at system pressure $P_v(T_{sat})$. (ii) a linear relation was used to relate the vapour pressure with temperature rather than the Clausius–Clapeyron equation used by [20] which underpredicts the vapour pressure and thus under-estimates the inertial growth velocity, see Eq. (13). In conclusion, a linear interpolation between the initial and final states was conducted for the vapour pressure and vapour density. Comparing the original model [20] with the modified version [21] indicated that the two models give exactly similar results when the initial to final density ratio is below 2. For water, this density ratio value corresponds to an initial superheat of about 22 K, which is a large range for boiling applications. In other words, assuming constant vapour density and using the Clausius–Clapeyron assumption adopted by Mikic et al. [20] is valid up to superheat degrees below 25 K. Avdeev and Zudin [19] adopted the same approach as [20] except that in the asymptotic stage, the heat flux at the bubble interface was corrected by the "interface permeability factor $\psi$" to account for heat transfer enhancement at the interface due to liquid/vapour flows: $q = \psi k_L \Delta T_{sL}/\sqrt{\alpha_L t} = \rho_v h_{fg} dR/dt$. Note that the Plesset and Zwick [15] solution for the asymptotic stage was used by Mikic et al. [20]. They managed to get an analytical equation for some special cases such as when the term $N = c_{pL}\Delta T_{sL}/h_{fg}$ in the permeability factor $\to 1$. However, in the general case $0 \le N < 1$, they failed to obtain a closed form solution similar to Mikic et al. [20] due to the complexity of the polynomials and inverse hyperbolic functions encountered in their analysis. Accordingly, they suggested the following approximate equation that combines inertia and thermal growth stages, which was based on dimensionless scaling analysis:

$$\frac{R}{l_{ch}} = \frac{r_1}{\left(1+F^3\right)^{1/3}} \tag{17}$$

$$l_{ch} = \frac{\alpha_L}{Ja^2\sqrt{2\Delta P/3\rho_L}}, F = \frac{2(t/t_0)^{1/4}}{3\psi}, r_1 = \frac{4}{3}\left[\left(1+\sqrt{t/t_0}\right)^{3/2} - 3\left(1+\sqrt{t/t_0}\right)^{\frac{1}{2}} + 2\right], t_0 = \frac{\alpha_L}{Ja^2(2\Delta P/3\rho_L)}$$

### 2.2. Bubble growth in heterogeneous boiling

Bubble growth in heterogenous boiling is more complex compared to homogeneous boiling due to the presence of the wall thermal boundary layer, which makes the superheat around the bubble nonuniform. In the above homogeneous models, the radius $R$ is proportional to $t^{1/2}$ in the asymptotic growth stage while in heterogeneous boiling, the exponent of time could be smaller than ½. For example, Strenge et al. [22] measured bubble growth in saturated boiling of n-pentane and diethyl ether at atmospheric pressure and found that the radius follows the relation $R \propto t^n$, with $n$ ranged from 0.19 to 0.475. The key differences amongst bubble growth models in heterogeneous boiling in the asymptotic stage arise from the assumption of the heat transfer mechanism to the bubble. Two main mechanisms were assumed by researchers namely: (i) growth due to evaporation of the liquid trapped in the microlayer underneath the bubble and (ii) growth due to evaporation from the superheated boundary layer around the curved surface of the bubble. From now on, to distinguish between the two mechanisms, the first one will be called "microlayer evaporation" and the second one will be called "boundary layer evaporation". Fig. 3 depicts a schematic drawing for bubble growth mechanisms adopted by some researchers to help the reader understand the difference between each model. In Fig. 3a, the bubble grows due to evaporation from the boundary layer carried by the bubble from the boiling surface. In Fig. 3b, the bubble protrudes outside the wall thermal boundary layer (WTBL) and grows as a hemisphere due to microlayer evaporation. The mechanism in Fig. 3c is similar to Fig. 3a except that the boundary layer was displaced and thus covers only part of the bubble. In Fig. 3d, the bubble grows due to a combined evaporation from the microlayer and from the superheated layer around the bubble. The different models suggested by researchers for bubble growth in heterogeneous boiling are discussed in the following sub-sections. They are classified into (i) empirical models, (ii) boundary layer evaporation models and (iii) microlayer evaporation models. It is worth mentioning that in all heterogeneous growth models, the average wall superheat ($\Delta T_w$) was used in the definition of $Ja$ number rather than the liquid superheat $\Delta T_{sL}$ ($\Delta T_{sL} = T_{L\infty} - T_{sat}$) in homogeneous boiling.

#### 2.2.1. Empirical models

Some researchers suggested bubble growth models in heterogeneous boiling based on fitting their experimental data. Cole and Shulman [28] measured bubble growth at high Jakob numbers (24 – 792) in saturated boiling of toluene, acetone, n-pentane, $CCl_4$, methanol and water on a polished zirconium ribbon. They used their data to evaluate some of the homogeneous growth models and concluded that the experimental growth factor $\beta = f(Ja)$ was small compared to the homogeneous models, which was attributed to the nonuniform superheat in heterogeneous boiling. They correlated their data in the form given by Eq. (18). The effect of the nonuniform superheat appears in the empirical constant (2.5) and the smaller exponent of $Ja$ compared to homogeneous boiling (the exponent of $Ja$ in homogeneous boiling is 1).

$$R = 2.5 Ja^{0.75}\sqrt{\alpha_L t} \tag{18}$$

Lee et al. [29] studied bubble growth in saturated boiling of R11 and R113 on a glass substrate. Compared to homogeneous models, they found that the time exponent was 0.2, which is smaller than the 0.5 value in homogeneous boiling. In addition to the two tested refrigerants, they collected data from literature for n-butane and water and suggested an empirical model based on dimensionless analysis. They correlated the dimensionless radius ($R^+ = R/l_{ch}$) with the dimensionless time ($t^+ = t/t_{ch}$) in the form given by Eq. (19) using characteristic length scale $l_{ch}$ and time scale $t_{ch}$ defined below.

$$R^+ = \frac{R}{l_{ch}} = 11.2\left(t^+\right)^{0.2}\tanh\left[0.345\left(t^+\right)^{0.8}\right] + 0.072 \tag{19}$$

$$l_{ch} = \frac{\sqrt{27}}{2} Ja\alpha_L\sqrt{\frac{\rho_L R_d}{\sigma}}, t_{ch} = \frac{9}{4} Ja\alpha_L\frac{\rho_L R_d}{\sigma}$$

Du et al. [30] collected data from literature for saturated boiling of water on copper, stainless steel, nickel and silver in the pressure range 0.02 – 95.7 bar ($Ja$ = 0.0904 – 2689). They found that the bubble growth can be fitted in the form given by Eq. (20) with the growth factor $\beta$ depends on $Ja$ while the time exponent $n$ depends on system pressure. The variation of the exponent $n$ with pressure was attributed to the dominant factors that control the

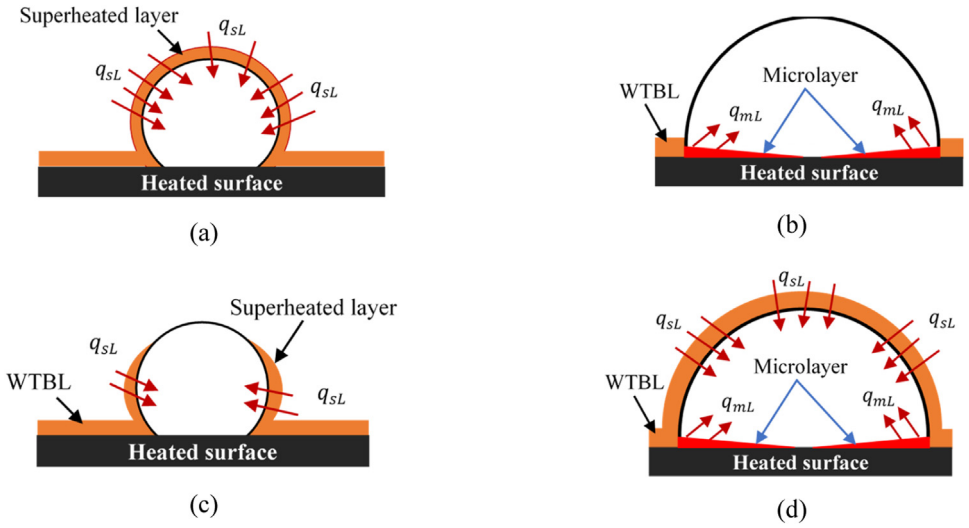


**Fig. 3.** Asymptotic bubble growth mechanisms in heterogeneous boiling: (a) and (c) boundary layer evaporation, Zuber [23], Han and Griffith [24], and Van Stralen [25]. (b) microlayer evaporation, Cooper [26], (d) combined microlayer and superheated liquid evaporation, Cooper [26] and Van Stralen et al. [27]. *WTBL: wall thermal boundary layer.*

growth rate, e.g. at low pressure, the growth is controlled by inertia while at high pressure it is controlled by heat transfer. Benjamin and Balakrishnan [31] collected data from literature for saturated boiling on upward facing flat metallic surfaces and fluids including water, $CCl_4$, n-hexane, n-pentane and acetone. They found that the data can be fitted by Eq. (21).

$$R = \beta \alpha_L^{1/2} t^n,\ \beta = 2.1077 Ja^{0.7902} \tag{20}$$

$$n = 1.0012e^{-P/0.3257} - 0.9624e^{-P/0.6161} + 0.5,\ \text{P: in MPa}$$

$$R = \frac{1}{2} BAr^{0.135} Ja^{0.5} \sqrt{\alpha_L t} \tag{21}$$

$Ar = (g/\nu_L^2)(\sigma/\rho_L g)^{3/2}$, $B = 1.55$, [water, CCl4, n-hexane] and $B = 1/1.55$, [n-pentane and acetone]

Abdollahi et al. [32] proposed a semi-empirical model for bubble growth in nucleate boiling. The functional form of the model was derived first for homogeneous boiling then used to fit experimental data in heterogeneous boiling. They ignored the bubble curvature and used the temperature gradient from the 1D transient heat conduction equation in the energy balance at the bubble interface and thus obtained Eq. (22) for the bubble growth velocity. The vapour temperature in Eq. (22) was assumed to vary with time according to the relation in Eq. (23), which satisfies the two extreme cases of growth (inertia) ($T_{L\infty} = T_v$) at $t = 0$ and asymptotic stage ($T_{sat} = T_v$) at $t = \infty$. The coefficient $\gamma$ in Eq. (23) depends on fluid properties and with small values, the vapour temperature approaches the saturation temperature slowly and with large values it decreases rapidly to the saturation temperature. Accordingly, substituting from Eq. (23) into (22) resulted in Eq. (24). In the inertia-controlled stage ($t \to 0$), Eq. (24) reduces to Eq. (25). Comparing Eq. (25) with the Rayleigh inertial growth velocity in Eq. (13), the coefficient $\gamma$ was obtained as Eq. (26).

$$\frac{dR}{dt} = \frac{1}{\sqrt{\pi}} \sqrt{\frac{\alpha_L}{t}} Ja \frac{T_{L\infty} - T_v}{T_{L\infty} - T_{sat}} \tag{22}$$

$$\frac{T_{L\infty} - T_v}{T_{L\infty} - T_{sat}} = erf\left(\gamma \sqrt{t}\right) \tag{23}$$

$$\frac{dR}{dt} = \sqrt{\frac{\alpha_L}{\pi}} Ja \frac{erf\left(\gamma \sqrt{t}\right)}{\sqrt{t}} \tag{24}$$

$$\left.\frac{dR}{dt}\right|_{t=0} = \sqrt{\frac{\alpha_L}{\pi}} Ja \frac{2\gamma}{\sqrt{\pi}} \tag{25}$$

$$\gamma = \frac{\pi}{\sqrt{6}} \sqrt{\frac{c_{pL}}{\alpha_L T_{sat}}} \frac{1}{Ja^{3/2}} (T_{L\infty} - T_{sat}) \tag{26}$$

In other words, this model combines the inertia and asymptotic stages in a similar manner to Mikic et al. [20] but adopting a different assumption for the variation of vapour temperature with pressure rather than the Clausius–Clapeyron equation. The obtained final expression for bubble growth in uniformly superheated liquid was thus given as:

$$R = \sqrt{\frac{\alpha_L}{\pi}} Ja \left\{ \sqrt{t} erf\left(\gamma \sqrt{t}\right) + \frac{2}{\alpha_L \sqrt{\pi}} \exp\left(-\gamma^2 t\right) \right\} + R_0 \tag{27}$$

They reported that the second term in brackets is small and thus can be ignored and the above equation was reduced to:

$$R = \sqrt{\frac{\alpha_L}{\pi}} Ja \sqrt{t} erf\left(\gamma \sqrt{t}\right) + R_0 \tag{28}$$

They used the above function form and fitted experimental data collected from literature for nucleate boiling (water, ethanol, methanol, benzene and $CCl_4$) using the same characteristic time and length scale defined in Eq. (19) adopted by Lee et al. [29] and obtained the following equation:

$$R = \begin{cases} 6.9577\sqrt{3}\sqrt{Ja\alpha_L}\sqrt{t} erf\left(\frac{3.8323 t^{1/2}}{t_{ch}}\right) + 0.028425 l_{ch}, & Ja > 24 \\ 2.5\sqrt{3}\sqrt{Ja\alpha_L}\sqrt{t} rf\left(\frac{0.1966 t^{1/2}}{t_{ch}}\right) + 0.7 l_{ch} & Ja < 15 \\ \sqrt{\frac{\alpha_L}{\pi}} Ja \sqrt{t} erf\left(\gamma \sqrt{t}\right) + \frac{2\sigma T_{sat}}{\rho_v h_{fg} \Delta T_w} & 24 \le Ja \le 15 \end{cases} \tag{29}$$

### 2.2.2. Boundary layer-based models

Zuber [23] modified the homogenous growth model suggested by Fritz and Ende [16] to capture the non-uniform superheat in heterogeneous boiling. The model was based on heat balance at the interface with the "thin boundary layer" approximation, which has a uniform thickness $\sqrt{\pi \alpha_L t}$. In homogeneous boiling, there is only one heat flux vector in the direction towards the bubble interface (the bubble is surrounded by a superheated shell insulated from the liquid side). On the contrary, in heterogeneous boiling, because the temperature of the liquid bulk is smaller than the temperature around the bubble, part of the heat can be transferred towards the bubble surface with the temperature potential

$(T_{max} - T_{sat})$ and another part can be towards the liquid bulk with temperature potential $(T_{max} - T_{Lb})$. In other words, the liquid temperature inside the boundary layer around the bubble has a peak value $T_{max}$ and it decays towards the bubble interface and towards the liquid bulk. This peak temperature was assumed equal to the boiling surface temperature $T_w$ and thus the part of heat flux towards the liquid bulk $q_{Lb}$ was assumed equal the wall heat flux. Based on this, the energy balance at the bubble interface was modified in heterogeneous boiling as Eq. (30) and resulted in the bubble radius in Eq. (31).

$$\rho_v h_{fg} \frac{dR}{dt} = b\left[k_L \frac{T_w - T_{sat}}{\sqrt{\pi \alpha_L t}} - q_{Lb}\right] \tag{30}$$

$$R = b\frac{2}{\sqrt{\pi}} Ja \sqrt{\alpha_L t}\left[1 - \frac{q_w \sqrt{\pi \alpha_L t}}{2k_L(T_w - T_{sat})}\right] \tag{31}$$

The factor $b$ was used to correct for the effect of bubble curvature on the temperature gradient arising from the assumption of flat interface, $1 \le b \le \sqrt{3}$, with a recommended value $b = \pi/2$ based on comparison with experimental data. Han and Griffith [24] assumed that the bubble grows as a truncated sphere and remains surrounded with the wall thermal boundary layer during its growth period and thus the bubble grows due to evaporation from the superheated liquid in this layer. To simplify the problem, they ignored the bubble curvature and thus solved the 1D transient heat conduction equation for a semi-infinite plate with the assumption that the initial temperature distribution in the boundary layer is linear. The thickness of the superheated liquid layer around the bubble was assumed uniform and equal to the transient conduction thickness estimated at the end of the waiting time, $\delta = \sqrt{\pi \alpha_L t_w}$. To account for the spherical geometry of the bubble, the 1D solution of the semi-infinite plate assumption was corrected using shape factors (for volume and surface area) that depend on the dynamic contact angle $\theta_d$. The total heat transfer rate entering the bubble was assumed consisting of two components: heat transfer due to vapour convection at the bubble base (dry area) and heat transfer due to conduction across the bubble interface, see Eq. (32) for the energy balance.

$$\rho_v h_{fg} \varphi_v 4\pi R^2 \frac{dR}{dt} = \varphi_c \varphi_s 4\pi R^2 k_L \left(\frac{\partial T}{\partial x}\right)_{x=0} + \varphi_b 4\pi R^2 h_v (T_w - T_{sat}) \tag{32}$$

In the above equation, $\varphi_v$ is volume correction factor $[0.25(2 + \cos\theta_d(2 + \sin^2\theta_d))]$, $\varphi_c$ is curvature correction factor $1 \le \varphi_c \le \sqrt{3}$, $\varphi_s$ is surface area correction factor $[0.5(1 + \cos\theta_d)]$, $\varphi_b$ is bubble base correction factor $[0.25\sin^2\theta_d]$ and $h_v$is a vapour convection heat transfer coefficient. They gave a general equation for the curvature correction factor, Eq. (33) that depends on the waiting time and average radius. The solution of Eq. (32) resulted in Eq. (34) for the bubble radius a function of time.

$$\varphi_c = \left[\sqrt{3} + \frac{\theta_d}{\pi}\left(1 - \sqrt{3}\right)\right]\left[\left(1 - \frac{\theta_d}{\pi}\right)\frac{\left(\sqrt{3}\pi/2\right)R_{av} + \sqrt{\pi \alpha_L t_w}}{R_{av} + \sqrt{\pi \alpha_L t_w}} + \frac{\theta_d}{\pi}\right] \tag{33}$$

$$R_{av} = \frac{1}{t}\int_0^t R(t)dt$$

$$R = R_c + \frac{\varphi_s \varphi_c}{\varphi_v}\frac{\rho_l c_{pl} \alpha}{\rho_v h_{fg}} \times \left\{\frac{2\Delta T_w}{\sqrt{\pi t}} t^{\frac{1}{2}} - \frac{\Delta T_w - \Delta T_\infty}{\delta}\frac{\delta^2}{4\alpha_L}\left[\frac{4\alpha_L t}{\delta^2}\mathrm{erf}\frac{\delta}{\sqrt{4\alpha_L t}} + \frac{2}{\sqrt{\pi}}\frac{\sqrt{4\alpha_L t}}{\delta}\right.\right.$$

$$\left.\left. \times \exp\left(-\frac{\delta^2}{4\alpha_L t}\right) - 2\mathrm{erf}\frac{\delta}{\sqrt{4\alpha_L t}}\right]\right\} + \frac{\varphi_b h_v \Delta T_w}{\varphi_v \rho_v h_{fg}} t \tag{34}$$

$$\Delta T_w = T_w - T_{sat},\ \Delta T_\infty = T_{L\infty} - T_{sat},\ \delta = \sqrt{\pi \alpha_L t_w},\ t_w = \frac{9}{4\pi \alpha_L}\left[\frac{(\Delta T_w + \Delta T_{sub})R_c}{T_w - T_{sat}\left[1 + 2\sigma/\left(R_c \rho_v h_{fg}\right)\right]}\right]^2$$

Van Stralen [25] assumed that when the bubble grows, it did not carry the wall thermal boundary layer as was suggested by Han and Griffith [24]. Instead, the superheated liquid at the upper surface of the bubble is displaced and with the radial expansion of the bubble, this superheated liquid accumulates around the bubble up to a certain height $y$ measured from the boiling surface which may be smaller than or equal to the bubble height. He assumed that the boundary layer around the bubble up to this height has a uniform thickness and he called it the "relaxation layer". Thus, the bubble was assumed to grow due to evaporation at a spherical segment with height smaller than the bubble height as if the bubble is partially heated. Contrary to the above models that assumed constant superheat during the entire growth period. Van Stralen [25] assumed that the liquid superheat in the "relaxation layer" decreases exponentially with time from its initial maximum value $(\Delta T_w)$, see Eq. (35). This was inspired from the relaxation phenomenon in physics, i.e. when a system at equilibrium is perturbed it takes a delay time to return back to its initial equilibrium state. Thus, the bubble growth was assumed to follow the relaxation phenomenon by disturbing the wall superheat (thermal boundary layer) periodically after the waiting period. Van Stralen [25] considered bubble departure time $t_d$ as the characteristic time in Eq. (35). Conducting the energy balance for a partially heated bubble including the time dependant superheat resulted in a solution similar to the Plesset and Zwick [15] model for homogeneous boiling (Eq. (36)) but multiplied by a factor $b^* \le 1$ $(b^* = y/2R)$ defined by Eq. (37) which represents the fraction of bubble surface area covered with the superheated liquid layer.

$$\Delta T = \Delta T_w \exp\left(-\sqrt{\frac{t}{t_d}}\right) \tag{35}$$

$$R = b^* \sqrt{\frac{12}{\pi}} Ja \exp\left(-\sqrt{\frac{t}{t_d}}\right)\sqrt{\alpha_L t} \tag{36}$$

$$b^* = \frac{2.7183 R_d \rho_v h_{fg}}{\sqrt{12/\pi}\sqrt{\rho_L c_{pL} k_L}\Delta T_w \sqrt{t_d}} \tag{37}$$

Mikic et al. [20] extended their homogeneous growth model (Eq. (16)) that combines the inertia and asymptotic stages to be applicable for heterogeneous boiling. In the inertial growth velocity, Eq. (13) was assumed valid also in heterogeneous boiling but the factor 2/3 should be replaced with $\pi/7$. It is worth mentioning that the 2/3 factor is the theoretical value in the 2nd term of the r.h.s. of Eq. (1) for symmetric bubble growth in an infinite liquid body. In heterogeneous boiling, bubble growth is asymmetric and thus the inertia term should be smaller than that of homogeneous boiling. That is why they recommended a factor $\pi/7$. For the asymptotic growth stage, they solved the transient 1D heat conduction equation in semi-infinite plate assuming that heat is transferred from the wall into the liquid bulk by conduction during the waiting period. At the end of the waiting period, the bubble forms and thus heat is transferred from the superheated liquid into the bubble (the bubble was assumed a sudden heat sink in the wall thermal boundary layer). On doing so, they obtained the temperature distribution in the liquid near the wall over the entire ebullition cycle (from reformation of the boundary layer up

to departure) as given by Eq. (38) and the temperature gradient required for energy balance at the bubble interface was given by Eq. (39) and corrected for bubble sphericity using the factor $\sqrt{3}$ obtained by Plesset and Zwick [15]. The energy balance (Eq. (40)) resulted in the asymptotic growth velocity (Eq. (41)) which was connected with the inertia growth stage through $T_v$ in a similar manner as they did in the homogeneous model. The final model equation was given as Eq. (42), which is valid for $t^+ \gg 1$.

$$\frac{T-T_{L\infty}}{T_w-TL_\infty} = erfc\ \frac{y}{\sqrt{4\alpha_L t}} - erfc\ \frac{y}{\sqrt{4\alpha_L(t+t_w)}} \tag{38}$$

$$\frac{\partial T}{\partial y} = \sqrt{3}\left\{\frac{T_w-T_v}{\sqrt{\pi\alpha_L t}} - \frac{T_w-T_{L\infty}}{\sqrt{\pi\alpha_L(t+t_w)}}\right\} \tag{39}$$

$$\rho_v h_{fg}\frac{dR}{dt} = \sqrt{3}k_L\left\{\frac{T_w-T_v}{\sqrt{\pi\alpha_L t}} - \frac{T_w-T_{L\infty}}{\sqrt{\pi\alpha_L(t+t_{wt})}}\right\} \tag{40}$$

$$\frac{dR}{dt} = \frac{B}{2\sqrt{t}}\left\{\frac{T_w-T_v}{\Delta T} - \frac{T_w-T_{L\infty}}{T_w-T_{sat}}\left(\frac{t}{t+t_w}\right)^{1/2}\right\} \tag{41}$$

$$R^+ = \sqrt{t^+}\left\{1-\frac{T_w-T_{L\infty}}{T_w-T_{sat}}\left[\left(1+\frac{t_w^+}{t^+}\right)^{1/2} - \left(\frac{t_w^+}{t^+}\right)^{1/2}\right]\right\} \tag{42}$$

$$R^+ = \frac{AR}{B^2},\ t^+ = \frac{A^2 t}{B^2},\ B = \sqrt{\frac{12}{\pi}}\alpha_L Ja,\ A = \sqrt{\frac{\pi}{7}\frac{\rho_v h_{fg}(T_{L\infty}-T_{sat})}{\rho_L T_{sat}}}$$

Forster [33] assumed that the bubble grows as a hemisphere due to evaporation from the superheated liquid around the bubble. In his derivation, the liquid superheat in the wall thermal boundary layer was assumed to decrease exponentially with the vertical distance y according to Eq. (43). Ignoring the bubble curvature, writing the distance y in polar coordinates and assuming that the 1D transient heat conduction in semi-infinite plate is valid, he obtained Eq. (44) for the temperature gradient at the interface. Using this gradient in the energy balance around the bubble surface in polar coordinates resulted in Eq. (45), which describes the asymptotic bubble growth on a heated surface. The integral in this equation was solved using power series, as given by Eq. (46). It is interesting to note that the general solution in Eq. (46) can be reduced to the homogeneous growth models when the ratio $R/\delta_{th}$ is very small, i.e. the bubble is smaller than the wall thermal boundary layer and thus $R \propto t^{1/2}$. When the bubble becomes larger than the wall boundary layer, the exponent of time decreases to 0.25. Eq. (46) was corrected by a factor $b$ in the l.h.s to account for the curvature which was ignored in the semi-infinite body.

$$\Delta T = \Delta T_w \exp\left(-y/\delta_{th}\right) \tag{43}$$

$$\frac{\partial T}{\partial r} = \frac{\Delta T_w \exp\left(-r\cos\varphi/\delta_{th}\right)}{\sqrt{\pi\alpha_L t}} \tag{44}$$

$$\frac{2}{\sqrt{\pi}}Ja\sqrt{\alpha_L t} = \int_0^R \frac{rdr}{\delta_{th}\left(1-e^{-r/\delta_{th}}\right)} \tag{45}$$

$$b\frac{2}{\sqrt{\pi}}Ja\sqrt{\alpha_L t} = R\left\{1+\frac{1}{4}\frac{R}{\delta_{th}} + \frac{1}{36}\left(\frac{R}{\delta_{th}}\right)^2 + \sum_{n=4,6,..}^{\infty}\frac{(-1)^{\frac{n}{2}+1}}{n!(n+1)}\frac{1}{4}\left(\frac{R}{\delta_{th}}\right)^n\right\},$$
$$b = \frac{1}{2}\left[1+\sqrt{1+2\pi/Ja}\right] \tag{46}$$

Lesage et al. [34] presented a model for bubble growth in saturated boiling assuming that bubble growth occurs due to evaporation from the superheated layer, which is valid for low Bond number ($Bo = \Delta\rho g R_c^2/\sigma$). In their model, the bubble shape was a truncated sphere with cylindrical neck pinning to the cavity, i.e. no spreading over the surface. The assumed bubble shape was based on a numerical model suggested by them, which was validated using data for saturated boiling of n-pentane on a surface with single cavity of diameter 90 μm at superheat 2 and 6 K. The temperature profile of the liquid in the wall thermal boundary layer was assumed the same as given by Mikic et al. [20] in Eq. (38). The difference between the two models is that Mikic et al. corrected the effect of curvature on temperature gradient by a factor $\sqrt{3}$ and the bubble boundary layer thickness was uniform $\delta = \sqrt{\pi\alpha t}$, which is the same as the wall thermal boundary layer thickness. On the contrary, Lesage et al. claimed that the boundary layer thickness around the bubble is smaller than the wall boundary layer thickness $\delta$. Thus, they suggested an effective bubble boundary layer thickness $\delta_{eff}$ measured in the direction $\zeta$ normal to the interface. They considered the factor $\sqrt{3}$ used by Mikic et al. [20] to be equivalent to the ratio $\delta/\delta_{eff}$. On doing so, the temperature profile Eq. (38) was modified as given by Eq. (47). This temperature gradient was used in the energy balance at the interface and the final equation for bubble growth was given as Eq. (48). In this equation, $R_c$ is the cavity mouth radius and is valid for $Ja \le 237$ and low $Bo < 0.07$. It is worth mentioning that for this range of $Bo$, the bubble shape is spherical.

$$\frac{T-T_{L\infty}}{T_w-T_{L\infty}} = erfc\ \frac{\zeta}{\sqrt{4\alpha_L t/3}} - erfc\ \frac{\zeta}{\sqrt{4\alpha\left(t+\delta^2/\pi\alpha_L\right)/3}} \tag{47}$$

$$\left[R+\sqrt{R^2+R_c^2}-R_c\right] = \frac{4Ja\sqrt{\alpha_L}}{\sqrt{\pi/3}}\left(\sqrt{t}-\sqrt{t+\frac{\delta^2}{\pi\alpha_L/3}}+\sqrt{\frac{\delta^2}{\pi\alpha_L/3}}\right),$$
$$\delta = \sqrt{\pi\alpha_L t_w} \tag{48}$$

Cho and Wang [35] assumed that the temperature distribution in the wall thermal boundary layer is linear and an applied energy balance at the bubble interface taking into account the bubble shape as a function of contact angle. The bubble shape was assumed to be a static pendant bubble that protrudes outside the thermal boundary layer with a fixed static contact angle during its growth cycle. They also included contribution from microlayer evaporation through an empirical coefficient $c_b$. Based on the energy balance at the interface, they obtained the following equation:

$$R = \begin{cases} \frac{2\delta_{th}}{c}\left[1-\exp\left(-\frac{c_b bc^2\Delta T_w\sqrt{t}}{\delta_{th}}\right)\right] & 0 \le t < t_\delta \\ \sqrt{2}\sqrt{c_b b\delta_{th}\Delta T_w\sqrt{t} - \frac{\delta_{th}^2(\ln 4-1)}{2c^2}} & t \ge t_\delta \end{cases} \tag{49}$$

$c = 2\cos\frac{\theta}{2}$, $t_\delta = \left(\frac{\delta_{th}\ln 2}{c_b bc^2\Delta T_w}\right)^2$ $c_b = 0.534$ – based on data for water in saturated boiling,

$$\delta_{th} = 3.22\frac{k_L}{h_b},\ b = \frac{k_L\left[(\pi-2.4)\cos\theta + 2.4\sec\frac{\theta}{2}\right]}{2\pi\rho_v h_{fg}\sqrt{\alpha_L}}$$

The characteristic time $t_\delta$ is the time for the bubble to protrude outside the thermal boundary layer. Their model indicates that when the bubble is inside the boundary layer the radius is proportional to the square root of time while when it protrudes outside the boundary layer the relation follows $t^{0.25}$, which agrees with Forster [33].

### 2.2.3. Microlayer-based models

In all microlayer-based models, the bubble was assumed to grow as a hemisphere, i.e. the bubble shape did not change during

the whole growth period. The advantage of these models is that it did not depend on the waiting time and the temperature field around the bubble as reported by Cooper [26]. Additionally, the bubble growth rate can be obtained from a balance between heat conduction across the microlayer (with an average initial thickness ($\delta_0/2$)) and the latent heat of evaporation, as given by the following equation:

$$k_L A_{bc} \frac{2\Delta T_w}{\delta_0(t)} = \frac{\mathrm{d}}{dt}\left(m_v h_{fg}\right) \tag{50}$$

For a hemisphere and assuming constant vapour density and latent heat, the above equation can be written as:

$$k_L \pi R^2 \frac{2\Delta T_w}{\delta_0(t)} = \rho_v h_{fg} \frac{1}{2} 4\pi R^2 \frac{\mathrm{dR}}{dt} \tag{51}$$

$$\frac{\mathrm{dR}}{dt} = \frac{k_L \Delta T_w}{\rho_v h_{fg} \delta_0(t)} \tag{52}$$

Thus, the key parameter in all microlayer-based models is the determination of the instantaneous microlayer thickness. Cooper and Lloyd [36] assumed that when the bubble grows rapidly in the initial growth stage, a viscous boundary layer develops underneath the bubble in a manner similar to flow over a flat plate. Thus, they conducted boundary layer analysis by solving the Navier-Stokes equation assuming that bubble growth follows a power law $R = C_1 t^n$. In their model, an analytical solution was only possible for a case when $n = 0.5$.

$$\delta_0(t) = \frac{\pi^2}{\pi^2 + 1} \frac{\sqrt{\pi}}{2} \sqrt{\nu_L t} = C_2 \sqrt{\nu_L t} = 0.8\sqrt{\nu_L t} \tag{53}$$

It is worth mentioning that the theoretical constant $C_2$ depends only on the exponent of time $n$ in the power law and thus the value 0.8 was for $n = 0.5$. Substituting Eq. (53) into Eq. (52) and after integration, the well-known bubble growth model suggested by Cooper [26] will be obtained, which is defined by Eq. (54).

$$R = 2.5 JaPr^{-1/2} \sqrt{\alpha_L t} \tag{54}$$

Cooper [26] gave another equation for a bubble which protruded outside the wall thermal boundary layer ($R \gg \delta_{th}$) and combined the microlayer evaporation with evaporation from that curved part of the hemispherical bubble immersed inside the wall thermal boundary layer. The heat flux from the superheated liquid was modelled in a similar manner as the homogeneous growth model by Plesset and Zwick [15] while Eq. (54) was used for the contribution from the microlayer evaporation. On doing so, he obtained Eq. (55) for the combined contribution of microlayer evaporation and evaporation/condensation at the curved part of the bubble. In saturated boiling, the first term in Eq. (55) becomes zero because $T_{Lb} = T_{sat}$. When the bubble size is smaller than the thermal boundary layer, the bubble remains surrounded with the superheated liquid with superheat equals nearly the wall superheat. In this case, he recommended Eq. (56) that considers evaporation from microlayer and evaporation from the whole curved surface of the bubble.

$$R = \sqrt{\frac{12}{\pi}} \frac{T_{Lb} - T_{sat}}{T_w - T_{sat}} Ja \sqrt{\alpha_L t} + 2.5 JaPr^{-1/2} \sqrt{\alpha_L t} \tag{55}$$

$$R = \left(1 + 0.78\sqrt{Pr}\right) 2.5 JaPr^{-1/2} \sqrt{\alpha_L t} \tag{56}$$

Van Ouwerkerk [37] assumed that bubble growth follows the relation $R \propto t^{1/2}$ as was adopted by Cooper and Lloyd [36]. Firstly, he solved the Navier-Stokes equation and obtained the initial microlayer thickness given by Eq. (57). Secondly, he solved the conjugate heat transfer problem numerically assuming that bubble growth occurs due to microlayer evaporation and evaporation from the hemispherical surface of the bubble. He included the heat capacity of the liquid in the microlayer, which was ignored in Cooper [26] model. The approximate solution ($R = \beta\sqrt{\alpha_L t}$) for the growth constant $\beta$ that fitted their numerical data was given as Eq. (58).

$$\delta_0(t) = 0.9\sqrt{\nu_L t} \tag{57}$$

$$\beta = \sqrt{2\nu_L}\left\{0.9\frac{\rho_L}{\rho_v}\left(1 + \frac{0.405Pr}{F^2}\right)^{-1/2} + \frac{\sqrt{6}}{3\sqrt{\pi}} JaPr^{-1/2}\right\}F = \frac{c_{pL}\Delta T_w}{3\sqrt{\pi} h_{fg}} \tag{58}$$

Labuntsov and Yagov [38], as cited in Zudin [39], divided the bubble base area into microlayer (thin layer) and macrolayer (thick layer) and assumed that the bubble grows as a truncated sphere due to evaporation from these two regions. The thermal capacity of the liquid in the microlayer was ignored similar to Cooper [26] and thus heat is transferred from the boiling surface to the base area by conduction. Because the geometry of the micro and macro-layers cannot be determined accurately from the experiments, they lumped all unknowns into empirical constants. For example, the microlayer thickness was assumed to vary linearly with the radial distance from the nucleation site, $\delta_0 = \beta_1 \mathrm{r}$ with $\beta_1$ an empirical constant. The heat transfer rate by conduction across the microlayer was given as:

$$Q_{ml} = \int_0^{R_{mL}} k_L \frac{\Delta T_w}{\delta} 2\pi r dr = \int_0^{R_{mL}} k_L \frac{\Delta T_w}{\beta_1 r} 2\pi r dr = \frac{2\pi}{\beta_1} k_L \Delta T_w R_{mL} = \frac{2\pi}{\beta_1} k_L \Delta T_w \beta_2 R = \beta_3 k_L \Delta T_w R \tag{59}$$

$$\beta_3 = \frac{2\pi\beta_2}{\beta_1}$$

In the above equation, the microlayer radius $R_{mL}$ was related to the bubble radius $R$ through another empirical constant $\beta_2$ ($R_{mL} = \beta_2 R$). For the macro-layer (thick curved part near the wall), the heat flux was calculated from the homogeneous model given by Plesset and Zwick as follows:

$$q_{sL} = \beta_4 k_L \sqrt{\frac{12}{\pi}} \frac{\Delta T_w}{\sqrt{\alpha_L t}} \tag{60}$$

The empirical factor $\beta_4$ in the above equation was used to account for the fraction of bubble surface area surrounded by the superheated liquid in the macro-layer and the fact that the liquid superheat should be a fraction of the wall superheat. Thus, the heat transfer rate conducted to the bubble through the macrolayer was given as Eq. (61). Applying the total energy balance at the bubble base results in Eq. (62).

$$Q_{sL} = \beta_4 k_L \frac{\Delta T_w}{\sqrt{\alpha_L t}} R^2 \tag{61}$$

$$\rho_v h_{fg} \frac{dV}{dt} = Q_{mL} + Q_{sL} = \beta_3 k_L \Delta T_w R + \beta_4 k_L \frac{\Delta T_w}{\sqrt{\alpha_L t}} R^2 \tag{62}$$

$$R\frac{dR}{dt} = \beta_4 Ja \alpha_L + \beta_5 RJa \sqrt{\frac{\alpha_L}{t}} \tag{63}$$

Substituting from $R = \beta\sqrt{\alpha_L t}$ into Eq. (63) and lumping all empirical constants into two constants $\chi$ and E resulted in the following quadratic equation for the bubble growth factor $\beta$:

$$\frac{1}{2}\beta^2 - \chi \mathrm{Ja}\beta - \mathrm{E}Ja = 0 \tag{64}$$

Solving for $\beta$ results in:

$$\beta = \chi \mathrm{Ja} + \sqrt{(\chi \mathrm{Ja})^2 + 2\mathrm{E}Ja} \tag{65}$$

The empirical coefficient $\chi$ and E that fitted a wide range of experimental data ($0.1 < Ja < 500$) was found to be 0.3 and 6, respectively.

Van Stralen et al. [27] suggested a model that combines contribution from the relaxation layer, microlayer and liquid inertia. The bubble growth due to relaxation layer was given previously as Eq. (36). For the contribution from the microlayer, they obtained the initial microlayer thickness assuming the flow underneath the bubble is similar to laminar boundary layer in parallel flow over a uniformly superheated flat plate. This allowed them to use the *Pohlhausen* exact solution for heat transfer in the boundary layer over a flat plate defined by Eq. (66), for the local Nusselt number. Additionally, to calculate Reynolds number, they assumed that the radius of the hemisphere $R$ follows the relation $R \sim t^n$ and thus the thermal boundary layer thickness was obtained from Eq. (66) as given by Eq. (67). For the asymptotic growth case when $n = 0.5$, the microlayer thickness was given as Eq. (68) which when substituted in Eq. (52) results in the bubble growth radius $R$ due to microlayer evaporation defined by Eq. (69).

$$Nu(r) = \frac{hr}{k_L} = \frac{q_w(r)r}{k_L\Delta T} = \frac{k_L\Delta Tr}{k_L\Delta T\delta_{th}(r)} = \frac{r}{\delta_{th}(r)} = 0.332Re^{0.5}(r)Pr^{\frac{1}{3}} = 0.332\left(\frac{\rho\dot{R}R}{\mu}\right)^{1/2}Pr^{1/3} \quad (66)$$

$$\delta_{th} = \frac{k_L\Delta T_w}{q_w} = 3.012\left(\frac{r}{R^*}\right)^{1/2n}\left(\frac{\nu_L R}{\dot{R}}\right)^{1/2}Pr^{-1/3} = 3.012\left(\frac{r}{R}\right)^{1/2n}\left(\frac{\nu_L t}{n}\right)^{1/2}Pr^{-1/3} \quad (67)$$

$$\delta_{th} = 4.26Pr^{-1/3}\sqrt{\nu_L t}, \quad (68)$$

$$R = 0.47Pr^{-1/6}Ja\sqrt{\alpha_L t} \quad (69)$$

It is worth mentioning that the difference between the microlayer thickness obtained by Van Stralen et al. [27] compared to Cooper and Llyod [36] and Van Ouwerker [37] is arising from the fact that [27] obtained the thickness based on heat transfer analysis while [36,37] obtained the thickness based on hydrodynamics analysis. Van Stralen et al. [27] combined the contribution from liquid inertia $R_1$ defined below, microlayer evaporation and evaporation from the relaxation layer into one model in the form given by Eq. (70). The contribution of microlayer and relaxation layer were added together and given as $R_2$ defined below. The factor $b^*$ was defined previously in Eq. (37).

$$R = \frac{1}{1/R1 + 1/R2} = \frac{R_1R_2}{R_1 + R_2} \quad (70)$$

$$R_1 = 0.8165\sqrt{\frac{\rho_v h_{fg}\Delta T_w \exp\left(-\sqrt{t/t_d}\right)}{\rho_L T_{sat}}t}$$

$$R_2 = 1.9544\left\{b^*\exp\left(-\sqrt{t/t_d}\right) + \frac{\Delta T_{Ls}}{\Delta T_w}\right\}Ja\sqrt{\alpha_L t} + 0.373Pr^{-1/6}\exp\left(-\sqrt{t/t_d}\right)Ja\sqrt{\alpha_L t}$$

Mei at al. [40] solved numerically the conjugate heat transfer problem assuming that the bubble grows due to microlayer evaporation only. The bubble was assumed to be a truncated sphere with a microlayer of wedge shape with a wedge angle $\varphi << 1$ rad. To capture the bubble shape, a shape factor $c = r_{cont}/R$, which was related to the wedge angle through the initial microlayer thickness given by Cooper and Lloyd [36] in Eq. (53) except that the theoretical constant 0.8 was left to be determined empirically. The change in bubble volume was captured by a shape function $f(c)$ as defined in Eq. (71); $c = 0$ for a sphere and $c = 1$ for a hemisphere. Applying the energy balance and considering the bubble shape function, the bubble growth equation was given by Eq. (72). The shape factor $c$ (depends on $Ja$) and the front constant in the initial microlayer thickness of Cooper and Lloyd [36] were determined empirically as given by Eqs. (73) and (74). This model was validated using data from literature for $Ja = 0.52$ – 1974 and fluids including water and hydrocarbons.

$$V_b = \frac{4}{3}\pi R^2 f(c),\ f(c) = 1 - 0.75\left[1 - \sqrt{1-c^2}\right]^2 + 0.25\left[1 - \sqrt{1-c^2}\right]^3 \quad (71)$$

$$R = \frac{c^2}{c_1 f(c)}JaPr^{-1/2}\sqrt{\alpha_L t} \quad (72)$$

$$c = \left\{\left(0.4134Ja^{0.1655}\right)^{-6} + (1 - \exp(-0.0005Ja)^{-6}\right\}^{-1/6} \quad (73)$$

$$c_1 = 0.00525Ja^{0.752}Pr^{-0.5}\left(\frac{k_L}{k_w}\right)^{-0.113}\left(\frac{\alpha_L}{\alpha_w}\right)^{-0.117} \quad (74)$$

Prisnyakov [18] claimed that neglecting the expansion work in the energy balance equation results in overestimation to the bubble growth. Thus, he applied the first law of thermodynamics including the expansion work for a truncated bubble growing at a heated surface and assumed that the vapour obeys the ideal gas laws. The heat transfer rate to the bubble was assumed to be from the liquid side through the curved surface and from the base side through the microlayer. The heat flux at the bubble interface from the liquid side was obtained from the semi-infinite plate assumption (similar to Fritz and Ende [16]) while the heat flux at the bubble base was assumed equal the wall heat flux. The interfacial area and volume of the truncated bubble were corrected by a shape factor (depends on the shape angle). With this energy balance, they gave Eq. (75) for bubble growth, which is valid for Jakob number up to 500 with its simplified version Eq. (76) when $\rho_v/\rho_L \ll 1$ or $(f_\rho = 1)$ and $2\sigma/R \ll P_{sat}$.

$$\left(1 + \frac{\gamma}{\gamma - 1}f_\rho N_1\right)(R - R_0) + \frac{2}{3}\frac{3f_\rho\gamma - 1}{\gamma - 1}N_2R_0\ln\frac{R}{R_0} = f_\theta Ja\left[\frac{2}{\sqrt{\pi}}\sqrt{\alpha_L t} + f_q N_3 t\right] \quad (75)$$

$$R = R_0 + \frac{2}{3}f_\theta Ja\left[\frac{2}{\sqrt{\pi}}\sqrt{\alpha_L t} + f_q N_3 t\right] \quad (76)$$

$$N_1 = \frac{P_{sat}}{\rho_v h_{fg}},\ N_2 = \frac{\sigma}{\rho_v h_{fgR_0}},\ N_3 = \frac{q_w}{\rho_L c_{pL}\Delta T}\gamma = \left[1 - \frac{2P_{sat}}{\rho_v h_{fg}}\right]^{-1},$$

$$f_\theta = \frac{0.5(1 + \cos\theta)}{0.5\left(1 + 0.5\cos\theta\left(1 + \sin^2\theta\right)\right)},\ f_q = \frac{1}{2}(1 - \cos\theta),\ f_\rho = 1 - \rho_v/\rho_L$$

Buyvich and Webbon [41] assumed that the bubble is a spherical segment separated from the wall by a microlayer, which was assumed to be flat (the wedge shape was ignored). They claimed that formulating the bubble growth problem through applying the momentum conservation is not appropriate due to the uncertain local stresses acting on the bubble and its surrounding liquid. Accordingly, they suggested formulating the dynamic equation using thermodynamics principles assuming that the total mechanical energy (kinetic and potential energy) is constant during the whole

course of bubble growth. The kinetic energy included the displacement of the bubble centre of mass in the vertical direction and the bubble expansion that results in motion in the radial direction. The potential energy included the potential energy in the gravity field, the surface tension energy and the vapour compression energy. The surface tension force between the liquid and vapour was included and it was found that it affects the bubble shape and its direction is similar to the buoyancy force. This was not included in the momentum balance adopted by other researchers. After formulating the dynamic equation, they solved the boundary layer problem to obtain the initial microlayer thickness as, $\delta_0 = 1.294\sqrt{\nu_L t}$. In formulating the asymptotic bubble growth, the heat flux to the bubble was divided into two components; one from the microlayer $q_{mL} = k_L \Delta T/\delta_0$ and one from the liquid side, $q_{sL} = k_L \Delta T/\delta_{sL}$. The conduction layer thickness in the liquid side $\delta_{sL}$ was obtained from the homogeneous bubble growth models as $\delta_{sL} = (2/C)\sqrt{\alpha_L t}$ where the growth law is $R = CJa\sqrt{\alpha_L t}$. The constant $C$ equals (1 – 2) but they left it to be an empirical parameter. They envisioned the bubble growth problem as follows: at early stage of growth the bubble shape is hemisphere due to the strong effect of liquid inertia that flatten the bubble while at a late stage of growth near departure the shape becomes spherical due to dominance of buoyancy and surface tension forces. The time after which the bubble shape changes from hemispherical to spherical was given as:

$$t^{3/2} + \frac{6\sigma t^{1/2}}{(1-\kappa)[CJa(1+N_m)]^2 \rho_l g \alpha_l} = \frac{3}{4}\frac{(1+\kappa/5)CJa(1+N_m)\alpha_l^{0.5}}{(1-\kappa)g},$$
$$\kappa = \rho_v/\rho_l, N_m = 1/CHPr^{1/2}, \; H = 1.294 \tag{77}$$

For time less than or equal the time predicted from the above equation, the bubble grows as a hemisphere with radius predicted using Eq. (78) but for time larger than the above time the bubble is a sphere and the radius was given as Eq. (79). The dimensionless parameter $N_m$ was introduced to estimate the contribution from the microlayer; when its value is less than 1, most of the heat enters the bubble from the superheated liquid.

$$R = CJa(1+N_m)\sqrt{\alpha_L t} \tag{78}$$

$$R = CJa\sqrt{\alpha_L t}, \text{ when } N_m \leq 1 \tag{79}$$

## 3. Experimental setup

### 3.1. Boiling chamber and test section

Fig. 4a depicts the schematic drawing of the experimental facility. It consists of the following: (i) rectangular boiling chamber (250 × 250 × 300 mm) made of stainless steel with four transparent visualization windows (158 × 220 mm), (ii) two helical coil heat exchangers (one on the top side of the chamber to work as a condenser and one immersed in the liquid to work as a liquid subcooler), (iii) circulation chiller to supply the cooling water-glycol mixture to the condenser and the sub-cooler, (iv) test section insulation block made of Polyether Ether Ketone (PEEK) that accommodate the copper test piece, see Figs. 4b and 4c, (v) immersion cartridge heater of power 1500 W to control the liquid bulk temperature and conduct liquid degassing before the test, (vi) data logger cDAQ from National Instruments, connected to a PC with Labview software to record the data, (vii) 1.5 kW DC power supply (Electro-Automatik) for supplying the heat to the test section, (viii) High-speed video camera (Phantom Miro Lab110) with NAVITAR 12X zoom lens system, (ix) two T-type thermocouples for measuring the liquid and vapour temperature and one pressure transducer (Omega, PX319, 0 – 3.5 bar) for measuring the system pressure.

The test section was made of oxygen-free copper and was insulated with a PEEK housing as seen in the exploded view in Fig. 4b and the assembly drawing in Fig. 4c. The copper test piece has a diameter of 30 mm and a height of 42.5 mm. It has five holes of diameter 0.6 mm at 6 mm equal distance along the vertical centreline to insert five thermocouples ($T_1$-$T_5$ with $T_5$ below the surface), and an O-ring shoulder of size 2.5 mm width and 2 mm depth leaving 25 mm diameter as a boiling surface, see Figs. 5b and 5c. The test piece was connected to a copper heater block using M10 thread connector (made of copper) and the thermal contact resistance was reduced by a thermal paste, see Fig. 5a for the assembly of the test section and the heater block. The heater block has four vertical holes (see Fig. 5c) with diameter 12 mm to accommodate four cartridge heaters (400 W each), which are connected to the DC power supply. The test section was manufactured using High Precision Micro Milling Machine (HERMLE C20U) and the boiling surface was finished by diamond turning machine to obtain a smooth surface. The surface was analysed using Surface Metrology System (NP FLEX-3D) and the $S_a$ value of the tested surface was 49.6 nm. The surface wettability was characterized by measuring the static contact angle for a water droplet at room temperature using contact angle measurement instrument First Ten Angstroms (FTA1000 series). The measured contact angle on the plain copper surface was 85.5.

The temperature reading of the five vertical thermocouples was plotted versus the vertical distance and the gradient was used to calculate the applied flux $q$ using Eq. (80). The measured temperature versus distance exhibited linear fitting with a correlation coefficient $R^2$ 0.99 except the lowest heat flux with $R^2$ 0.95, which verifies the 1D assumption in calculating $q$. The temperature difference between the wall and the saturation temperature (wall superheat) was calculated using Eq. (81). The saturation temperature was based on the pressure measured using the pressure transducer, which matched the measured liquid and vapour temperatures. Because the last thermocouple ($T_5$) was located at distance $\Delta y$ = 3.5 mm below the surface, the wall temperature was corrected using Eq. (82) to account for this temperature drop. All thermocouples were calibrated and the maximum systematic error in the temperature measurements was ± 0.5 K while the random error was ± 0.003 K, resulting in combined uncertainty of ± 0.5 K (0.7% of the reading). The systematic and random errors were corrected using the calibration equation. The propagated uncertainty analysis was calculated according to the method given in Coleman and Steel [42] and the highest uncertainty in the heat flux was 7%.

$$q_w = -k_{cu}\frac{dT}{dy} \tag{80}$$

$$\Delta T_w = T_w - T_{sat} \tag{81}$$

$$T_w = T_5 - \frac{q_w \Delta y}{k_{cu}} \tag{82}$$

The experiments were conducted using de-ionized water as a test fluid at atmospheric and sub-atmospheric pressures. The thermophysical properties of the fluid required for the calculations were obtained from the Engineering Equation Solver software (EES). All experiments were conducted after degassing the liquid and the boiling surface simultaneously. Liquid degassing was conducted by boiling the liquid vigorously using the 1.5 kW immersion heater and surface degassing was conducted by heating the test section until most of the nucleation sites become active (at about 30% of the critical heat flux value). The degassing process was deemed to be complete when the measured system pressure becomes equal to the saturation pressure at the measured liquid temperature (the measured liquid and vapour temperature are equal). After degassing, the heat supplied to the test section was switched off until the surface cools down to a temperature below the saturation temperature (all nucleation sites become deactivated). Then,

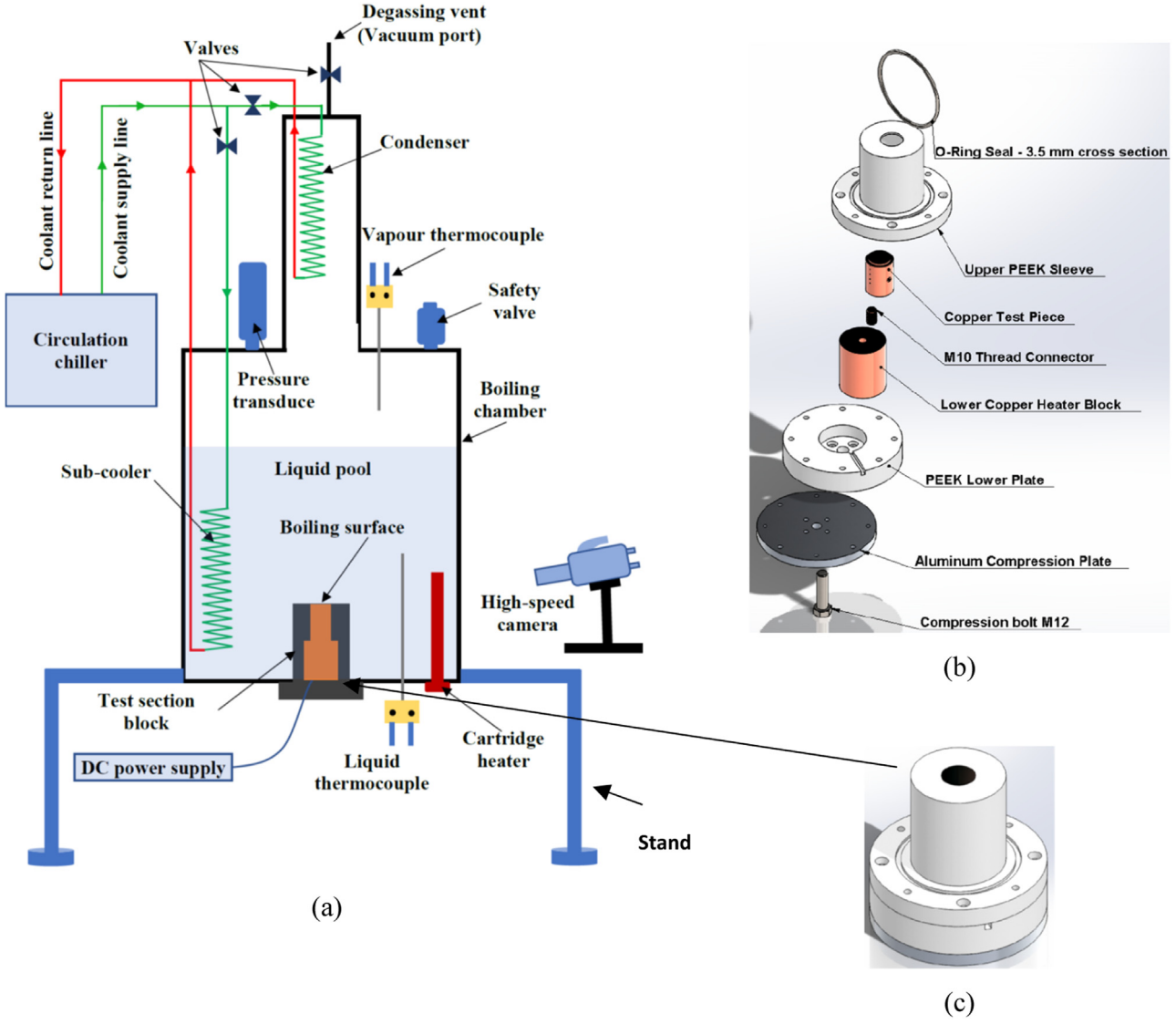


**Fig. 4.** (a) Schematic drawing of the experimental facility, (b) Exploded view of the test section, and (c) The test section assembly, [9].

the heat flux was increased gradually in small steps until boiling starts. The details of the bubble size measurements are described in ref. [9].

### 3.2. Experimental validation

Many researchers validated their experimental system by conducting boiling experiments and comparing the experimental boiling curve with the well-known Rohsenow [2] pool boiling correlation. This approach may not be accurate because boiling depends strongly on the surface microstructure. In the present study, experimental system validation was conducted using natural convection single-phase experiments rather than boiling experiments. Fig. 6 depicts the heat flux plotted versus the temperature difference between the surface ($T_w$) and the liquid ($T_L$). The results were compared with the natural convection correlation reported in Bergman et al. [43], see Eq. (83). It is obvious that there is a good agreement between the measurements and the prediction with average deviation of 8.8%, which verifies the accuracy of the experimental measurement system.

$$Nu = \begin{cases} 0.54Ra^{1/4} \;\; 10^4 \le Ra \langle 10^7, \;\; Pr \rangle 0.7 \\ 0.15Ra^{1/3} \;\; 10^7 \le Ra < 10^{11}, \;\; all \; Pr \end{cases} \tag{83}$$

## 4. Models assessment

This section presents and discusses the assessment of the homogeneous and heterogeneous bubble growth models presented in Section 2. The models are assessed using experimental data for three pressures (0.15 – 1 bar) and different values of wall superheat. In the current study, the models are assessed based on the trend comparison and the mean absolute error percentage (MAE%) defined by Eq. (84). It is worth mentioning that the comparison based on the MAE% may result in a misleading conclusion especially when the growth model is used to predict the departure radius. For example, a model may predict a trend that crosses the experimental data with reasonable MAE% but the error at departure may be very large. Because the latent heat transfer rate depends on the cube of departure radius ($Q_{LH} = (4/3)\pi R^3 \rho_v f_{bd} h_{fg}$), any small error in the departure radius will result in large error in the predicted heat transfer rate. For instance, a 30% error in the departure radius will result in about 120% error in the latent heat transfer rate. Accordingly, the MAE%-based comparison will be used as a rough guide to infer the performance of the assessed models.

$$MAE \; \% = \frac{1}{N} \sum_{1}^{N} \frac{\left| R_{exp} - R_{ped} \right|}{R_{exp}} \times 100 \tag{84}$$

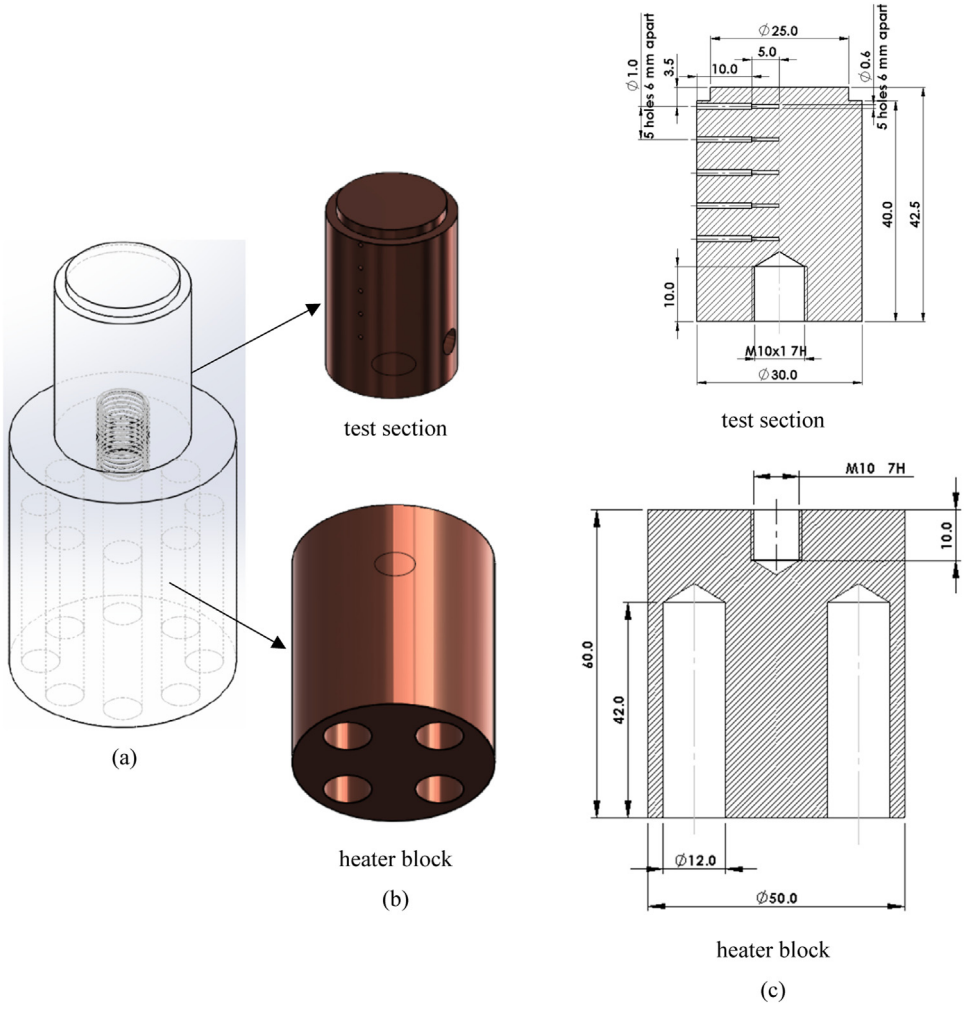


**Fig. 5.** (a) CAD drawing of the copper test section and the heater block connected with M10 copper threaded connector, (b) CAD drawing for test section (top) and copper heater block (bottom), and (c) 2D drawing of the test section (top) and heater block, [9]. (Dimensions are in mm).

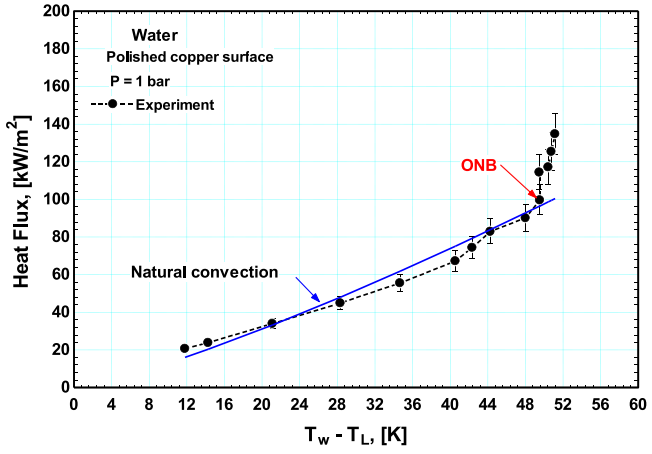


**Fig. 6.** Experimental validation using single-phase natural convection, [9].

### 4.1. Assessment of homogeneous models

It is important to assess bubble growth models in homogeneous boiling because some researchers used these models in the prediction of bubble departure diameter and heat transfer rates in nucleate boiling. Eleven models were included in the comparison and the equations are summarized in Table A1 in the Appendix A. Figs. 7, 8 and 9 show the experimental data compared with the models at $P$ = 1, 0.5 and 0.15 bar, respectively. All experimental data indicates that the bubble grows at a faster rate at the beginning for a short time period then it grows at a much slower rate. Mahmoud and Karayiannis [9] discussed these results in more detail and concluded that all experimental data are in the asymptotic growth stage, i.e. heat transfer-controlled growth. In other words, the initial rapid growth is not due to the inertia-controlled growth stage which is also obvious from the comparison with the Rayleigh [12] model included in figures. The MAE (averaged over the whole growth period) for each model is summarized in Table 1 for the three tested pressures and superheats while Table 2 summarises the error at departure. The following points can be concluded:

1. ***Pressure 1 bar:*** Fig. 7(a-d) shows the comparison at atmospheric pressure and superheat 5.6, 9.4, 10 and 15 K. It shows that the models by Fritz and Ende [16] (curve 1), Prisnyakov [18] (curve 10) and Abdollahi et al. [32] (curve 11) always underpredict the experimental data with MAE in the range 18.5 – 31.6%, 44.8 – 52.6% and 58 – 63.4%, respectively. These models predicted the data at departure (end point in each curve) with error 0.1 – 18.7%, 33.4 – 45.8% and 49.8 – 58.7% in the same order. The small error at departure predicted by the Fritz and

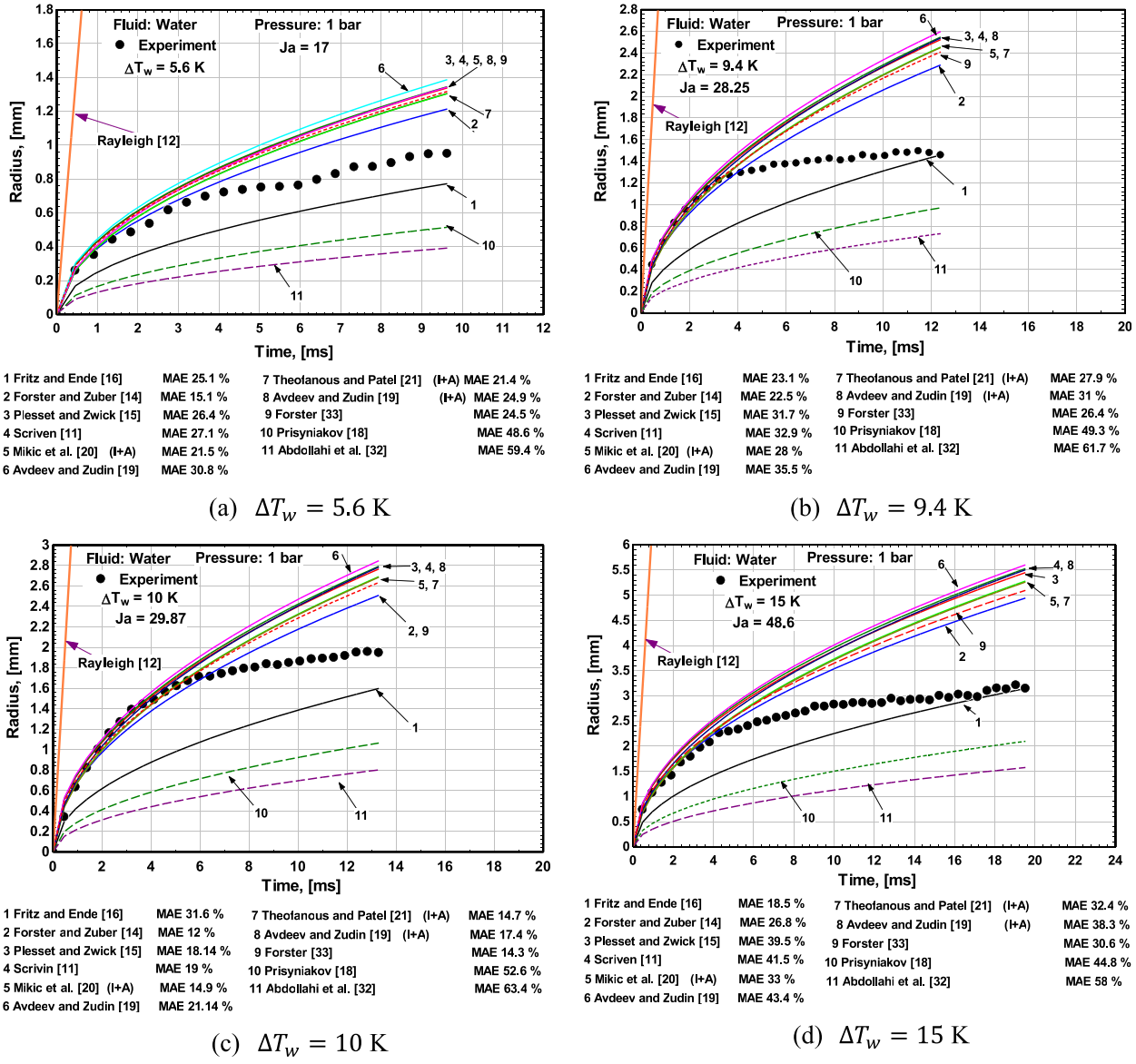


**Fig. 7.** Evaluation of homogeneous bubble growth models at $P = 1$ bar.

**Table 1**
Summary of the mean absolute error percentage (MAE%) of homogeneous bubble growth models.

| Model | $P = 1$ bar | | | | $P = 0.5$ bar | | | $P = 0.15$ bar | | | MAE % @@Average |
|---|---|---|---|---|---|---|---|---|---|---|---|
| | MAE % | | | | MAE % | | | MAE % | | | |
| | 5.6K | 9.4K | 10K | 15K | 12.7K | 17.1K | 19.5K | 15.1K | 16.3K | 18.4K | |
| Fritz and Ende [16] | 25.1 | 23.1 | 31.6 | 18.5 | 86.2 | 95.4 | 63.4 | 283.6 | 243.5 | 210 | 108.04 |
| Forster and Zuber [14] | 15.1 | 22.5 | 12 | 26.8 | 192.6 | 205.8 | 156.7 | 502.5 | 439.6 | 386.9 | 196.1 |
| Plesset and Zwick [15] | 26.4 | 31.7 | 18.14 | 39.5 | 222.6 | 237 | 183.1 | 564.4 | 495 | 436.9 | 225.5 |
| Scriven [11] | 27.1 | 32.9 | 19 | 41.5 | 226.5 | 242.5 | 188.4 | 573.9 | 504.2 | 446.4 | 230.2 |
| Mikic et al. [20] | 21.5 | 28 | 14.9 | 33 | 184.3 | 203.9 | 156.8 | 304.3 | 282.3 | 249.7 | 148 |
| Avdeev and Zudin [19] | 30.8 | 35.5 | 21.14 | 43.4 | 229.7 | 245.6 | 191 | 576.9 | 507 | 448.9 | 233 |
| Theofanous and Patel [21] | 21.4 | 27.9 | 14.7 | 32.4 | 180.5 | 199.4 | 152.7 | 277.9 | 257.8 | 225.1 | 139 |
| Avdeev and Zudin [19] $(I + A)$ | 24.9 | 31 | 17.4 | 38.3 | 196.4 | 219.2 | 170.8 | 335.4 | 312.5 | 280.1 | 162.6 |
| Forster [33] | 24.5 | 26.4 | 14.3 | 30.6 | 199 | 211 | 160.7 | 505.9 | 442.5 | 389.3 | 200.4 |
| Prisnyakov [18] | 48.6 | 49.3 | 52.6 | 44.8 | 25.4 | 30.9 | 14.3 | 155.7 | 129 | 106.7 | **65.7** |
| Abdollahi et al. [32] | 59.4 | 61.7 | 63.4 | 58 | 16 | 13.5 | 18.6 | 92.2 | 72.1 | 55.2 | **51** |

**Table 2**
Summary of the error percentage of homogeneous bubble growth models at departure.

| Model | $P = 1$ bar | | | | $P = 0.5$ bar | | | $P = 0.15$ bar | | | MAE % @@Average |
|---|---|---|---|---|---|---|---|---|---|---|---|
| | MAE % | | | | MAE % | | | MAE % | | | |
| | 5.6K | 9.4K | 10K | 15K | 12.7K | 17.1K | 19.5K | 15.1K | 16.3K | 18.4K | |
| Fritz and Ende [16] | 18.7 | 0.1 | 18 | 0.12 | 132.5 | 163.4 | 108 | 407.8 | 319.7 | 291.2 | **145.9** |
| Forster and Zuber [14] | 27.7 | 56.9 | 28.8 | 56.9 | 265.3 | 313.8 | 226.8 | 697.8 | 599.2 | 514.6 | 278.8 |
| Plesset and Zwick [15] | 40.8 | 73 | 42 | 73 | 302.8 | 356.1 | 260.4 | 779.6 | 626.9 | 577.7 | 313.2 |
| Scriven [11] | 41.5 | 74.6 | 43.4 | 75.5 | 307.6 | 363.9 | 267 | 792.3 | 638.2 | 589.6 | 319.4 |
| Mikic et al. [20] $(I + A)$ | 37.4 | 68.3 | 38.1 | 67.7 | 274.1 | 329.5 | 240.3 | 537.7 | 451.1 | 419.6 | 246.4 |
| Avdeev and Zudin [19] | 45.9 | 78.1 | 46.1 | 77.9 | 311.6 | 368 | 270.6 | 796.3 | 641.6 | 592.8 | 322.9 |
| Theofanous and Patel [21] $(I + A)$ | 37.2 | 67.9 | 37.8 | 67 | 271 | 325.8 | 237 | 506.1 | 425.2 | 392.7 | 236.8 |
| Avdeev and Zudin [19] $(I + A)$ | 41.3 | 74 | 43 | 74.8 | 289.3 | 350 | 257.6 | 580.4 | 488.6 | 458.1 | 265.7 |
| Forster [33] | 38.5 | 65.2 | 35.3 | 61.8 | 273.3 | 320.8 | 231.8 | 702.3 | 562.8 | 517.5 | 280.9 |
| Prisnyakov [18] | 45.8 | 33.4 | 45.3 | 33.4 | 55 | 75.6 | 38.7 | 238.5 | 179.8 | 160.9 | **90.6** |
| Abdollahi et al. [32] | 58.7 | 49.8 | 58.8 | 50 | 16.5 | 13.5 | 4.1 | 154.2 | 110.1 | 95.8 | **61.2** |

Ende model is because the values predicted by the model approach the experimental data as time increases while the trend of the other two models is nearly parallel to the experimental trend. As mentioned in Section 2, the Fritz and Ende [16] model can be considered as a benchmark because it ignored the effect of bubble curvature and radial motion on the temperature gradient around the bubble. Prisnyakov [18] also ignored the effect of bubble curvature but included the expansion work in the first law of thermodynamics. This model predicted values which are lower than that predicted by the Fritz and Ende [16] model but with a trend nearly similar to the experimental trend, which means that including the bubble expansion work in the energy balance results in a lower growth rate. The model by Abdollahi et al. [32] assumed a certain function for the instantaneous vapour temperature in the bubble boundary layer rather than the Clausius–Clapeyron equation used in other models. In other words, they assumed that the superheat varies with time rather than a fixed superheat as adopted in the other models. Additionally, they ignored the effect of bubble curvature, which is similar to the Fritz and Ende [16] and the Prisnyakov [18] models. The model predicted values which are lower than the values predicted by [16] and [18]. It is worth mentioning that the curvature and radial motion have the effect of increasing the temperature gradient and thus evaporation heat flux. Accordingly, as expected, these three models predicted values which are significantly lower than the values predicted by the other models (curves 2 – 9) in Fig.7 which considered the effect of curvature and radial motion. These models (curves 2 – 9) exhibited excellent predictions up to about 4 – 6 ms then they overpredicted the data with the deviation increasing with time. The small differences amongst these models is due to the fact that they were based on nearly similar analysis (solution of momentum and energy equations). Additionally, it is obvious that there is no significant difference between the complex models that combined the inertial growth stage with the asymptotic growth (curves 5, 7, 8) and the simple asymptotic models (curves 2, 3, 4, 6, 9). Based on Fig. 7, the best performing model in terms of MAE is the Forster and Zuber model [14] which predicted the data of the four superheats with MAE in the range 12 – 26.8% and error at departure in the range 27.7 – 56.9%. Additionally, it is obvious from Table 1, at $P = 1$ bar, that some models exhibited low MAE% only for some superheat. Additionally, Table 2 indicates that although some models predicted the data with low MAE values, they gave large deviation at departure. In other words, if these models were used to predict the departure radius provided that the departure time is known, and were used in the heat transfer models, significant discrepancies will result.

2. ***Pressure 0.5 bar:*** Fig. 8(a-c) show the comparison at 0.5 bar and superheat 15.1, 17.2 and 19.5 K. The following observations can be drawn from these figures: (i) the slope of the curve that represents Rayleigh [12] solution for the inertia-controlled growth decreased slightly and agreed with all models only in the first 0.5 ms after which a clear deviation was observed. None of the experimental data points agreed with the inertia-controlled growth as was the case at atmospheric pressure. (ii) the models by Prisnyakov [18] and Abdollahi et al. [32], which underpredicted all the data at atmospheric pressure with high MAE, exhibited better performance at 0.5 bar. These models predicted the data with MAE in the range 14.3 – 30.9% and 13.5 – 18.6% with error at departure 38.7 – 75.6% and 4.1 – 16.5%, respectively. Thus, in terms of the MAE and the error at departure, the model by Abdollahi et al. [32] is the best performing model at 0.5 bar. Although the Fritz and Ende [16] model exhibited reasonable performance at atmospheric pressure (MAE 18.5 – 31.6% and error at departure 0.1 – 18.7%), it significantly overpredicted the data with MAE 63.4 – 95.4% and error at departure 108 – 163.4%. (iii) the models described by curves 2 – 9, which predicted part of the growth curve at 1 bar very well (up to 4 – 6 ms), significantly overpredicted the data at 0.5 bar in the whole growth period. The MAE of these models ranged from 152.7 to 245.6% and error at departure 226.8 – 368%. The poor performance of these models at 0.5 bar compared to data at 1 bar may be attributed to the change in bubble shape. At atmospheric pressure, the bubble shape is nearly spherical during most of the growth period which agrees with the assumptions adopted in these models, e.g. symmetric growth of spherical bubbles. At sub-atmospheric pressure, the bubble shape changes from hemisphere in the early stages to a flattened spheroidal shape in most of the growth period. Additionally, the smaller bubble size and the nearly spherical shape at atmospheric pressure may help keep most of the wall thermal boundary layer around the bubble, which makes the bubble share part of the uniform superheat assumption in homogeneous models. At sub-atmospheric pressure, the flattened shape and large bubble size makes evaporation restricted to small part of the bubble surface area near the wall. Another reason could be due to the error arising from the Clausius–Clapeyron assumption in the models (2 – 9), which seems to be valid at high pressures.
3. ***Pressure 0.15 bar:*** Figs. 9(a-c) show the comparison at 0.15 bar and superheat 15.1, 16.3 and 18.4 K. The following differences can be observed compared to the comparison at 1 and 0.5 bar: (i) the slope of the inertia-controlled growth curve by Rayleigh decreased significantly and the curve crossed the data predicted by some of the other asymptotic growth models up to about

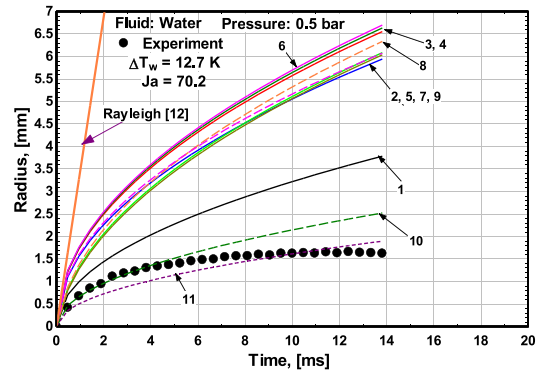


| | | | |
|---|---|---|---|
| 1 Fritz and Ende [16] | MAE 86.2 % | 7 Theofanous and Patel [21] (I+A) | MAE 180.5 % |
| 2 Forster and Zuber [14] | MAE 192.6 % | 8 Avdeev and Zudin [19] (I+A) | MAE 196.4 % |
| 3 Plesset and Zwick [15] | MAE 222.6 % | 9 Forster [33] | MAE 199 % |
| 4 Scriven [11] | MAE 226.5 % | 10 Prisyniakov [18] | MAE 25.4 % |
| 5 Mikic et al. [20] (I+A) | MAE 184.3 % | 11 Abdollahi et al. [32] | MAE 16 % |
| 6 Avdeev and Zudin [19] | MAE 229.7 % | | |

(a) $\Delta T_w = 12.7$ K

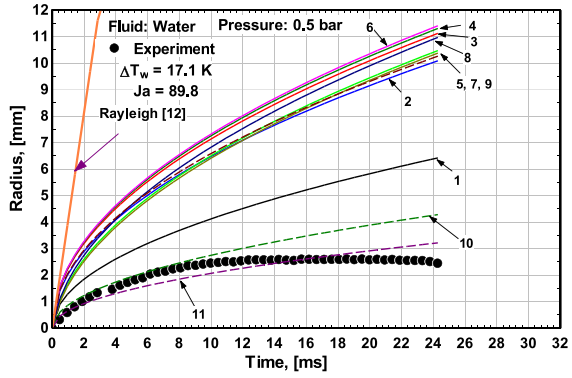


| | | | |
|---|---|---|---|
| 1 Fritz and Ende [16] | MAE 95.4% | 7 Theofanous and Patel [21] (I+A) | MAE 199.4 % |
| 2 Forster and Zuber [14] | MAE 205.8 % | 8 Avdeev and Zudin [19] (I+A) | MAE 219.2 % |
| 3 Plesset and Zwick [15] | MAE 237 % | 9 Forster [33] | MAE 211 % |
| 4 Scriven [11] | MAE 242.5 % | 10 Prisyniakov [18] | MAE 30.9 % |
| 5 Mikic et al. [20] (I+A) | MAE 203.9 % | 11 Abdollahi et al. [32] | MAE 13.5 % |
| 6 Avdeev and Zudin [19] | MAE 245.6 % | | |

(b) $\Delta T_w = 17.1$ K

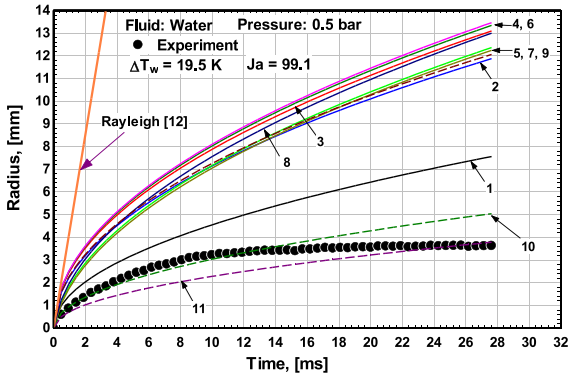


| | | | |
|---|---|---|---|
| 1 Fritz and Ende [16] | MAE 63.4% | 7 Theofanous and Patel [21] (I+A) | MAE 152.7 % |
| 2 Forster and Zuber [14] | MAE 156.7 % | 8 Avdeev and Zudin [19] (I+A) | MAE 170.8 % |
| 3 Plesset and Zwick [15] | MAE 183.1 % | 9 Forster [33] | MAE 160.7 % |
| 4 Scriven [11] | MAE 188.4 % | 10 Prisyniakov [18] | MAE 14.3 % |
| 5 Mikic et al. [20] (I+A) | MAE 156.8 % | 11 Abdollahi et al. [32] | MAE 18.6 % |
| 6 Avdeev and Zudin [19] | MAE 191 % | | |

(c) $\Delta T_w = 19.5$ K

**Fig. 8.** Evaluation of homogeneous bubble growth models at $P = 0.5$ bar.

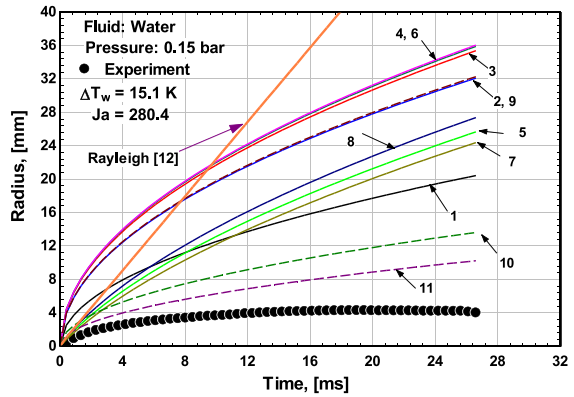


| | | | |
|---|---|---|---|
| 1 Fritz and Ende [16] | MAE 283.6 % | 7 Theofanous and Patel [21] (I+A) | MAE 277.9 % |
| 2 Forster and Zuber [14] | MAE 502.5 % | 8 Avdeev and Zudin [19] (I+A) | MAE 335.4 % |
| 3 Plesset and Zwick [15] | MAE 564.4 % | 9 Forster [33] | MAE 505.9 % |
| 4 Scriven [11] | MAE 573.9 % | 10 Prisyniakov [18] | MAE 155.7 % |
| 5 Mikic et al. [20] (I+A) | MAE 304.3 % | 11 Abdollahi et al. [32] | MAE 92.2 % |
| 6 Avdeev and Zudin [19] | MAE 576.9 % | | |

(a) $\Delta T_w = 15.1$ K

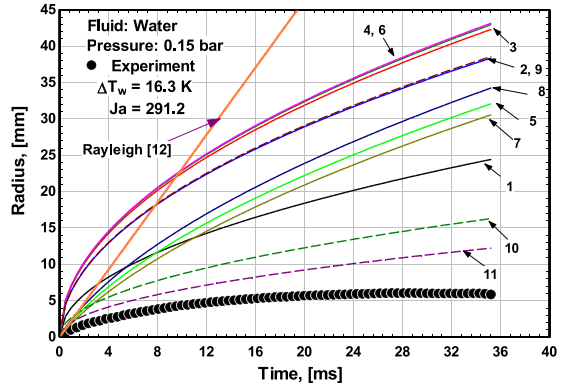


| | | | |
|---|---|---|---|
| 1 Fritz and Ende [16] | MAE 243.5 % | 7 Theofanous and Patel [21] (I+A) | MAE 257.8 % |
| 2 Forster and Zuber [14] | MAE 439.6 % | 8 Avdeev and Zudin [19] (I+A) | MAE 312.5 % |
| 3 Plesset and Zwick [15] | MAE 495 % | 9 Forster [33] | MAE 442.5 % |
| 4 Scriven [11] | MAE 504.2 % | 10 Prisyniakov [18] | MAE 129 % |
| 5 Mikic et al. [20] (I+A) | MAE 282.3 % | 11 Abdollahi et al. [32] | MAE 72.1 % |
| 6 Avdeev and Zudin [19] | MAE 507 % | | |

(b) $\Delta T_w = 16.3$ K

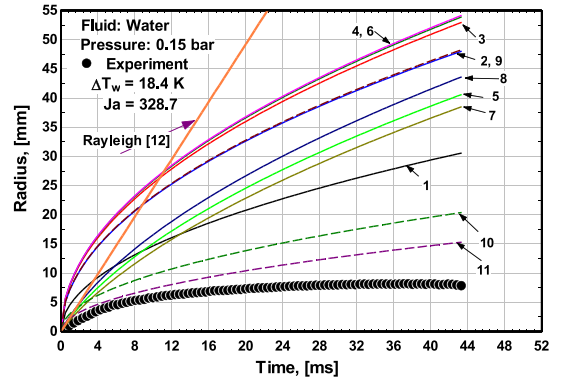


| | | | |
|---|---|---|---|
| 1 Fritz and Ende [16] | MAE 210 % | 7 Theofanous and Patel [21] (I+A) | MAE 225.1 % |
| 2 Forster and Zuber [14] | MAE 386.9 % | 8 Avdeev and Zudin [19] (I+A) | MAE 280.1 % |
| 3 Plesset and Zwick [15] | MAE 436.9 % | 9 Forster [33] | MAE 389.3 % |
| 4 Scriven [11] | MAE 446.4 % | 10 Prisyniakov [18] | MAE 106.7 % |
| 5 Mikic et al. [20] (I+A) | MAE 249.7 % | 11 Abdollahi et al. [32] | MAE 55.2 % |
| 6 Avdeev and Zudin [19] | MAE 448.9 % | | |

(c) $\Delta T_w = 18.4$ K

**Fig. 9.** Evaluation of homogeneous bubble growth models at 0.15 bar.

**Table 3**
MAE% and error at departure predicted using empirical growth models.

| Model | $P = 1$ bar | | | | $P = 0.5$ bar | | | $P = 0.15$ bar | | | MAE % @@Average |
|---|---|---|---|---|---|---|---|---|---|---|---|
| | MAE % | | | | MAE % | | | MAE % | | | |
| | 5.6K | 9.4K | 10K | 15K | 12.7K | 17.1K | 19.5K | 15.1K | 16.3K | 18.4K | |
| Cole and Shulman [28] | 18.7 | 26.9 | 34.9 | 34.3 | 40.7 | 44.4 | 20.6 | 109 | 84.2 | 61.3 | 47.5 |
| Du et al. [30] | 18 | 12.7 | 9.2 | 8.6 | 66.3 | 69.6 | 41.6 | 100.6 | 83.4 | 61.9 | 47.2 |
| Lee et al. [29] | 54.4 | 17.1 | 7 | 16 | 85.1 | 73.3 | 47 | 52.2 | 35.4 | 31.6 | 41.9 |
| Benjamin and Balakrishnan [31] | 14 | 31.5 | 39.9 | 45.2 | 15.5 | 14.7 | 21.9 | 14.6 | 16.4 | 29.4 | 24.3 |
| Abdollahi et al. [32] | 61.1 | 53 | 34.3 | 20.4 | 135.9 | 124.7 | 81.6 | 145.1 | 118.2 | 85.5 | 85.9 |
| | Error at departure | | | | | | | | | | |
| Cole and Shulman [28] | 11.3 | 3.9 | 21.9 | 20.2 | 75.7 | 94.4 | 53.4 | 175.1 | 125 | 103.6 | 68.5 |
| Du et al. [30] | 22.1 | 33 | 7.8 | 7.8 | 101.6 | 121.7 | 75.2 | 168.3 | 128 | 107.9 | 77.3 |
| Lee et al. [29] | 57.6 | 29 | 11.6 | 15.7 | 132.8 | 144.4 | 96.3 | 140 | 88.1 | 53 | 76.9 |
| Benjamin and Balakrishnan [31] | 5.9 | 9.9 | 27.9 | 33.8 | 26.6 | 30.1 | 0.7 | 25.6 | 3.8 | 8.9 | **17.3** |
| Abdollahi et al. [32] | 59.1 | 100.9 | 60.9 | 47.7 | 194.3 | 202.3 | 130.9 | 221.8 | 165.9 | 133.4 | 131.7 |

10 ms. (ii) The Prisnyakov [18] and Abdollahi et al. [32] models, which predicted the data very well at 0.5 bar, overpredicted the data with MAE 106.7 – 155.7% and 55.2 – 92.2% and error at departure 160.9 – 238.5% and 95.8 – 154.2%, respectively. (iii) the models described by curves 2 – 9 that exhibited nearly similar performance at 1 and 0.5 bar (some models were nearly coincident) showed clear differences and separate curves at 0.15 bar. For example, models 5, 7 and 9 exhibited nearly similar performance at 1 and 0.5 bar while they behaved differently at 0.15 bar. These three models combined the inertia and asymptotic growth stages using different assumptions for the relation between pressure difference and temperature difference. The performance of the models described by curves 1 – 9 was getting poor with MAE in the range 210 – 573.9% and error at departure as 291.2 – 796.3%.

In conclusion, the evaluation of homogeneous growth models demonstrated that some models predict part of the growth curves at atmospheric pressure in the early stage of growth up to 4 – 6 ms followed by large deviation when the experimental data enters the slow growth stage. At 0.5 bar, the models by Prisnyakov [18] and Abdollahi et al. [32] gave reasonable predictions while other models exhibited poor prediction. At 0.15 bar, none of the models could predict the experimental data. Thus, the homogeneous growth models should be used in heterogeneous boiling with some precautions.

### 4.2. Assessment of heterogenous models

Because heterogeneous bubble growth models were suggested based on different assumptions regarding the mechanism of heat transfer to the bubble, it is better to segregate the models into the following three categories: (i) empirical models which are based on fitting a range of experimental data as a function of dimensionless groups. (ii) models based on evaporation from the superheated boundary layer around the curved surface of the bubble. (iii) models that include evaporation from the superheated liquid trapped in the microlayer underneath the bubble. All heterogeneous bubble growth models included in the comparison are summarized in Table A2 of the Appendix A.

#### 4.2.1. Empirical models

The experimental data were compared with five empirical models as seen in Figs. 10, 11 and 12 for the three tested pressure; 1, 0.5 and 0.15 bar, respectively. The comparison includes the models suggested by Cole and Shulman [28], Du et al. [30], the Lee et al. [29], Benjamin and Balakrishnan [31] and Abdollahi et al. [32]. The statistical assessment of these models is summarized in Table 3.

1. ***Pressure 1 bar:*** Fig. 10a indicates, for 5.6 K superheat, that the models suggested by Benjamin and Balakrishnan [31] (curve 4), Du et al. [30] (curve 2), and Cole and Shulman [28] (curve 1) predict the experimental data and trend very well with MAE 14, 18 and 18.7% and error at departure 5.9, 22.1 and 11.3%, respectively. As presented in Section 2, the Cole and Shulman [28] and the Benjamin and Balakrishnan [31] models predict that $R \propto t^{1/2}$ and the exponent of $Ja$ was 0.6 and 0.5, respectively. This may explain the small difference between the two models. The model by Du et al. [30] predicts that the time exponent depends on system pressure (the exponent is 0.271 at 1 bar), which is smaller than the 0.5 value in [28] and [31] and the exponent of $Ja$ was 0.79, which is larger compared to [28] and [31]. This explains why this model predicts values larger than those predicted by [28] and [31]. The model by Abdollahi et al. [32] (curve 5) underpredicted the data significantly with MAE 61.1% and error at departure 59.1% while the Lee et al. [29] model (curve 3) overpredicted the data significantly with MAE 54.4% and error at departure 57.6%. Fig. 10b indicates, for 9.4 K, that the Cole and Shulman [28] and the Benjamin and Balakrishnan [31] models exhibited nearly similar performance and underpredicted the data with MAE 26.9 and 31.5% and error at departure 3.9 and 9.9%, respectively. The small error at departure is because the values predicted using these models approach the experimental data towards the end of the curve. The Du et al. [30] model exhibited excellent predictions up to about 7 ms after which the model deviated from the experimental data with overprediction by MAE 12.7% and error at departure 33%. The small MAE is due to the partial agreement with the data over part of the growth period. The Lee et al. [29] model behaved nearly similar to the Du et al. [30] model except that the model predicts a slower growth rate. The MAE of this model was MAE 17.1% and the error at departure was 29%. The Abdollahi et al. [32] model exhibited small deviation at the beginning then the deviation increased significantly with time with MAE 53% and error at departure 100.9%. At 10 K superheat, Fig. 10c shows that the performance of the Cole and Shulman [28] and the Benjamin and Balakrishnan [31] models was nearly similar to Fig. 10b where they underpredicted the data with MAE 34.9 and 39.9%, respectively and error at departure 21.9 and 27.9%. The Lee et al. [29] model exhibited excellent agreement in terms of values and trend with the lowest MAE of 7% and error at departure 11.6%. Also, the Du et al. [30] model gave excellent prediction with MAE of 9.2% although the trend was slightly different compared to the experimental data. The Abdollahi et al. [32] model showed the same performance as Fig. 10b but with a lower MAE value of

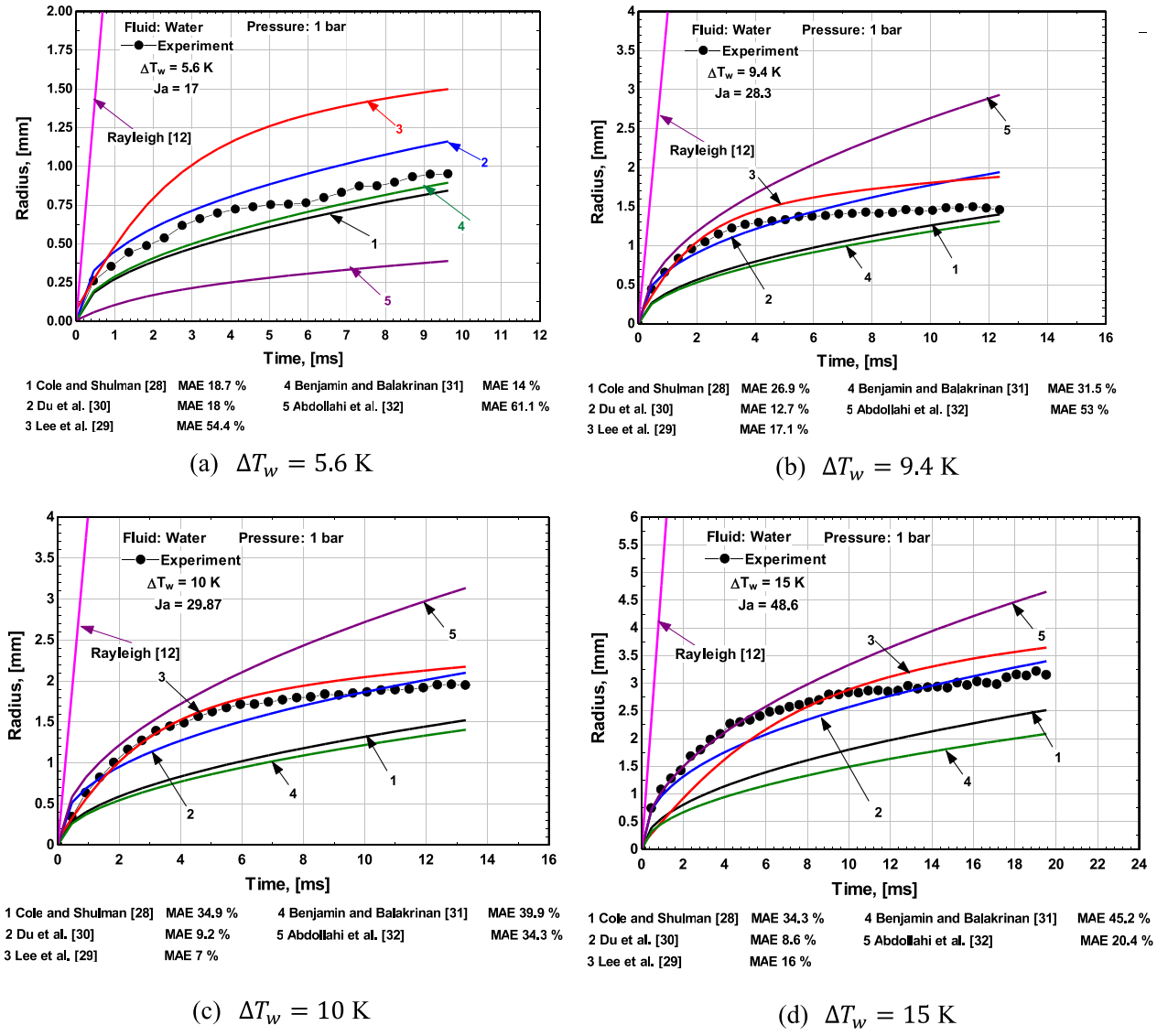


**Fig. 10.** Assessment of empirical heterogeneous bubble growth models at $P = 1$ bar.

34.3% and error at departure 60.9%. Fig. 10d indicates, for the highest superheat, that the difference between the Cole and Shulman [28] and the Benjamin and Balakrishnan [31] models is getting large compared to Figs. 10(a-c) for lower superheat. They underpredict the data with MAE 34.3 and 45.2% and error at departure 20.2 and 33.8%, respectively. The Lee et al. [29] model underpredicted the data for time below 10 ms then overpredicted the data up to departure (the model crosses the data) with MAE of 16% and error at departure 15.7%. The Du et al. [30] model exhibited excellent prediction up to 2 ms then slightly underpredicted the data with excellent prediction towards the end of the growth period. The MAE of this model was 8.6% and the error at departure was 7.8%. Contrary to the large MAE predicted by the Abdollahi et al. [32] model at low superheats, it showed excellent prediction up to 6 ms then overpredicted the data with deviation that increases with time. Due to the partial agreement, the MAE decreased to 20.4% while the error at departure was 47.7%. Based on Table 3, it may be concluded that the best performing model at atmospheric pressure is the Du et al. [30] model in terms of the MAE while based in the error at departure the Cole and Shulman [28] has the lowest deviation.

2. ***Pressure 0.5 and 0.15 bar:*** Figs. 11 and 12 depict the comparison at 0.5 and 0.15 bar, respectively. The behaviour of all models was similar to that occurred at 1 bar except that the trend predicted by the Lee et al. [29] model has changed. After the early stage of growth, it predicted slow growth rate at atmospheric pressure, which was nearly similar to the experimental data. By contrast, at 0.5 and 0.15 bar, the model predicted a faster growth rate compared to the atmospheric pressure case, i.e. it was nearly linear at 0.15 bar. The Benjamin and Balakrishnan [31] exhibited the lowest MAE for the three superheats at 0.5 bar with values in the range 14.7 – 22% and error at departure 0.7 – 30%. The performance of this model did not change significantly at 0.15 bar where the MAE ranged from 16.4 to 29.4% and the error at departure was 3.8 – 25.6%. The Cole and Shulman [28] model gave a MAE value below 30% only for the 19.5 K superheat at 0.5 bar. All other models gave MAE in the range 40.7 – 135.9% at 0.5 bar and 31.6 – 145.1% at 0.15 bar. Based on Table 3, the model by Benjamin and Balakr-

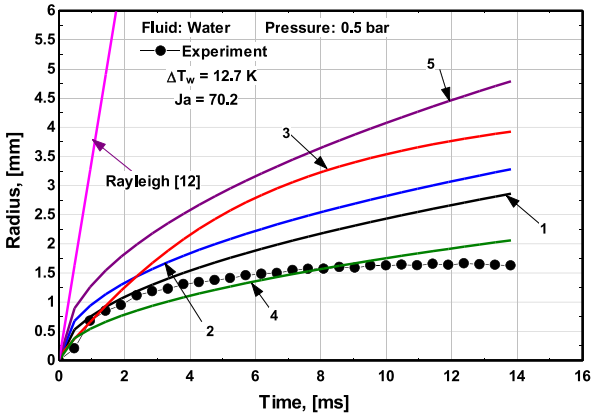


(a) $\Delta T_w = 12.7$ K

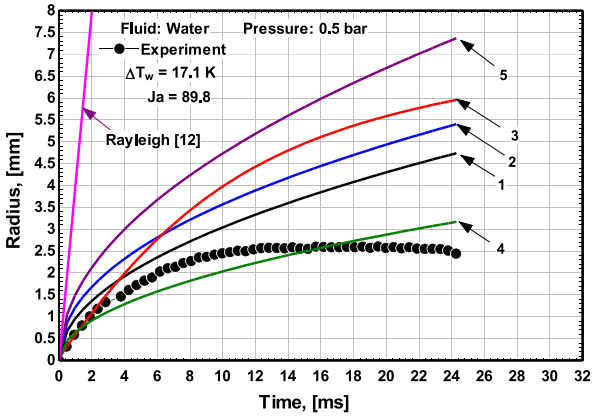


(b) $\Delta T_w = 17.1$ K

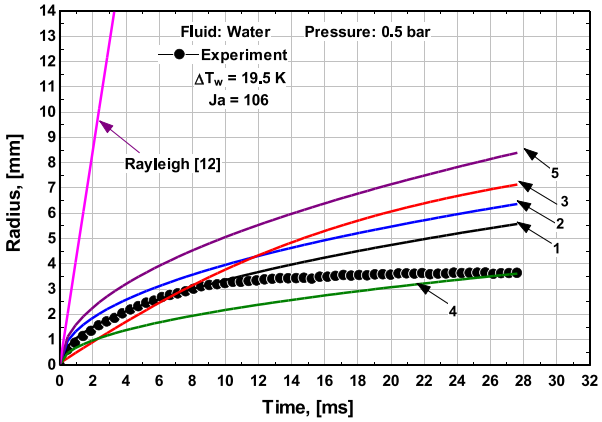


(c) $\Delta T_w = 19.5$ K

**Fig. 11.** Assessment of empirical heterogeneous bubble growth models at $P = 0.5$ bar.

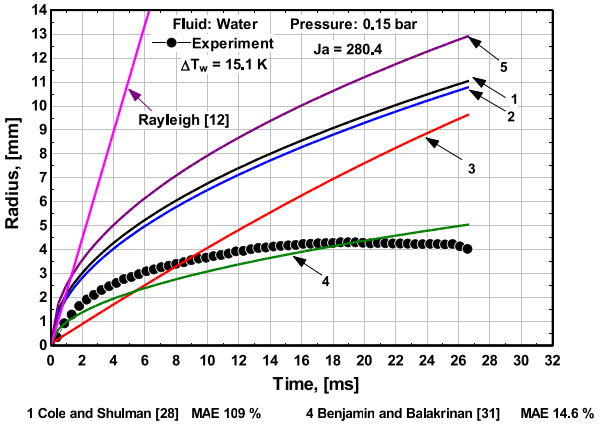


(a) $\Delta T_w = 15.1$ K

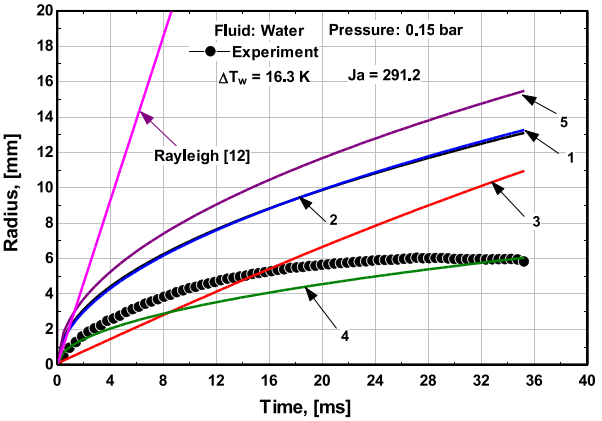


(b) $\Delta T_w = 16.3$ K

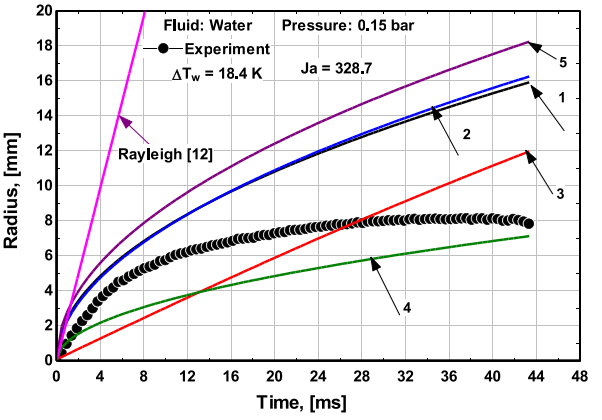


(c) $\Delta T_w = 18.4$ K

**Fig. 12.** Assessment of empirical heterogeneous bubble growth models at $P = 0.15$ bar.

ishnan [31] exhibited the best overall performance for the three examined pressures at different superheat. It predicted all data with MAE 24.3% and error at departure 17.3%. The better performance of this model may be attributed to the inclusion of the Archimedes number, which considers the effect of gravity, which was ignored by all other models.

*4.2.2. Boundary layer-based models*

Seven models [20,23–25,33–35] for bubble growth due to evaporation from the superheated liquid in the boundary layer around the bubble are evaluated in this section. Because bubble growth rate in uniform superheat represents the upper limit of growth, it is expected that the effect of nonuniform superheat is to reduce the growth rate in heterogeneous boiling. Zuber [23] assumed spherical bubble which is initially fully surrounded with the wall thermal boundary layer of uniform thickness and superheat ($T_{sL} \approx T_w$). When evaporation starts, the bubble surface cools down to the saturation temperature $T_{sat}$ and thus part of the heat will be conducted towards the bubble surface with temperature difference ($T_w - T_{sat}$) while the other part will be conducted towards the liquid bulk with temperature difference ($T_w - T_{Lb}$) due to the nonuniform liquid superheat. If the liquid bulk temperature $T_b$ equals the superheated wall temperature (uniform superheat), the model is reduced to bubble growth in homogeneous boiling. This model predicts that the $R \propto t^{1/2}$. Forster [33] considered the effect of nonuniform superheat by assuming that the bubble grows in a wall thermal boundary layer in which the liquid superheat decreases exponentially in the direction normal to the boiling surface. This model predicts that the $R \propto t^{1/2}$ when the bubble is inside the wall thermal boundary layer and the relation changes to $R \propto t^{1/4}$ when it protrudes outside the boundary layer. Han and Griffith [24] assumed that the bubble grows as a truncated sphere and is fully surrounded with the wall thermal boundary layer, which is formed periodically during the waiting period. The superheat was assumed to vary linearly in the bubble thermal boundary layer. It is difficult to infer the time exponent from their model but in the case of uniform superheat and spherical bubble, the model was reduced to homogenous growth models with time exponent 0.5. Van Stralen [25] assumed that the bubble is a truncated sphere similar to [24] but is partially surrounded with the superheated boundary layer. Contrary to the above models which assumed that the superheat does not vary with time during the whole bubble growth period, Van Stralen [25] assumed that bubble growth is a relaxation phenomenon, i.e. the superheat around that part of the bubble decreases exponentially during a relaxation time (delay time), which was taken as the departure time. He assumed that the bubble grows with a fixed shape with a fixed contact shape angle of 60°. In conclusion, he modified the homogeneous growth model to account for partial heating and the time dependant superheat. The bubble height which is surrounded with the superheated layer "relaxation layer" was related to the shape angle. Because this angle was assumed fixed, the part of the bubble surrounded with the boundary layer can be obtained at any time, recommended at departure. This model predicts that in the early stage, the radius follows the relation $R \propto t^{1/2}$ and the exponent decreases rapidly with time. The model was also based on satisfying that the growth velocity tends to zero towards departure. Mikic et al. [20] gave a model assuming that a spherical bubble forms at the end of the waiting period due to evaporation from superheated liquid in the boundary layer after subtracting the conduction heat flux towards the liquid bulk. This principle is nearly similar to Zuber [23] but it considers the effect of waiting time. When the waiting time is zero or when the liquid bulk temperature equals the superheated wall temperature (uniform superheat), the model reduces to the Plesset and Zwick [15] model. Finally, they combined this asymptotic solution with the Rayleigh solution to consider the inertia-growth stage. Lesage et al. [34] assumed spherical bubble connected with the surface with a cylindrical neck and corrected the temperature profile in the wall thermal boundary layer used by Mikic et al. [20] to account for the premise that the bubble boundary layer thickness should be smaller than the wall thermal boundary layer thickness adopted by all researchers. Cho and Wang [35] assumed that the bubble grows as a truncated sphere protruding outside the wall thermal boundary layer in which the liquid temperature was assumed to decrease linearly. The bubble was assumed to grow due to evaporation from that curved part of the bubble surface immersed in the wall thermal boundary layer. They also included a factor determined empirically to account for contribution from the microlayer. In their model, they identified a critical time after which the bubble penetrates the boundary layer. The overall performance of these models is summarized in Table 4.

Fig. 13a indicates, for the lowest superheat, that six models predicted the data very well with MAE below 30%. These models are arranged as follows: (1) the Mikic et al. [20] model (MAE 3.2% and $Er_d$ 4.1%). It is worth mentioning that the waiting time required for this model was predicted from the Han and Griffith [24] model. (2) the Lesage et al. [34] model (MAE 5.7% and $Er_d$ 8.9%). As mentioned above, this model was based on the temperature distribution used in the Mikic et al. [20] corrected by the effective bubble boundary layer thickness. (3) the Zuber [23] model (MAE 7.3% and $Er_d$ 14.7%). (4) the Han and Griffith [24] model (MAE 12.2% and $Er_d$ 5.5%). (5) the Forster [33] model (MAE 19.7% and $Er_d$ 12.5%). (6) the Van Stralen [25] model (MAE 23.9% and $Er_d$ 3.6%). This model predicted rapid growth with large deviation at the beginning then a significant decrease in bubble growth rate with small deviation, e.g. the growth rate approaches zero near departure. The model by Cho and Wang [35] underpredicted the data significantly at this superheat with MAE 46% and error at departure 43.7%. The underprediction may be attributed to the fact that the model assumes bubble growth due to evaporation at the curved part of the bubble surface immersed in the wall thermal boundary layer. This is contrary to the other models that considered the bubble is surrounded with the wall thermal boundary layer. The same conclusion can be reached in Figs. 13b, c, d for superheat 9.4, 10 and 15 K where the same six models predicted the data very well with better performance for the Van Stralen [25] model, see Table 4 for the error values. The only exception was the model by Forster [33] which underpredicted the data with MAE 37.7%. It is obvious that this model shows a clear jump after certain time (see curve 2). This time corresponds to the moment when the bubble protrudes outside the wall thermal boundary layer (according to the model the exponent of time changes from 0.5, when the bubble grows inside the wall boundary layer, to 0.25, when it grows outside the wall boundary layer). Additionally, this model described the bubble growth using one continuous function, i.e. smooth transition between the two stages (inside and outside the wall boundary layer). It is worth mentioning that the fraction of the bubble surface which is surrounded with the relaxation layer was supposed to be less than or equal to 1 according to the Van Stralen [25] model. However, the predicted value at departure as recommended by the model was in the range 1.6 – 2. In other words, the bubble is fully surrounded by the wall thermal boundary layer at atmospheric pressure. This is justified by the perfect prediction in terms of values and trend by this model. Generally, it is obvious that most of the boundary-layer based models predicted the data at atmospheric pressure very well.

Fig. 14 shows the comparison at 0.5 bar and superheat 12.7, 17.1 and 19.5 K. Contrary to the atmospheric pressure case that exhibited good performance for all models except the Cho and Wang [3] model, only three models exhibited excellent agreement at 0.5 bar. These models are the Van Stralen [25], the Forster [33] and the Cho and Wang [35] models which predicted the data

**Table 4**
MAE% and error at departure predicted using boundary layer-based models.

| Model | $P = 1$ bar | | | | $P = 0.5$ bar | | | $P = 0.15$ bar | | | MAE % @@Average |
|---|---|---|---|---|---|---|---|---|---|---|---|
| | MAE % | | | | MAE % | | | MAE % | | | |
| | 5.6K | 9.4K | 10K | 15K | 12.7K | 17.1K | 19.5K | 15.1K | 16.3K | 18.4K | |
| Zuber [23] | 7.3 | 15.2 | 8.8 | 12.9 | 177 | 201.6 | 144.5 | 462 | 388.6 | 339.8 | 171.3 |
| Forster [33] | 19.7 | 8.9 | 21.1 | 37.7 | 29 | 17.6 | 18.1 | 40.7 | 20 | 30.2 | **24.3** |
| Han and Griffith [24] | 12.2 | 15.4 | 20.1 | 14.2 | 111 | 132.2 | 100.1 | 341.2 | 292.7 | 254.3 | 129.3 |
| Van Stralen [25] | 21.5 | 3.2 | 5.2 | 10.5 | 22.1 | 21.7 | 20.9 | 18.8 | 22.9 | 15.6 | **16.2** |
| Mikic et al. [20] | 3.2 | 7.7 | 14.7 | 9.7 | 107 | 147.4 | 68.2 | 333.7 | 281.3 | 228.8 | 118.5 |
| Lesage et al. [34] | 5.7 | 7.7 | 18.2 | 14.1 | 89.7 | 133.9 | 95.2 | 304.2 | 253.5 | 203.7 | 164.8 |
| Cho and Wang [35] | 46 | 48.6 | 53.9 | 53 | 13 | 19.4 | 9.1 | 53.8 | 28.3 | 20.7 | 34.6 |
| **Error at departure** ($Er_d$) | | | | | | | | | | | |
| Zuber [23] | 14.7 | 39.5 | 9.2 | 12.5 | 237.2 | 258 | 192 | 620.2 | 467.4 | 427.1 | 225.4 |
| Forster [33] | 12.5 | 1.4 | 21.1 | 38.4 | 67.2 | 24 | 10 | 40 | 4.5 | 14.3 | **23.3** |
| Han and Griffith [24] | 5.5 | 15.7 | 4.6 | 6.6 | 162.3 | 212 | 154.4 | 480.5 | 379.8 | 374.4 | 179.6 |
| Van Stralen [25] | 3.6 | 0.2 | 2.3 | 5.2 | 22.8 | 25.1 | 18.8 | 29.9 | 24 | 21.4 | **15.3** |
| Mikic et al. [20] | 4.1 | 13.1 | 8 | 5.4 | 113 | 177 | 67.2 | 369 | 271.4 | 224.8 | 122.9 |
| Lesage et al. [34] | 8.9 | 6.6 | 13.6 | 12 | 141.2 | 153.8 | 100.8 | 326.5 | 235.5 | 192 | 195.1 |
| Cho and Wang [35] | 43.7 | 34.8 | 46.9 | 48.1 | 24.8 | 36.5 | 2.6 | 67.6 | 19 | 3.4 | 32.7 |

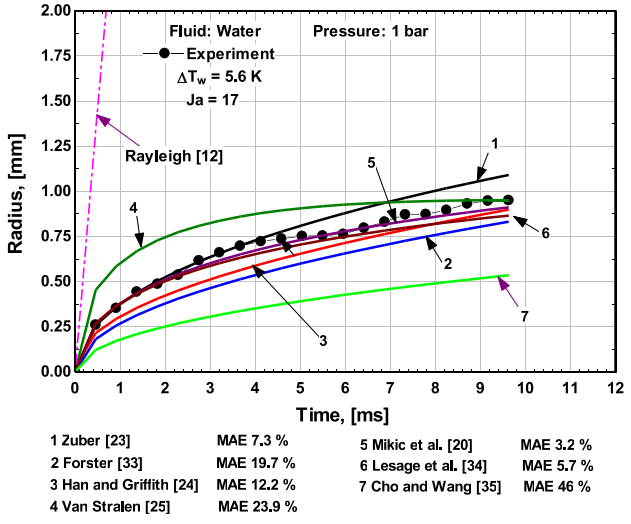


(a) $\Delta T_w = 5.6$

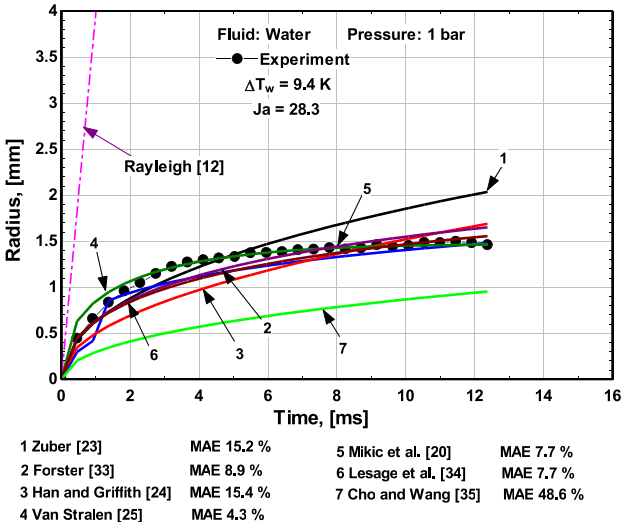


(b) $\Delta T_w = 9.4$

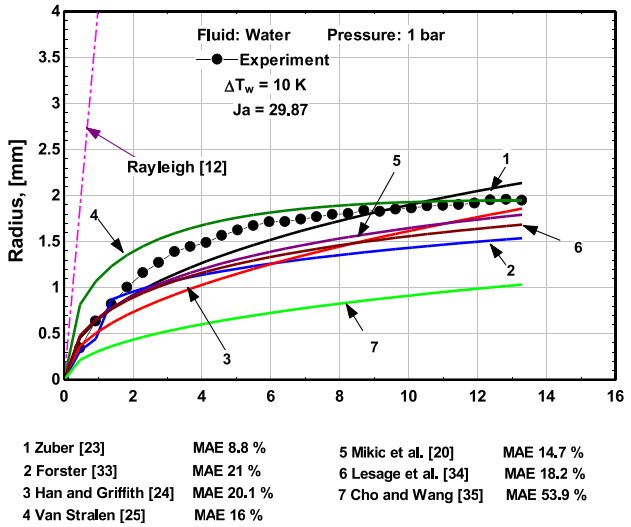


(c) $\Delta T_w = 10$

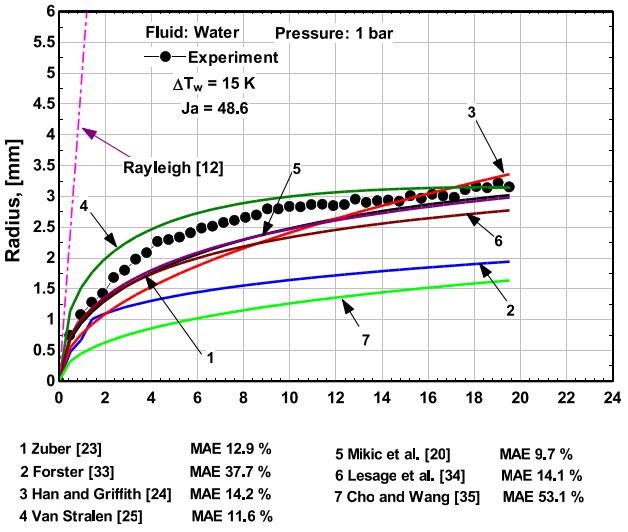


(d) $\Delta T_w = 15$

**Fig. 13.** Assessment of superheated layer-based models at $P = 1$ bar.

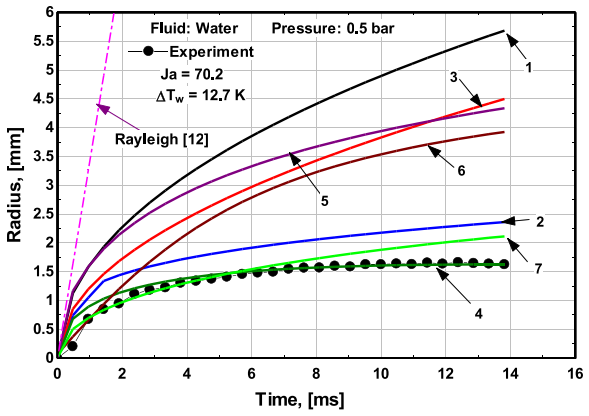


| | | | |
|---|---|---|---|
| 1 Zuber [23] | MAE 177 % | 5 Mikic et al. [20] | MAE 146.1 % |
| 2 Forster [33] | MAE 17.6 % | 6 Lesage et al. [34] | MAE 89.7 % |
| 3 Han and Griffith [24] | MAE 111 % | 7 Cho and Wang [35] | MAE 13 % |
| 4 Van Stralen [25] | MAE 12.7 % | | |

(a) $\Delta T_w = 12.7$

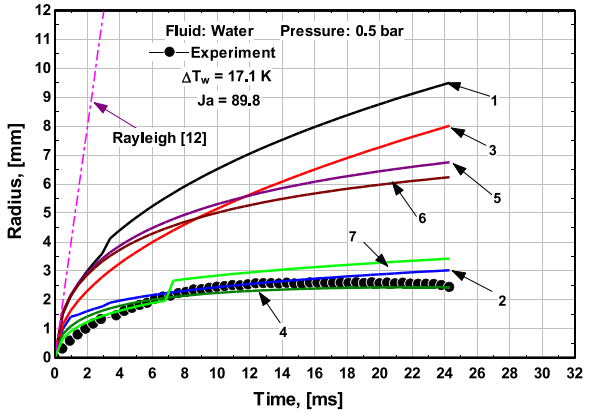


| | | | |
|---|---|---|---|
| 1 Zuber [23] | MAE 201.6 % | 5 Mikic et al. [20] | MAE 147.4 % |
| 2 Forster [33] | MAE 19 % | 6 Lesage et al. [34] | MAE 133.9 % |
| 3 Han and Griffith [24] | MAE 132 % | 7 Cho and Wang [35] | MAE 19 % |
| 4 Van Stralen [25] | MAE 13.9 % | | |

(b) $\Delta T_w = 17.1$

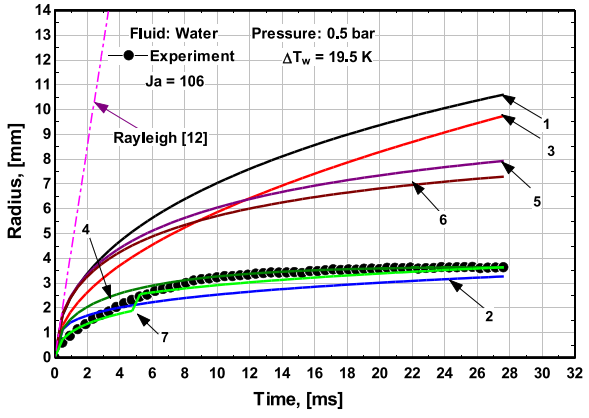


| | | | |
|---|---|---|---|
| 1 Zuber [23] | MAE 144.5 % | 5 Mikic et al. [20] | MAE 107.2 % |
| 2 Forster [33] | MAE 18.1 % | 6 Lesage et al. [34] | MAE 95.2 % |
| 3 Han and Griffith [24] | MAE 100.1 % | 7 Cho and Wang [35] | MAE 9.1 % |
| 4 Van Stralen [25] | MAE 9 % | | |

(c) $\Delta T_w = 19.5$

**Fig. 14.** Assessment of superheated layer-based models at $P = 0.5$ bar.

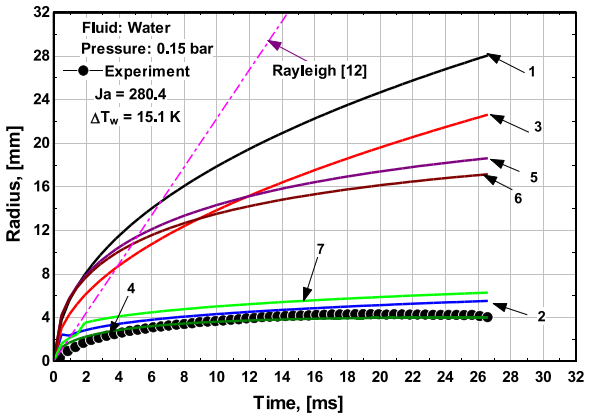


| | | | |
|---|---|---|---|
| 1 Zuber [23] | MAE 456 % | 5 Mikic et al. [20] | MAE 333.7 % |
| 2 Forster [33] | MAE 40.7 % | 6 Lesage et al. [34] | MAE 304.2 % |
| 3 Han and Griffith [24] | MAE 341.2 % | 7 Cho and Wang [35] | MAE 53.8 % |
| 4 Van Stralen [25] | MAE 14.2 % | | |

(a) $\Delta T_w = 15.1$

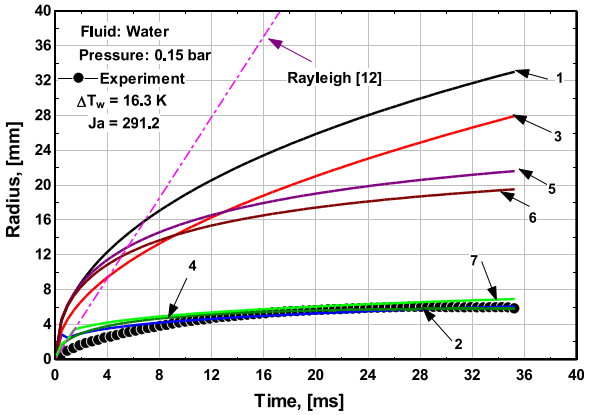


| | | | |
|---|---|---|---|
| 1 Zuber [23] | MAE 388.6 % | 5 Mikic et al. [20] | MAE 281.3 % |
| 2 Forster [33] | MAE 20 % | 6 Lesage et al. [34] | MAE 253.5 % |
| 3 Han and Griffith [24] | MAE 292.7 % | 7 Cho and Wang [35] | MAE 28.3 % |
| 4 Van Stralen [25] | MAE 18.6 % | | |

(b) $\Delta T_w = 16.3$

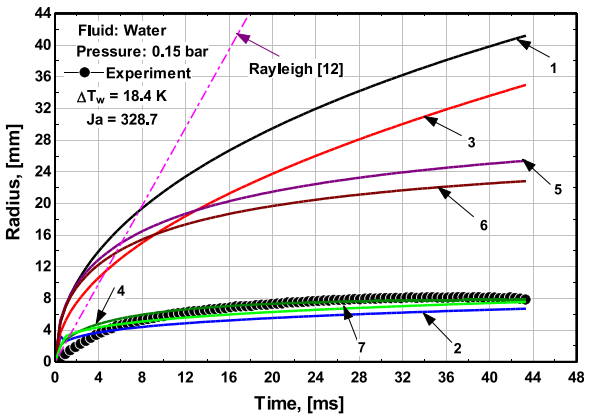


| | | | |
|---|---|---|---|
| 1 Zuber [23] | MAE 339.8 % | 5 Mikic et al. [20] | MAE 228.8 % |
| 2 Forster [33] | MAE 30.2 % | 6 Lesage et al. [34] | MAE 203.7 % |
| 3 Han and Griffith [24] | MAE 254.3 % | 7 Cho and Wang [35] | MAE 20.7 % |
| 4 Van Stralen [25] | MAE 15.6 % | | |

(c) $\Delta T_w = 18.4$

**Fig. 15.** Assessment of superheated layer-based models at $P = 0.15$ bar.

**Table 5**
MAE% and error at departure predicted using microlayer-based models.

| Model | $P = 1$ bar | | | | $P = 0.5$ bar | | | $P = 0.15$ bar | | | MAE % @@Average |
|---|---|---|---|---|---|---|---|---|---|---|---|
| | MAE % | | | | MAE % | | | MAE % | | | |
| | 5.6K | 9.4K | 10K | 15K | 12.7K | 17.1K | 19.5K | 15.1K | 16.3K | 18.4K | |
| Cooper [26] | 21.6 | 27.9 | 16.5 | 25.8 | 177.6 | 206.7 | 164.6 | 359.5 | 324.8 | 283.4 | 160.8 |
| Van Ouwerker [37] | 25.8 | 24.1 | 31.4 | 24.7 | 81.9 | 99.2 | 70.5 | 272.3 | 239.5 | 206.5 | 107.6 |
| Labuntsov and Yagov [38] | 21.5 | 31.4 | 39.1 | 39.2 | 32 | 37.7 | 17.6 | 123.3 | 105.1 | 83.3 | 53 |
| Van Stralen et al. [27] | 39.1 | 38.6 | 44.4 | 39.2 | 50.2 | 66 | 43.2 | 163.2 | 143.4 | 119.6 | 74.7 |
| Van Stralen et al. [27] (BL+ML+$I$) | 21.5 | 3.2 | 5.2 | 10.5 | 22.1 | 27.7 | 17.6 | 18.8 | 22.9 | 15.6 | **16.5** |
| Mei et al. [39] | 42 | 22.2 | 11.5 | 12.6 | 86.8 | 77.5 | 43 | 81.7 | 60.7 | 35.2 | 47.3 |
| Prisnyakov [18] | 41.1 | 41.3 | 46.7 | 39.8 | 40.4 | 55.8 | 35.4 | 286.2 | 171.3 | 144.8 | 90.3 |
| Buyvich and Webbon [41] | 6.9 | 17 | 16.9 | 32.6 | 23.5 | 29.2 | 24.7 | 209.1 | 185.8 | 171.9 | 71.8 |
| | **Error at departure** ($Er_d$) | | | | | | | | | | |
| Cooper [26] | 25.3 | 67.7 | 38.5 | 55.7 | 246.5 | 313 | 236.7 | 504.6 | 419 | 383.9 | 229.1 |
| Van Ouwerker [37] | 19.5 | 0.3 | 17.7 | 8.1 | 127.1 | 168.1 | 117.1 | 390 | 318.7 | 286.8 | 145.3 |
| Labuntsov and Yagov [38] | 14.6 | 9.9 | 27 | 26.3 | 64.8 | 85.4 | 47.8 | 194 | 150.6 | 131.1 | 75.2 |
| Van Stralen et al. [27] | 34.9 | 19.3 | 33.4 | 25.1 | 57.8 | 123.5 | 82.3 | 246.4 | 197.4 | 177.3 | 99.7 |
| Van Stralen et al. [27] (BL+ML+$I$) | 3.6 | 0.2 | 2.3 | 5.2 | 22.8 | 25.1 | 47.8 | 29.9 | 24 | 21.4 | **18.2** |
| Mei et al. [39] | 58.9 | 56.3 | 25.5 | 16.8 | 133.2 | 139 | 82 | 139.1 | 96.4 | 70.6 | 81.8 |
| Prisnyakov [18] | 37.4 | 22.8 | 35.8 | 26.1 | 75.7 | 110.9 | 73.8 | 192.4 | 233 | 210.9 | 101.9 |
| Buyvich and Webbon [41] | 12.1 | 39 | 2.4 | 16.1 | 17.5 | 20.7 | 1.6 | 306.6 | 249.1 | 243.1 | 90.8 |

with MAE 9 – 13.9%, 17.6 – 19% and 9.1 – 19% with error at departure 18.8 – 25.1%, 10 – 67.2% and 2.6 – 36.5%, respectively. The Zuber [23], the Han and Griffith [24], the Mikic et al. [20] and the Leseage et al. [34] overpredicted the data significantly. The same conclusion can be reached in Fig. 15 at 0.15 bar. It may be concluded that the model by Van Stralen [2] predicted the data very well at all pressures. It worth noting that the growth curve predicted by the Cho and Wang [35] model exhibited a sudden drop at a certain time for some conditions (see Fig.14b, c). This drop is due to the fact that this model gave two equations for the bubble growth problem, see Eq. (49). The first equation describes bubble growth when the bubble size is smaller than the thickness of the wall thermal boundary layer, while the second equation describes bubble growth when the bubble protrudes outside the wall thermal boundary layer. They gave an expression for $t_\delta$ (see Eq. (49)), the critical time at which the bubble protrudes outside the wall thermal boundary layer. The appearance of the sudden drop in the growth curve at some conditions and the absence at some other conditions is due to the fact that the critical time depends on fluid properties and wall superheat. Thus, when the critical time is very small (less than about 1 or 2 ms), we only see one equation and cannot detect the sudden drop observed at some conditions.

*4.2.3. Models including microlayer evaporation*

This section compares 8 models that attributed bubble growth either to microlayer evaporation only such as Cooper [26], Van Stralen et al. [27], and Mei et al. [39] or considering the microlayer as one of the contributing mechanisms such as Labuntsov and Yagov [38], Van Stralen et al. [27], van Ouwerkerk [37], Prisnyakov [18] and Buyvich and Webbon [41]. Figs. 16, 17 and 18 shows the comparison at pressure 1, 0.5 and 0.15 bar, respectively. The statistical performance of each model is summarized in Table 5. The following points can be concluded from this comparison for each model:

1. The Cooper [26] (curve 1) exhibited excellent agreement with the experimental data up to 4 – 6 ms at atmospheric pressure, see Fig. 16. After this time, the model overpredicted the data with deviation increasing with time. The partial agreement of this model at atmospheric pressure resulted in low MAE (16.5 – 27.9%) while the error at departure was large (25.3 – 67.7%). This model has been discussed extensively in Mahmoud and Karayiannis [9] and the excellent agreement up to 4 – 6 ms was coincident with the end of the expansion stage (maximum contact radius), i.e. end of microlayer evaporation. Additionally, this good agreement was due to the fact that the initial microlayer thickness was predicted based on 0.5 time exponent, which is similar to the experimental exponent in this stage. In other words, the microlayer model should be compared with the data up to the end of microlayer evaporation (expansion stage) and the overprediction is expected because the model did not consider the growth during the departure stage. It is worth mentioning that, as discussed in the introduction section, Cooper [26] gave another two models that include contribution from microlayer evaporation and the boundary layer. In his formulation, the contribution was conducted in an additive manner. Because the comparison indicated that the microlayer only agrees partially at low time and overpredict the values at large times, it is expected that the other additive models will overpredict the data significantly. Thus, they were not included in the current comparison. Figs. 17 and 18 demonstrates that the Cooper [26] model exhibited poor performance at subatmospheric pressure with significant overprediction. This can be attributed to the fact that the initial microlayer thickness given in Cooper model represents a special case when the time exponent is 0.5. In fact, the initial microlayer thickness depends on the time exponent during the early stage of growth, which is expected to be larger than 0.5 in the first few milliseconds, see ref. [9] for more details. Accordingly, to generalize the Cooper microlayer evaporation model, a general expression for the initial microlayer thickness is required.
2. Van Ouwerker [37] solved the conjugate heat transfer problem including contribution from the microlayer and boundary layer without neglecting the heat capacity of the liquid in the microlayer as was done by Cooper [26]. This model (curve 2) always underpredict the experimental data with a trend that approaches the data towards the end of the growth period. It did not show excellent agreement in the first 4 – 6 ms as was the case by Cooper [26] model and gave reasonable prediction at atmospheric pressure as seen in Fig. 16. It predicted the data with MAE in the range 24.1 – 31.4% and low error at departure 0.3 – 19.5%. It is worth mentioning that this model was based on assuming that the bubble growth follows the law, $R = \beta t^{1/2}$. Similar to the Cooper [26] model, the performance of the Van

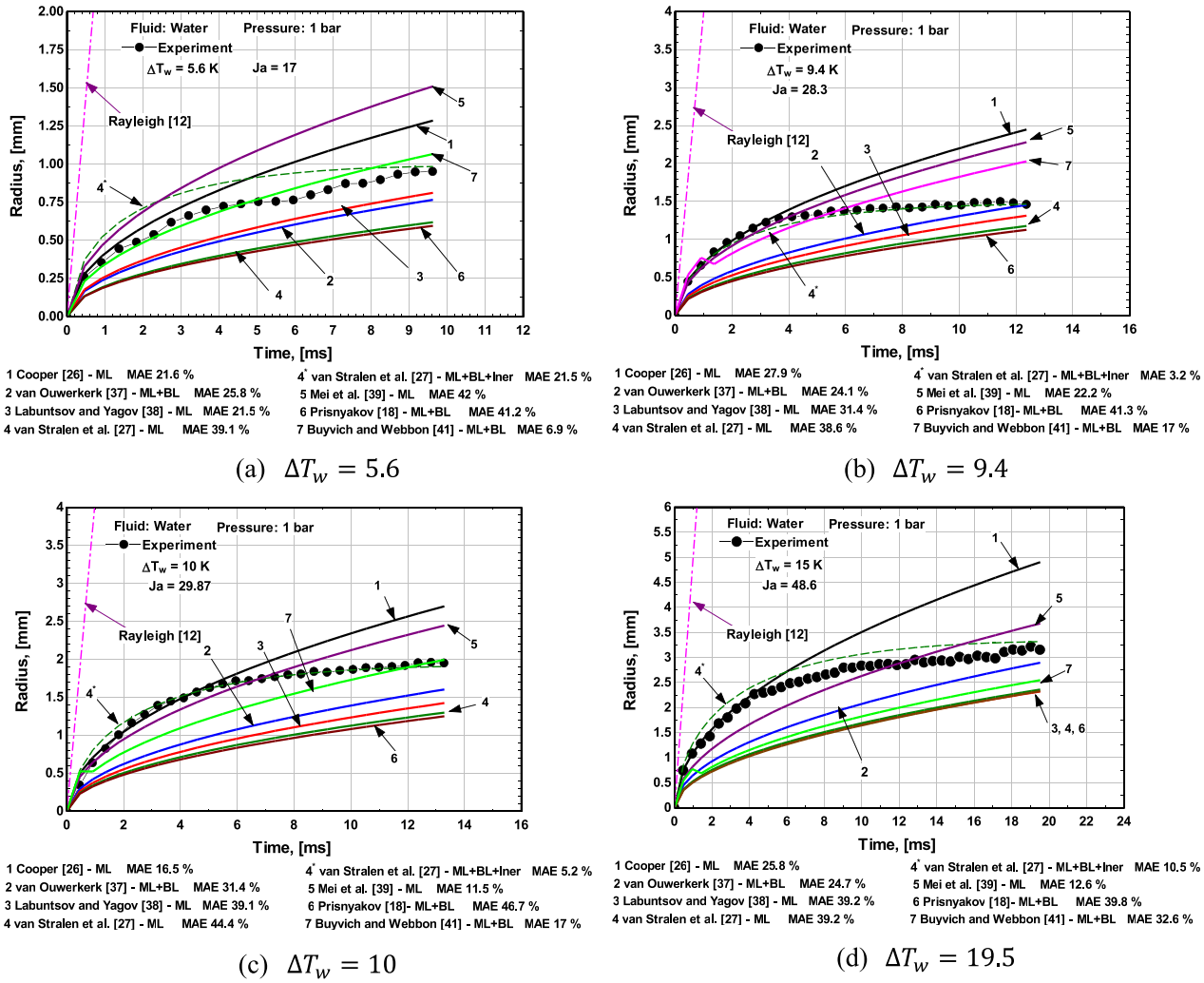


**Fig. 16.** Assessment of microlayer-based models at $P = 1$ bar.

Ouwerker [37] was poor at sub-atmospheric pressure with large overprediction.

3. Labuntsov and Yagov [38] presented a semi-empirical model that combines evaporation from the thin microlayer in the contact area and the thick layer below the bubble in the wedge region. They lumped all physical unknowns into empirical constants that were determined from experimental data. The comparison of this model (curve 3) indicates that the model always underpredicts the data at atmospheric pressure as seen in Fig. 16 with MAE 21.5 – 39.2% and error at departure 9.9 – 27%. At 0.5 bar, the model achieved some good agreement with the data in the early stage of growth then overpredicted the data as time increases, as seen in Fig. 17. The MAE of this model at 0.5 bar was 17.6 – 37.7% and error at departure 47.8 – 85.4%. The model overpredicted the data significantly at 0.15 bar during the whole growth period as seen in Fig. 18. In conclusion, the empirical constants should be optimized for the model to be more general.
4. Van Stralen et al. [27] suggested a model for bubble growth due to microlayer evaporation only. The microlayer thickness was obtained based on heat transfer over flat plate rather than solving the Navier-Stokes equations as adopted by Cooper [26] and Van Ouwerker [37]. The solution was obtained for a case when the time exponent is 0.5. The model (curve 4) underpredicted all the data at atmospheric pressure as seen in Fig. 16 with MAE in the range 38.6 – 44.4% and error at departure 19.3 – 34.9%. Contrary to the underprediction at atmospheric pressure, the model overpredicted the data at 0.5 and 0.15 bar as seen in Figs. 17 and 18. Again, the reasonable performance at atmospheric pressure and the poor performance at sub-atmospheric pressure may be due to the assumption of 0.5 exponent in the growth law, which was used to estimate Reynolds number to obtain the microlayer thickness. Again, for the model to be more general, the time exponent should be formulated as a function of operating conditions. The same authors [27] combined their microlayer evaporation model with the relaxation boundary layer model suggested by them as discussed in the previous section and incorporated the inertia-controlled growth in one model. This model is described here as curve 4*. In this model, the contribution of each mechanism was combined similar to the total electric resistance connected in parallel, rather than the additive approach adopted by other researchers. In other words, the model prediction approaches the most dominant mechanism. This model exhibited excellent prediction at all pressures where it gave MAE 3.2 – 21.5% at 1 bar, 17.6 – 27.7% at 0.5 bar and 15.6 – 22.9% at 0.15 bar. The over MAE of this model is 16.5%. It is worth noting that the performance of this model that combines all mechanisms in a complex way was not better than the simple “relaxation boundary layer” model suggested by them and discussed in the above section.

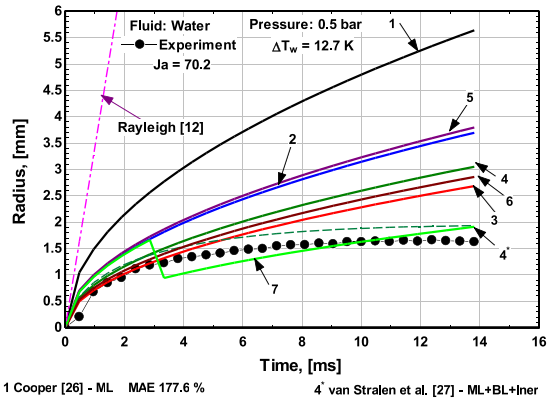


(a) $\Delta T_w = 12.7$

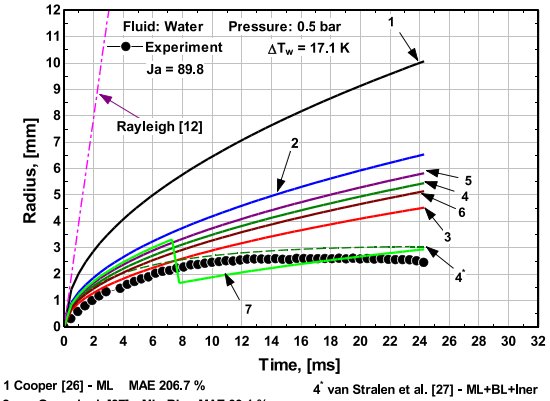


(b) $\Delta T_w = 17.1$

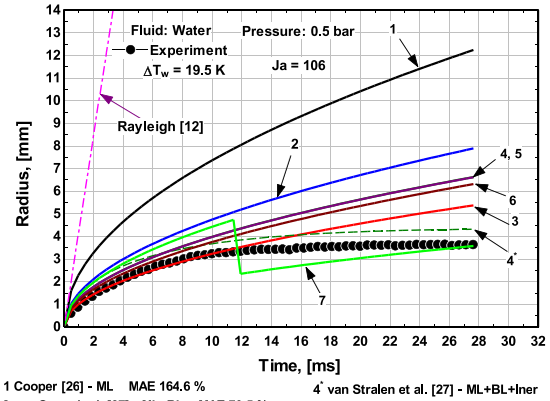


(c) $\Delta T_w = 19.5$

**Fig. 17.** Assessment of microlayer-based models at $P = 0.5$ bar.

5. Mei et al. [39] solved the conjugate heat transfer problem including microlayer evaporation only as a contributing mechanism for bubble growth. The model was sharing the functional form of the initial microlayer thickness given by Cooper [26] except that they left the front constant to be determined empirically. The difference between the Cooper [26] and the Mei et al. [39] model was small at low superheat then the dif-

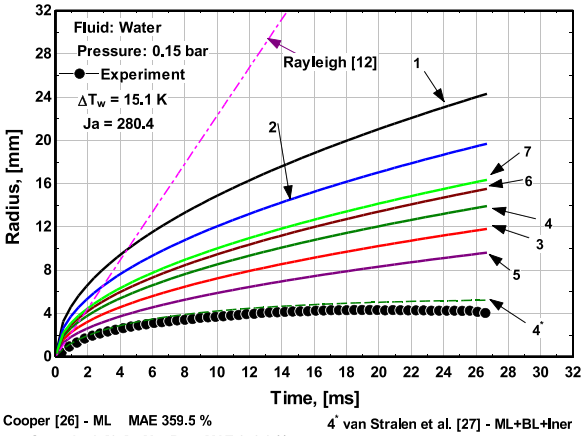


(a) $\Delta T_w = 15.1$

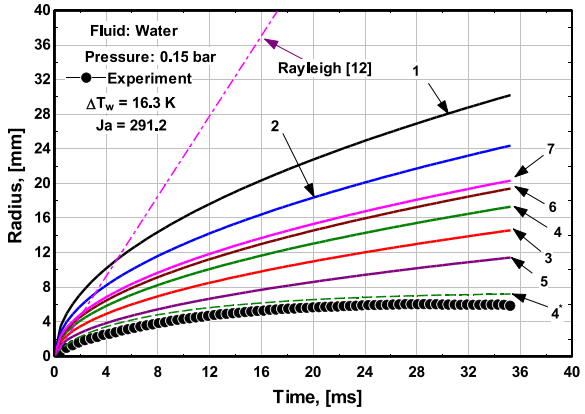


(b) $\Delta T_w = 16.3$

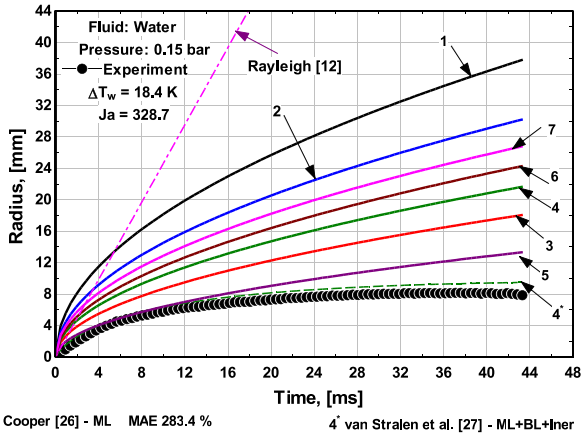


(c) $\Delta T_w = 18.4$

**Fig. 18.** Assessment of microlayer-based models at $P = 0.15$ bar.

ference is getting larger as superheat increases (the values by the Mei et al. model are always smaller than those predicted by the Cooper model). Fig. 16 indicates that the model gave reasonable prediction at atmospheric pressure except the lowest superheat with MAE in the range 11.5 – 42% and error at departure 16.8 – 58.9%. Similar to Cooper model, the model overpredicted the data significantly at 0.5 and 0.15 bar as seen in Figs. 17 and 18.

6. Prisnyakov [18] included the microlayer contribution in a different way. He did not model the initial microlayer thickness as was done in the above models. Instead, he applied the first law of thermodynamics and assumed that the total heat transfer rate entering the bubble is the sum of the heat flux at the contact region and the heat flux at the curved part of the bubble. The heat flux in the contact region was assumed equal to the wall heat flux. Thus, his model depends on the average wall heat flux. At atmospheric pressure as seen in Fig. 16, the model performance was nearly similar to the microlayer model given by Van Stralen et al. [27], i.e. it always predicts slightly lower values at all superheats. It underpredicted the experimental data by MAE 39.8 – 46.7% and error at departure 22.8 – 37.4%. The model overpredicted the data at 0.5 and 0.15 bar as seen in Figs. 17 and 18.
7. Buyvich and Webbon [41] applied the mechanical energy equation rather than the momentum equation and assumed bubble growth due to microlayer and boundary layer evaporation. The microlayer thickness was obtained from the Navier-Stokes equation and the boundary layer evaporation was modelled using the homogeneous growth model. It was assumed that the bubble has different shapes during its growth period, i.e. the shape changes from hemispherical to sphere. Thus, they could give an equation to predict the time at which the transition from shape to shape occurs. Fig. 16a indicates for the lowest superheat case that the model (curve 7) is one continuous curve indicating that the bubble grows with hemispherical shape. Increasing the superheat, as seen in Figs. 16b-c, the model is a two-part curve, where the bubble grows as a hemisphere for few milliseconds then the shape changes to a sphere. The two-part curve became very clear in Fig. 17. In other words, the sudden drop observed at some conditions is due to the two different equations used in the description of the bubble growth in this model. The model exhibited reasonable prediction at 1 and 0.5 bar as seen in Figs. 16 and 17 with MAE in the range 6.9 – 32.6% and 23.5 – 29.2% respectively and error at departure 2.4 – 39% and 1.6 – 20.7%, in the same order. On the contrary, at the lowest pressure, Fig. 18 demonstrates that the model overpredict the data significantly. This can be attributed to the fact that the predicted time at which transition from hemispherical to spherical growth occurs is extremely larger than the bubble growth period at the lowest pressure. This is obvious from observing one continuous curve that represent the hemispherical growth stage. At 0.5 bar, this transitional time occurred after nearly 50% of the growth period while the hemispherical growth period was much shorter at atmospheric pressure. It is worth mentioning that this model left the growth constant to be determined empirically without any recommendation. For the sake of comparison, a value $\pi/2$, which is in the mid-range was used (it should be between 1 and $\sqrt{3}$).

It may be concluded from the above comparison that the microlayer evaporation only or combined with boundary layer evaporation could not explain the bubble growth at the three examined pressures. There is only some partial agreement at some experimental conditions. This is contrary to the boundary layer models discussed above, which seems to explain the bubble growth in nucleate boiling much better than the microlayer-based models.

## 5. Recommendation

Based on the results of evaluating 11 models for bubble growth in homogeneous boiling and 20 models in heterogeneous boiling, only the “relaxation boundary layer” model suggested by Van Stralen [25] predicted all the data very well in terms of trend and values. It predicted all data with MAE 16.2% and error at departure of 15.3%. The limitation of this model is that the time and radius at departure must be known in advance. In the above comparison, the departure time and radius were taken directly from the experimental data. Accordingly, for the Van Stralen model to be generalized, accurate models for bubble departure radius and time are needed. To get an idea about the effect of superheat and pressure on departure radius and time, the experimental data are plotted in Fig. 19. The figure indicates that for a fixed pressure, the departure radius and departure time increase as superheat increases. Additionally, at the lowest pressure (0.15 bar), the departure radius and time increase at a higher rate compared to the 1 and 0.5 bar. The increase of departure radius with superheat is due to the increase in the excess enthalpy in the boundary layer around the bubble which increases the bubble growth rate and size. The increase in departure time with superheat can be attributed to the fact that as the superheat increases the initial bubble growth rate becomes larger and thus the bubble grows with a hemispherical shape with larger inertia force for a longer period, which means that the size of the bubble contact area becomes larger, see Mahmoud and Karayiannis [9] for more details. Accordingly, the surface tension force which keep the bubble attached to the surface dominates for a longer period and thus the bubble takes time for the buoyancy force to overcome the attaching forces (surface tension and inertia).

As mentioned above, to generalize the Van Stralen [25] model, models for departure radius and time are required. Accordingly, it is important to evaluate existing bubble departure models in the present section using the experimental data. Mohanty and Das [44] and Mahmoud and Karayiannis [10] conducted a review study which included a section on bubble dynamics and summarized the bubble departure models. Due to space limitation, the interested reader is referred to these references for more details about the equations. In this section, 19 models were selected for comparison with the experimental bubble departure radius and the results of comparison are summarized in Table 6. It demonstrated that five models [46,49,51,53,56] predicted the departure radius very well at atmospheric pressure while none of the models could predict the departure radius at 0.5 and 0.15 bar.

In literature, there is no correlations/models to predict the bubble departure time directly. Instead, the departure time was correlated with the departure diameter in the form $fD_d^n$. It is expected that the predicted departure time will not be accurate as well, since the comparison in Table 6 indicated that there is no general model for the prediction of bubble departure diameter. It may be concluded from this discussion that there is no general model for the prediction of bubble departure diameter and departure time. It is well known that bubble departure depends on the instantaneous local forces acting on the bubble during its growth, which are difficult to determine precisely. These forces depend significantly on the operating conditions and it is difficult to have a phenomenological model that capture the departure phenomenon at all pressures. Accordingly, the bubble departure data in this study were correlated for the sake of recommending a closed form model to predict the bubble growth rate, departure diameter and departure time (frequency). The best fit equation for the prediction of bubble

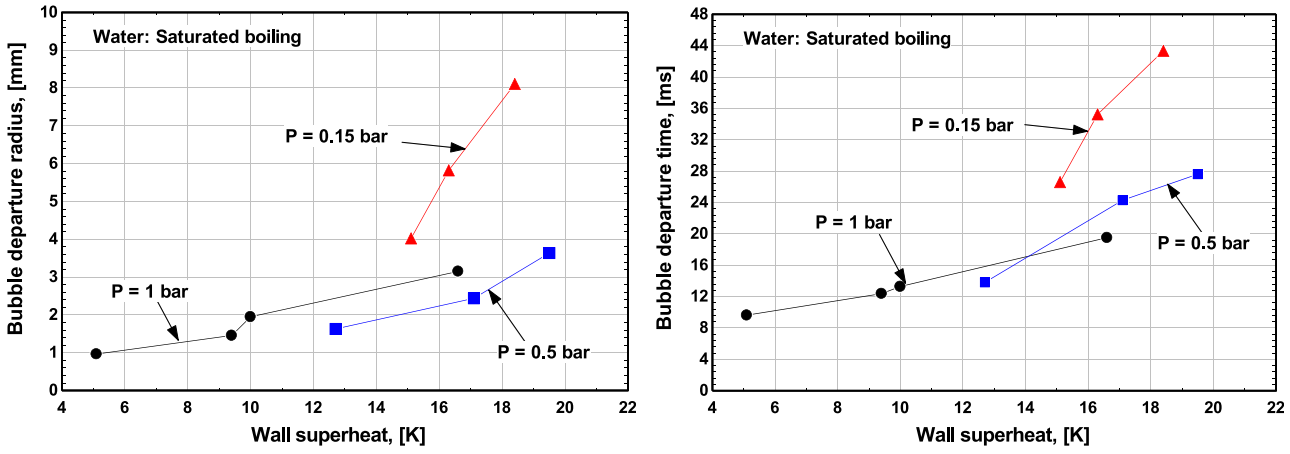


**Fig. 19.** Effect of pressure and superheat on (a) departure radius and (b) departure time.

**Table 6**
Evaluation of bubble departure models.

| Model | $P = 1$ bar | | | | $P = 0.5$ bar | | | $P = 0.15$ bar | | | MAE % @@Average |
|---|---|---|---|---|---|---|---|---|---|---|---|
| | MAE % | | | | MAE % | | | MAE % | | | |
| | 5.6K | 9.4K | 10K | 15K | 12.7K | 17.1K | 19.5K | 15.1K | 16.3K | 18.4K | |
| Saini et al. [46] | 15.6 | 28 | 2 | 5.4 | 188.5 | 159.2 | 98.2 | 321 | 213.9 | 163.9 | 119.57 |
| Fritz [47] | 21.8 | 19.6 | 39.8 | 62.8 | 26.3 | 50.8 | 67 | 69.3 | 78.8 | 84.1 | 52.03 |
| Ruckenstein [48] | 98.6 | 98.2 | 98.5 | 98.5 | 94.8 | 94.9 | 95.9 | 89.7 | 92.1 | 93.1 | 95.43 |
| Cole [49] | 11.6 | 2.1 | 22 | 27.7 | 129.1 | 105.9 | 57.5 | 256.4 | 165.7 | 123.4 | 90.14 |
| Cole and Rohenow [50] | 27.9 | 15.6 | 36.8 | 60.9 | 60.9 | 7.4 | 28 | 152.7 | 74.5 | 30 | 49.47 |
| Kipper [51] | 12.6 | 15 | 6.4 | 0.7 | 254.3 | 251.5 | 180.9 | 701.8 | 513.3 | 436.8 | 237.33 |
| Van Stralen [52] | 86.1 | 87.3 | 90.1 | 92 | 79.4 | 83.3 | 87.8 | 81 | 86.2 | 88.8 | 86.2 |
| Stephan [53] | 4.6 | 12.1 | 10.9 | 18.1 | 172.2 | 144.2 | 86.8 | 376.1 | 255 | 198.5 | 127.85 |
| Kutateladze and Gogonin [54] | 59.5 | 70.2 | 77.4 | 84.4 | 62.6 | 721.3 | 80.3 | 69.9 | 78.5 | 83.1 | 138.72 |
| Jensen and Memel [55] | 109.3 | 52.3 | 15.7 | 20.3 | 92.8 | 45.7 | 3.7 | 75.2 | 26.5 | 1.2 | 44.27 |
| Zeng et al. [56] | 9.4 | 19.2 | 3.1 | 2.9 | 266.9 | 264 | 190.9 | 730.6 | 535.4 | 456.2 | 247.86 |
| Lee et al. [29] | 41.3 | 8.9 | 7.6 | 28.5 | 481.1 | 603 | 513.2 | 2684.3 | 2141.1 | 2026.5 | 853.55 |
| Kim and Kim [57] | 55.9 | 47.7 | 15.5 | 5.1 | 160.9 | 114.5 | 57.6 | 173.4 | 99.3 | 61.5 | 79.14 |
| Phan et al. [58] | 48.7 | 66.1 | 74.6 | 84.3 | 68.9 | 79.3 | 86.1 | 87.1 | 91.1 | 93.3 | 77.95 |
| Phan et al. [59] | 52.2 | 68.5 | 76.4 | 85.4 | 74.1 | 82.72 | 88.4 | 91.1 | 93.9 | 95.4 | 80.812 |
| Nam et al. [60] | 295.9 | 161.1 | 95.6 | 20.9 | 139.4 | 59.7 | 7.1 | 0.2 | 31.1 | 48.6 | 85.96 |
| Cho and Wang [35] | 76.6 | 37 | 4.6 | 26.6 | 38 | 1.1 | 29.4 | 39.2 | 57 | 66.7 | 37.62 |
| Cole and Shulman [61] | 73.5 | 14.5 | 14.3 | 47 | 109.8 | 40 | 6.1 | 201.7 | 108.4 | 55.1 | 67.04 |
| Golorin et al. [62] | 59.6 | 62.3 | 70.6 | 76.2 | 37.9 | 49.5 | 63 | 41.6 | 57.5 | 65.7 | 58.39 |
| | Error in Departure time | | | | | | | | | | |
| Saddy and Jameson [45] | 14 | 7 | 9.8 | 19.8 | 54 | 6.5 | 2.1 | 88.9 | 50 | 32 | 32.2 |

departure radius was found to be:

$$R_d = C_1 Ja^{C_2}\left[\sqrt{\frac{\sigma}{g\Delta\rho}}\right]^{C_3}, \ [in\ mm] \tag{86}$$

$$C_1 = -143,527P_r^2 + 750.63P_r + 0.286$$

$$C_2 = -1.21\ln P_r - 5.352$$

$$C_3 = -1.287\ln P_r - 6.420$$

The empirical constants $C_1$, $C_2$, $C_3$ were found to correlate well with the reduced pressure $P_r = P/P_C$, i.e. the effect of pressure on departure size is captured through the reduced pressure. The same was conducted to correlate the bubble departure time with the average wall superheat and the empirical constants as a function of the reduced pressure, as given by Eq. (87). The new empirical models Eqs. (86) and ((87)) predicted the experimental departure radius of all data with MAE 8.2% and departure time with MAE 9.75%.

$$t_d = C_4\Delta T_w^{C_5}, [in\ sec] \tag{87}$$

$$C_4 = 24\times 10^{-6}\exp(906.48P_r)$$

$$C_5 = 2.82\exp(-233.5P_r)$$

Because only three pressures and three superheats were tested in the current study, it is important to examine whether the new suggested empirical model predicts the correct trend or not. Saddy and Jameson [45] applied the potential flow theory to a growing bubble on a nucleation site including the radial expansion and translational motion of the centre of mass of the bubble. Their model resulted in a balance between liquid inertia, buoyancy, surface tension and vapour inertia forces. The bubble growth was divided into two stages, expansion (growth) and transition (neck formation), and the Scriven [11] bubble growth model was used to

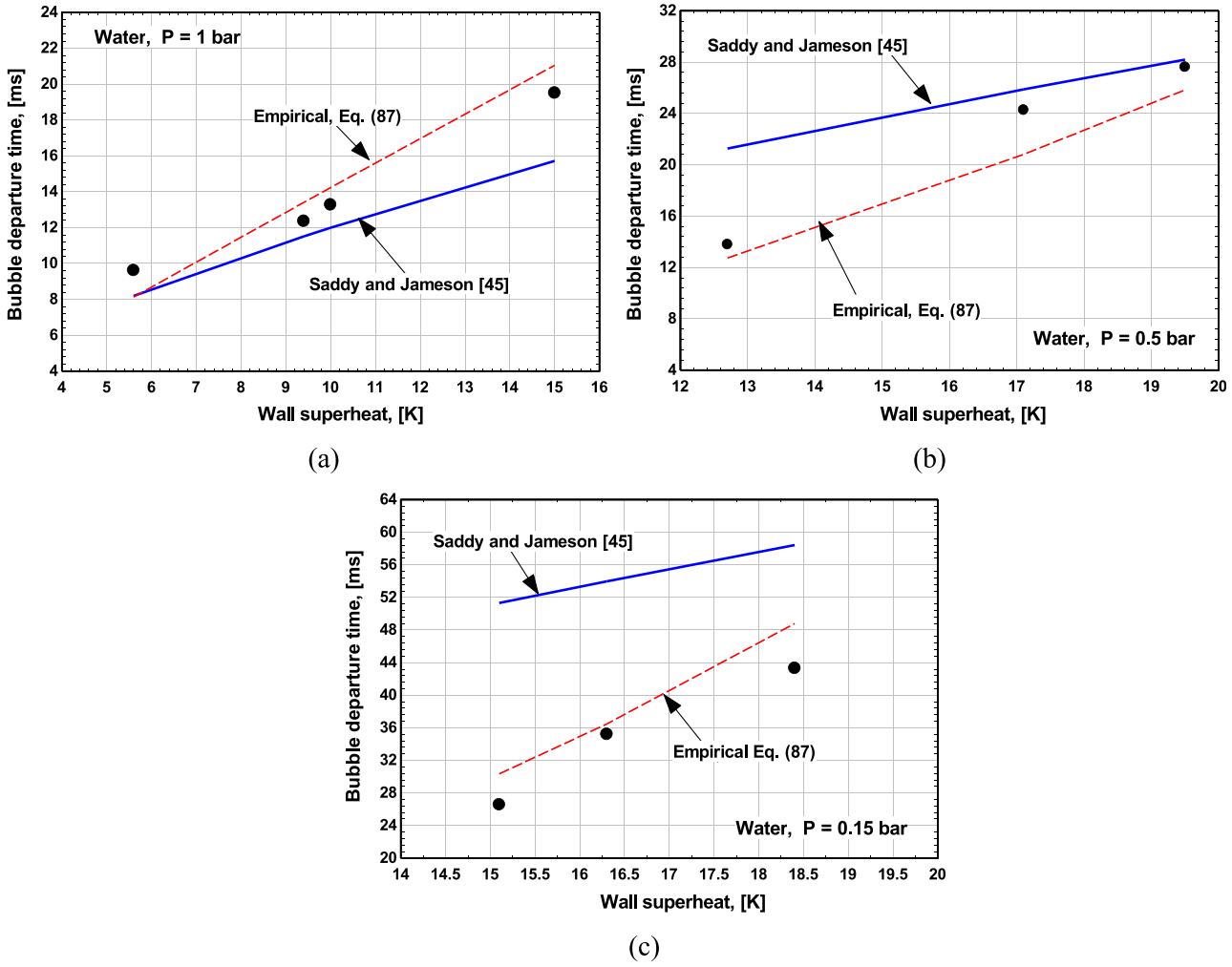


**Fig. 20.** Effect of superheat on the measured departure time compared with the theoretical model by Saddy and Jemeson [45] and the empirical model in Eq. (87): (a) $P = 1$ bar, (b) $P = 0.5$ bar and (c) $P = 0.15$ bar.

**Table 7**
Comparison of Eqs. (86) and (87) with experimental data from literature.

| Author | Conditions | | Measured | | Predicted | | % Error | |
|---|---|---|---|---|---|---|---|---|
| | P, [bar] | $\Delta T_w$, [K] | $R_d$, [mm] | $t_d$, [ms] | $R_d$, [mm] | $t_d$, [ms] | $E_d$@@% | $E_t$@@% |
| Yabuki and Nakapebbu [63] | 1 | 9 | 1.57 | 16.48 | 1.56 | 12.54 | 0.2 | 23.9 |
| Van Stralen et al. [64] | 0.13 | 19.7 | 13.62 | 77.32 | 14.68 | 62.14 | 7.8 | 19.6 |
| Jung and Kim [65] | 1 | 9 | 1.935 | 14.14 | 1.567 | 12.54 | 19 | 11.3 |

estimate the velocity and acceleration. Based on that they gave the following theoretical expression for the time at which the bubble forms the neck and enters the departure stage:

$$t_{crit}^{3/2} = \frac{273\beta_{sc}\sqrt{\alpha_L}}{256g}\left(1 + \frac{16R_c\sigma}{91\rho_L\beta_{Sc}^4\alpha_L^2}\right) \tag{88}$$

The above theoretical model was evaluated using our experimental data and the result of comparison is summarized in the last row in Table 6. It is obvious that Eq. (88) exhibited good prediction at $P = 1$ and 0.5 bar except the lowest superheat at 0.5 bar but could not predict the data at 0.15 bar. This theoretical model was used to test the trend predicted by our new empirical model given by Eq. (87) and the comparison is depicted in Fig. 20 for the three tested pressures. It is obvious that the new empirical model agrees with the theoretical model at all pressures in predicting the correct trend, i.e. departure time increases as superheat increases. Additionally, the theoretical model and empirical model gave nearly similar performance at atmospheric pressure. At sub-atmospheric pressure, the theoretical model exhibited large deviations at the lowest superheat for the 0.5 bar and significant overprediction as the pressure decreased to 0.15 bar. To verify the new empirical model for bubble departure radius Eq. (86)), comparison was conducted with the experimental data of Yabuki and Nakapeppu [63], Van Stralen et al. [64], and Jung and Kim [65] and the performance of Eqs. (86) and ((87) is summarized in Table 7. The new empirical models predicted the data of these researchers very well with error 0.2 – 19% for departure radius and 11.3 – 23.4% for departure time. Due to the fact that the new empirical models Eqs. (86) and ((87)) predict the correct trend and values very well, it may be recommended to be used with the Van Stralen [25] bubble growth model. To test the performance of the new recommendation, Eqs. (86) and (87) were used with the Van Stralen

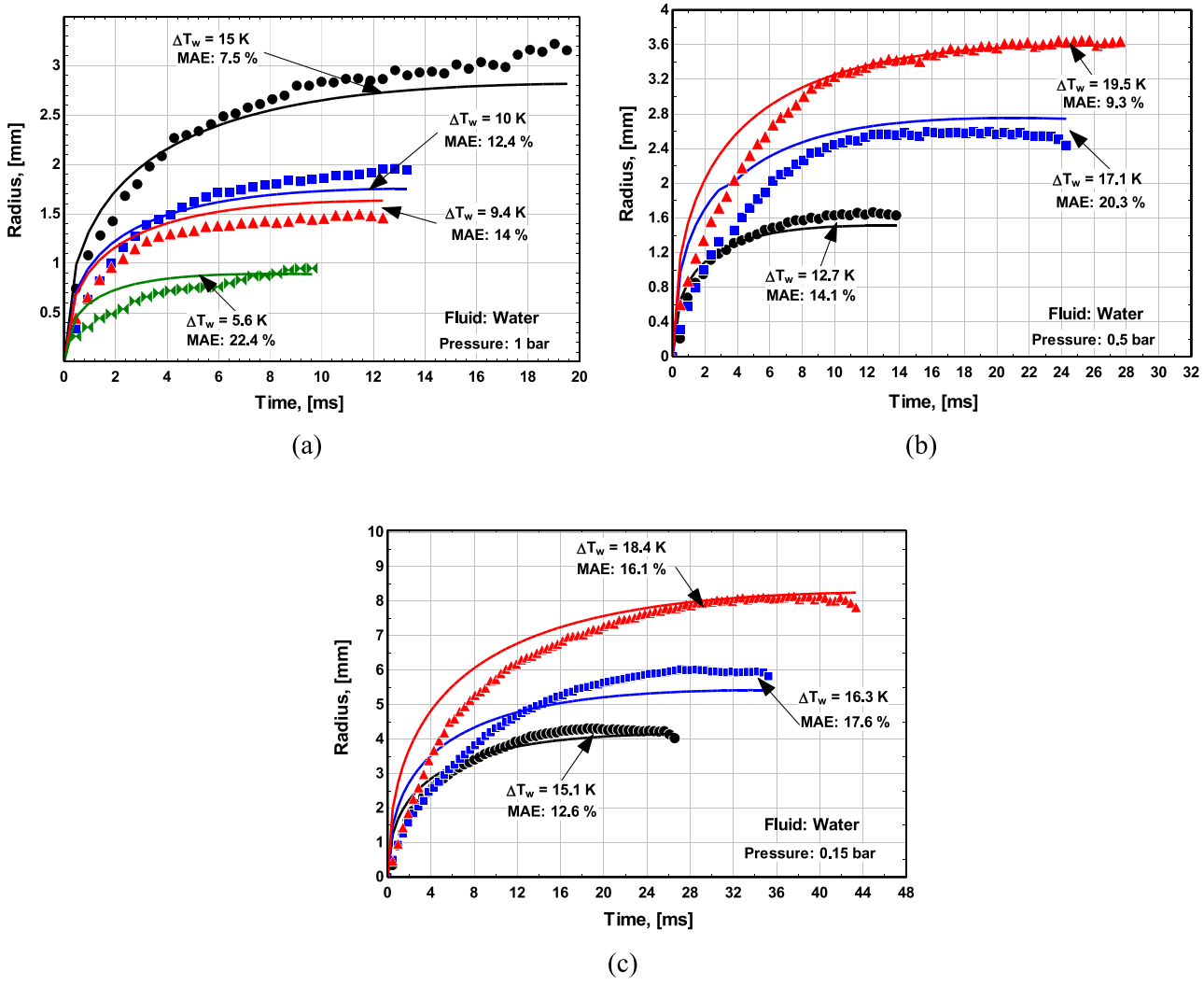


**Fig. 21.** Comparison of the new recommended model with the experimental data: (a) $P = 1$ bar, (b) $P = 0.5$ bar and (c) $P = 0.15$ bar.

[25] model and the results of comparison are shown in Fig. 21 for the three pressures. It is obvious that the model predicted all data in terms of trend and low MAE very well.

## 6. Conclusions

Bubble growth was measured in saturated boiling of deionized water on a smooth copper surface at three pressures (1, 0.5 and 0.15 bar) and different superheat. The experimental data were used to evaluate 11 models for bubble growth in homogeneous boiling and 20 models for bubble growth in heterogeneous boiling. The following points can be concluded:

1. There is nearly general agreement amongst researchers on bubble growth in homogeneous boiling, which appears from the work by [11,14,15,17,19] who nearly reached the same solution with small differences. On the contrary, several models were suggested for heterogeneous boiling with significant differences. The differences arise from the assumed bubble growth mechanism and the complex temperature distribution around the bubble, which is difficult to verify experimentally.
2. The evaluation of homogeneous growth models demonstrated that some models [11,14,15,19–21,33] predict part of the growth curve at atmospheric pressure in the early rapid growth stage (up to 4 – 6 ms) followed by significant overprediction in the slow growth stage (large deviation at departure). Also, there is no significant difference between the complex models that combine inertia and asymptotic stages [19–21] compared to the simple asymptotic models. At 0.5 bar, the models by Prisnyakov [18] and Abdollahi et al. [32] gave reasonable predictions while other models [11,14,15,19–21,33] exhibited poor prediction. At 0.15 bar, none of the models could predict the experimental data. Thus, the homogeneous growth models should be used in heterogeneous boiling with precautions.
3. In heterogeneous boiling, the evaluation of the empirical models indicated that the Du et al. [30] model gave the best performance at atmospheric pressure with MAE 8.6 – 18% while the Benjamin and Balakrishnan [31] model gave the best performance at sub-atmospheric pressures. It predicted the data with MAE 14.6 – 29.4%. The better performance of this model at sub-atmospheric pressure may be due to the inclusion of Archimedes number that considers the effect of gravity, which was ignored by all other empirical models. All examined empirical models could not predict the exact experimental trend.
4. The evaluation of boundary layer-based bubble growth models indicated that at atmospheric pressure, six models [20,23–25,33,34] exhibited excellent agreement with the experimental data. The Cho and Wang [35] exhibited the poor performance at atmospheric pressure. On the contrary, this model [35] and the Van Stralen [25] model exhibited excellent prediction at sub-

atmospheric pressure. In terms of trend and MAE, the best performing boundary layer-based model at the three tested pressures is the Van Stralen [25] model.

5. The models that were based on microlayer evaporation only could not explain the bubble growth at the three examined pressures. There is only some partial agreement at some experimental conditions. This, combined with the above point, may lead to the conclusion that bubble growth in saturated boiling of water occurs mostly due to evaporation from the superheated boundary layer around the bubble. The microlayer could be only a contributing mechanism.
6. All examined models failed to predict the correct experimental trend (rapid and slow growth stages) except the model by Van Stralen [25], which assumed that bubble growth is a "relaxation phenomenon", i.e. the superheat decreases exponentially during the whole growth period (from the beginning to departure). The relaxation time was considered equals the bubble departure time and the fraction of the bubble surface ($b^*$) which is surrounded by the relaxation layer was a function of the bubble departure radius as defined in Eq. (37). The comparison with this model indicated that at atmospheric pressure, this fraction is always larger than 1 (the bubble is fully surrounded with the relaxation layer) while it was smaller than 1 at sub-atmospheric pressure (part of the bubble is surrounded by the relaxation layer). This agrees with the fact that bubble size at sub-atmospheric pressure is much larger than the wall thermal boundary layer. This model was not widely used in literature because it requires the knowledge of departure time and radius in advance.
7. To generalize the Van Stralen [25] relaxation model, 19 models for bubble departure radius were evaluated in the present study. It demonstrated that five models [46,49,51,53,56] predicted the departure radius very well at atmospheric pressure while none of the models could predict the departure radius at 0.5 and 0.15 bar. Thus, there is no general model for departure radius can be recommended to be used with the Van Stralen [25] at all pressures. This encouraged the present authors to suggest empirical models for departure radius (Eq. (86)) and time (Eq. (87)) as a function of superheat and reduced pressure. The two empirical models were compared with some data from literature and exhibited excellent performance. Additionally, the empirical model for departure time agreed with the trend predicted by the theoretical model given by Saddy and Jameson [45], which verify that the functional form of our empirical model is correct.
8. The new suggested empirical models are recommended to be used with the Van Stralen [25] model for the prediction of bubble growth rate. This recommendation is valid for saturated boiling of water on metallic surfaces and may need further validation using other fluids and substrate materials.

## Author statement

T. G. Karayiannis planned the project. M. M. Mahmoud designed and constructed the original experimental facility under the supervision of T.G. Karayiannis. M. M. Mahmoud carried out the experiments and presented the results and first draft for changes and additions to T.G. Karayiannis. Both authors discussed the results and contributed to the final manuscript.

## Declaration of Competing Interest

The authors declare that they have no known competing financial interests or personal relationships that could have appeared to influence the work reported in this paper.

## Data availability

Data will be made available on request.

## Acknowledgements

The work was carried out with the support of the Engineering and Physical Sciences Research Council of the UK, under Grant: EP/S019502/1.

## Appendix A

Tables A1 and A2

**Table A1**
Bubble growth models in homogeneous boiling.

| Author | Model |
|---|---|
| Fritz and Ende [16] | $R = (2/\sqrt{\pi})Ja\sqrt{\alpha_L t}$ |
| Plesset and Zwick [15] | $R = \sqrt{12/\pi}Ja\sqrt{\alpha_L t}$ |
| Forster and Zuber [14] | $R = \sqrt{\pi}Ja\sqrt{\alpha_L t}$ |
| Scriven [11] | $R = \sqrt{12/\pi}[h_{fg}/\{h_{fg} - (c_{pL} - c_{pv})\Delta T\}]Ja\sqrt{\alpha_L t}$ |
| Forster [33] | $R = 0.5[1 + \sqrt{1 + 2\pi/Ja}]\sqrt{\pi}Ja\sqrt{\alpha_L t}$ |
| Prisnyakov [18] | $R = (4/3\sqrt{\pi})Ja\sqrt{\alpha_L t}$ |
| Avdeev and Zudin [19] | $R = \{\sqrt{3/\pi}Ja\psi + \sqrt{(3/\pi)(Ja\psi)^2 + 2Ja}\}\sqrt{\alpha_L t}$ |
| | $\psi = [1 + \sqrt{\pi/2}\{1/\sqrt{1-N} - 1\}]$, $N = c_{pL}\Delta T/h_{fg} = \varepsilon Ja = \rho_v/\rho_L Ja$ |
| Abdollahi et al. [32] | $R = \sqrt{\alpha_L/\pi}Ja\sqrt{t}erf(\beta\sqrt{t}) + R_0$ |
| | $\beta = \frac{\pi}{\sqrt{6}}\sqrt{\frac{c_{pL}}{\alpha_L T_{sat}}}\frac{1}{Ja^{3/2}}(T_\infty - T_{sat})$ $R_0 = \frac{2\sigma T_{sat}}{\rho_v h_{fg}\Delta T}$ |
| Mikic et al. [20] | $R^+ = \frac{2}{3}[(t^+ + 1)^{3/2} - (t^+)^{\frac{3}{2}} - 1]$ |
| | $R^+ = \frac{AR}{B^2}$, $t^+ = \frac{A^2 t}{B^2}$, $A = [\frac{2}{3}\frac{\rho_v h_{fg}\Delta T}{\rho_L T_{sat}}]^{1/2}$, $B = 2\sqrt{\frac{3}{\pi}\alpha_L}$Ja |
| Theofanous and Patel [19] | $R^+ = \frac{2}{3\beta}[(\beta^2 t^+ + 1)^{3/2} - (\beta^2 t^+)^{\frac{3}{2}} - 1]$, $R^+ = \frac{R}{B^2/A}$, $t^+ = \frac{t}{B^2/A^2}$, |
| | $A = [\frac{2}{3}\frac{\rho_v h_{fg}\Delta T}{\rho_L T_{sat}}]^{1/2}$, $B^2 = (\frac{12\alpha_L}{\pi})\{\frac{\rho_L c_{pL}(T_\infty - T_{sat})}{h_{fg}\rho_v(P_\infty)}\}^2$, $\beta = \sqrt{\frac{h_{fg}\rho_v(P_\infty)(T_\infty - T_{sat})}{T_{sat}\ (P_v(T_\infty) - P_\infty)}}$ |
| Avdeev and Zudin [19] | $r = \frac{r_1}{(1+F^3)^{1/3}}$, $r = \frac{R}{l}$, $l_{ch} = \frac{\alpha Ja^2}{U}$, $U = \sqrt{\frac{2\Delta P_0}{3\rho_L}}$, $F = \frac{2}{3}\frac{\tau^{1/4}}{\psi}$, $\tau = \frac{t}{t_0}$, $t_0 = \frac{\alpha_L Ja^2}{U^2}$ |
| | $r_1 = \frac{4}{3}[(1 + \sqrt{\tau})^{3/2} - 3(1 + \sqrt{\tau})^{\frac{1}{2}} + 2]$, $\psi = [1 + \sqrt{\frac{\pi}{2}}\{\frac{1}{\sqrt{1-N}} - 1\}]$, $N = \frac{c_{pL}\Delta T}{h_{fg}} = \frac{\rho_v}{\rho_L}Ja$ |

**Table A2**
Bubble growth models in heterogeneous boiling.

| Author | Model |
|---|---|
| Zuber [23] | $R = b(\frac{2}{\sqrt{\pi}})[1 - \frac{q_w\sqrt{\pi\alpha_L t}}{2k_L\Delta T}]Ja\sqrt{\alpha_L t}$ |
| | $b$: curvature correction factor (between 1 and $\sqrt{3}$) with recommended value of $\pi/2$ |
| Forster [33] | $R = \frac{\pi}{2}[\frac{2}{\sqrt{\pi}}Ja\sqrt{\alpha_L t} - \frac{1}{\pi}\frac{Ja^2\alpha t}{\delta_{th}} + \frac{7}{9\pi^{\frac{3}{2}}}\frac{(Ja^2\alpha_L t)^{\frac{3}{2}}}{\delta_{th}^2} - \ldots.]$ |
| | First three terms of a series solution |
| Han and Griffith [24] | $R = R_c + \frac{\varphi_s\varphi_c}{\varphi_v}\frac{\rho_L c_{pl}\alpha_L}{\rho_v h_{fg}}\{\frac{2\vartheta_w}{\sqrt{\pi t}}t^{\frac{1}{2}} - \frac{\vartheta_w - \vartheta_\infty}{\delta}\frac{\delta^2}{4\alpha_L}[\frac{4\alpha_L t}{\delta^2}\mathrm{erf}\frac{\delta}{\sqrt{4\alpha_L t}} + \frac{2}{\sqrt{\pi}}\frac{\sqrt{4\alpha_L t}}{\delta}\exp(-\frac{\delta^2}{4\alpha_L t}) - 2\mathrm{erf}\frac{\delta}{\sqrt{4\alpha_L t}}]\} + \frac{\varphi_b h_v\vartheta_w}{\varphi_v\rho_v h_{fg}}t$ |
| | $\varphi_c$ : curvature factor $1 < \varphi_c < \sqrt{3}$, $\varphi_s$:surface factor $(1+\cos\theta)/2$, $\varphi_b$ is base factor $\sin^2\theta/4$, $\varphi_v$: volume factor $(2+\cos(2+\sin^2\theta))/4$ $h_v$: vapour heat transfer coefficient. $\vartheta_w$ : degree of superheat, $R_c$ is cavity mouth radius, $\delta = \sqrt{\pi\alpha_L t_{wt}}$ |
| Cole and Shulman [28] | $R = 2.5Ja^{0.75}\sqrt{\alpha_L t}$ |
| Cooper [26] | $R = 2.5\frac{Ja}{Pr^{1/2}}\sqrt{\alpha_L t}$ (Microlayer only) |
| | $R = [0.8\sqrt{3/\pi}Pr^{1/2}][\frac{2}{0.8}\frac{\vartheta_{bulk}}{\psi}\sqrt{\nu}]\sqrt{t} + [\frac{2}{0.8}\frac{\vartheta_w}{\psi}\sqrt{\nu}]\sqrt{t}$ (microlayer and curved part) |
| | $\psi = \frac{\rho_v h_{fg}Pr}{\rho_L c_{pl}}$, $\vartheta_{bulk} = T_{bulk} - T_{sat}$, $\vartheta_w = T_w - T_{sat}$ |
| Prisnyakov [18] | $R = R_0 + \frac{2}{3}f_\theta Ja[2/\sqrt{\pi}\sqrt{\alpha_L t} + f_q N_3 t]$ |
| | $N_3 = \frac{q}{\rho_L c_{pL}\Delta T}$, $f_\theta = \frac{\frac{1}{2}(1+\cos\theta)}{\frac{1}{2}(1+\frac{1}{2}\cos\theta(1+\sin^2\theta))}$, $R_0 = \frac{2\sigma T_{sat}}{\rho_v h_{fg}\Delta T}$ $f_q = \frac{1}{2}(1-\cos\theta)$ |
| Mikic et al. [20] | $R^+ = (t^+)^{\frac{1}{2}}[1 - \vartheta\{(1+t_w^+/t^+)^{\frac{1}{2}} - (t_w^+/t^+)^{\frac{1}{2}}\}]$ (dimensionless form) |
| | $R^+ = AR/B^2$, $t^+ = A^2 t/B^2$, $t_w^+ = A^2 t_w/B^2$, |
| | $A = [\frac{\pi}{7}\frac{\rho_v h_{fg}\Delta T}{\rho_L T_{sat}}]^{1/2}$, $B = \sqrt{\frac{12}{\pi}\alpha_L}\mathrm{Ja}$, $\vartheta = \frac{T_w - T_\infty}{T_w - T_{sat}}$ |
| | $R = [1 - \vartheta(\sqrt{1 + t_w/t} - \sqrt{t_w/t})]2\sqrt{3/\pi}Ja\sqrt{\alpha_L t}$ (dimensional form) |
| Van Ouwerkerk [37] | $R = \{0.9\sqrt{2\nu_l}\frac{\rho_L}{\rho_v}[1 + \frac{2\pi h_{fg}^2(\nu_L/\alpha_L)(0.9)^2}{4(c_{pL}\Delta T)^2}]^{-1/2} + \frac{\sqrt{6}}{\sqrt{\pi}}\sqrt{\frac{\alpha_L}{\nu_L}}Ja\}\sqrt{t}$ |
| Labuntsov-Yagov [38] | $R = [0.3Ja + \sqrt{(0.3Ja)^2 + 12Ja}]\sqrt{\alpha_L t}$ |
| Van Stralen et al. [27] | $R = \frac{R_1 R_2}{R_1 + R_2}$ |
| | $R_1 = 0.8165t\sqrt{\frac{\rho_v h_{fg}\Delta T\exp-(t/t_g)^{1/2}}{\rho_L T_{sat}}}$, [Inertia term] |
| | $R_2 = 1.9544[\{b^*\exp-(t/t_g)^{1/2}\} + \frac{\Delta T_{lg}}{\Delta T}]Ja\sqrt{\alpha_L t} + 0.373Pr^{-1/6}\exp-(t/t_g)^{1/2}Ja\sqrt{\alpha_L t}$ |
| | $b^* = 1.3908\frac{R_2(t_d)}{Ja\sqrt{\alpha_L t}} - 0.1908Pr^{-\frac{1}{8}}$, $R_2$: [microlayer + relaxation layer] |
| Mei et al. [40] | $R = \sqrt{c/\varphi f(c)}Ja^{1/2}\sqrt{\alpha_L t}$ |
| | $\varphi = \frac{f(c)C_1^2 Pr}{c^3 Ja}$, $f(c) = 1 - \frac{3}{4}[1 - \sqrt{1-c^2}]^2 + \frac{1}{4}[1 - \sqrt{1-c^2}]^3$ |
| | $c = [(0.4134Ja^{0.1655})^{-6} + (1 - 0.1e^{-0.0005Ja})^{-6}]^{-1/6}$ |
| | $c_1 = 0.00525Ja^{0.752}Pr^{-0.5}(k_L/k_s)^{-0.113}(\alpha_L/\alpha_s)^{-0.117}$ |
| Buyevich and Webbon [41] | Hemispherical growth: $R = CJa[1 + N_m]\sqrt{\alpha_L t}$ |
| | Spherical growth: $R = CJa\sqrt{\alpha_L t}$ when $N_m \le 1$ |
| | C is the constant in $R = CJa\sqrt{\alpha_L t}$, $N_m = \frac{1}{1.294C\sqrt{Pr}}$ |
| | $t_1^{3/2} + \frac{6}{(1-\rho_v/\rho_L)[CJa(1+N_m)]^2}\frac{\sigma/\rho_l}{g\alpha_L}t_1^{1/2} = \frac{3}{4}\frac{(1+\rho_v/5\rho_l)CJa(1+N_m)\sqrt{\alpha_l}}{(1-\rho_v/\rho_L)g}$ |
| | $t_1$: the end of the hemispherical growth, $C$ was left to be empirical |
| Benjamin and Balakrishnan [31] | $R = 0.5BAr^{0.135}Ja^{1/2}\sqrt{\alpha_L t}$ |
| | $Ar = (g/\nu_L^2)\cdot(\sigma/\rho_L g)^{3/2}$, $B = 1.55$ [water, $CCl_4$, n-hexane] |
| | $B = 1/1.55$ [n-pentane, acetone] |
| Lee et al. [29] | $R^+ = 11.2t^{+1/5}\tanh 0.345t^{+4/5} + R_0^+$ |
| | $R^+ = R/R_c$, $t^+ = t/t_c$, $R_0^+ = 0.072$, $t_c = \frac{9}{2}Ja\alpha_L\frac{\rho_L R_d}{\sigma}$, $R_c = \sqrt{\frac{27}{2}}Ja\alpha_L\sqrt{\frac{\rho_L R_d}{\sigma}}$ |
| Lesage et al. [34] | $[R + \sqrt{R^2 + R_c^2} - R_c] = (4/\sqrt{\pi/3})Ja\sqrt{\alpha_L}(\sqrt{t} - \sqrt{t + \delta_0^2/(\pi\alpha_L/3)} + \sqrt{\delta_0^2/(\pi\alpha_L/3)})$ |
| | $\delta_0 = \sqrt{\pi\alpha_L t_{wt}}$, $R_c$: cavity mouth radius |
| Abdullahi et al. [32] | $R = 6.9577\sqrt{3Ja\sqrt{\alpha t}}erf(3.8323\sqrt{t}/t_c) + 0.028425R_c$, $Ja > 24$ |
| | $R = 2.5\sqrt{3Ja\sqrt{\alpha t}}erf(0.19660.1966/t_c) + 0.7R_c$, $Ja < 15$ |
| | $R = \sqrt{\alpha_L/\pi}Ja\sqrt{t}erf(\sqrt{\beta t}) + R_0$, $15 < Ja < 24$ |
| | $t_c = \frac{9}{4}\alpha_L Ja\frac{\rho_L R_d}{\sigma}$, $R_c = \frac{\sqrt{27}}{3}\alpha_L Ja\sqrt{\frac{\rho_L R_d}{\sigma}}$, $\beta = \frac{\pi}{\sqrt{6}}\sqrt{\frac{c_{pL}}{\alpha_L T_{sat}}}\frac{1}{Ja^{3/2}}(T_\infty - T_{sat})$, $R_0 = \frac{2\sigma T_{sat}}{\rho_v h_{fg}\Delta T}$ |
| Du et al. [30] | $R = f(Ja)\alpha_L^{1/2}t^n$ |
| | $n = 1.0012e^{-P/0.3257} - 0.9624e^{-P/0.6161} + 0.5$, P: in MPa $f(Ja) = 2.1077Ja^{0.7902}$ |
| Cho and Wang [35] | $R = \begin{cases} 2\delta_{th}/c[1 - \exp(-c_b bc^2\Delta T\sqrt{t}/\delta_{th})] & 0 \le t < t_\delta \\ \sqrt{2}\sqrt{c_b b\delta_{th}\Delta T\sqrt{t} - \delta_{th}^2(\ln 4 - 1)/2c^2} & t > t_\delta \end{cases}$ |
| | $c = 2\cos\frac{\theta}{2}$, $t_\delta = (\frac{\delta_{th}\ln 2}{c_b bc^2\Delta T})^2$, $b = \frac{k_L[(\pi - 2.4)\cos\theta + 2.4\sec\frac{\theta}{2}]}{2\pi\rho_v h_{fg}\sqrt{\alpha_L}}$, $\theta$: static contact angle. |
| | $c_b = 0.534$ (based on data for water at 1 atm), $\delta_{th} = 35.7(\nu\alpha_L/g\beta_l\Delta T)^{1/3}$ |

## References


[1] M. Jakob, Heat Transfer, 1, NY Wiley, New York, 1949.
[2] W.M. Rohsenow, A Method of Correlating Heat Transfer Data For Surface Boiling of Liquids, Massachusetts Institute of Technology, M. I. T. Division of Industrial Corporation, Cambridge, Massachusetts, 1951 Tech. Report No. 5.
[3] H.K. Forster, N. Zuber, Dynamics of vapor bubbles and boiling heat transfer, AIChE J. 1 (4) (1955) 531–535.
[4] C.-Y. Han, P. Griffith, The mechanism of heat transfer in nucleate pool boiling–Part II the heat flux-temperature difference relation, Int. J. Heat Mass Transf. 8 (1965) 905–914.
[5] B.B. Mikic, W.M. Rohsenow, A new correlation of pool boiling data including the effect of heating surface characteristics, Heat Transf. Eng., ASME (1969) 245–250 May.
[6] B. Yu, P. Cheng, A fractal model for nucleate pool boiling heat transfer, Heat Transf. Eng., ASME 124 (2002) 1117–1124 December.
[7] M. Kim, S.J. Kim, A mechanistic model for nucleate pool boiling including the effect of bubble coalescence on area fractions, Int. J. Heat Mass Transf. 163 (2020) 120453.
[8] M. Zupančič, P. Gregorčič, M. Bucci, C. Wang, G.M. Aguiar, M. Bucci, The wall heat flux partitioning during the pool boiling of water on thin metallic foils, Appl. Therm. Eng. 200 (2022) 117638.
[9] M.M. Mahmoud and T.G. Karayiannis, Bubble growth on a smooth metallic surface at atmospheric and sub-atmospheric pressure, Submitted to the Int. J. Heat Mass Transf. 2022.
[10] M.M. Mahmoud, T.G. Karayiannis, Pool boiling review – Part I: fundamental of boiling and relation to surface design, Therm. Sci. Eng. Prog. 25 (2021).
[11] L.E. Scriven, On the dynamics of phase growth, Chem. Eng. Sci. Genie Chim. 10 (1/2) (1959) 1–13.
[12] J.W.S. Rayleigh, Boiling Heat Transfer L.S. Tong and Y.S. Tang, CRL Press, 2010 2nd edt.
[13] V. Sernas, F.C. Hooper, The initial vapor bubble growth on a heated wall during nucleate boiling, Int. J. Heat Mass Transf. 12 (12) (1969) 1627–1630.
[14] H.K. Forster, Zuber N, Growth of a vapour bubble in a superheated liquid, J. Appl. Phys. 25 (4) (1954) 474–478.
[15] M.S. Plesset, S.A. Zwick, The growth of vapour bubbles in superheated liquids, J. Appl. Phys. 25 (4) (1954) 493–500.
[16] W. Fritz, W. Ende, Über den verdampfungsvorgang nach kinematographischen aufnahmen an dampfblasen, Phys. Zeitschr. 37 (1936) 391–401.
[17] S.G. Bankoff, Asymptotic growth of a bubble in a liquid with uniform initial superheat, Allp. Sci. Res. Section A. 12 (1963) 267–281.
[18] V.F. Prisnyakov, Bubble growth in liquids, Inzhenerno-Fizicheskii Zhurnal 18 (5) (May 1970) 844–848.
[19] A.A. Avdeev, Y.B. Zudin, Inertia-thermal governed vapour bubble growth in highly superheated liquid, in: Heat Mass Transf., 41, 2005, pp. 855–863.
[20] B.B. Mikic, W.M. Rohsenow, P. Griffith, On bubble growth rates, Int. J. Heat Mass Transf. 13 (1970) 657–666.
[21] T.G. Theofanous, P.D. Patel, Universal relations for bubble growth, Int. J. Heat Mass Transf. 19 (1976) 425–429.
[22] P.H. Strenge, A. Orell, J.W. Westwater, Microscopic study of bubble growth during nucleate boiling, A. I. ChE. J. 7 (4) (1961) 578–583 December.
[23] N. Zuber, The dynamics of vapour bubbles in nonuniform temperature fields, Int. J. Heat Mass Transf. 2 (1961) 83–98.
[24] C.-Y. Han, P. Griffith, The mechanism of heat transfer in nucleate pool boiling-Part I Bubble initiation, growth and departure, Int. J. Heat Mass Transf. 8 (1965) 887–904.
[25] S.J.D. Van Stralen, The mechanism of nucleate boiling in pure liquids and in binary mixtures-Part I, Int. J. Heat Mass Transf. 9 (1966) 955–1020.
[26] M.G. Cooper, The microlayer and bubble growth in nucleate pool boiling, Int. J. Heat Mass Transf. 12 (1969) 915–933.
[27] S.J.D. van Stralen, M.S. Sohal, R. Cole, W.M. Sluyter, Bubble growth rate in pure and binary systems: combined effect of relaxation and evaporation microlayers, Int. J. Heat Mass Transf. 18 (1975) 453–467.
[28] R. Cole, H.I. Shulman, Bubble growth rates at high Jakob numbers, Int. J. Heat Mass Transf. 9 (1966) 1377–1390.
[29] H.C. Lee, B.D. Oh, S.W. Bae, M.H. Kim, Single bubble growth in saturated pool boiling on a constant wall temperature surface, Int. J. Multiph. Flow 29 (2003) 1857–1874.
[30] J. Du, C. Zhao, H. Bo, A modified model for bubble growth rate and bubble departure diameter in nucleate pool boiling covering a wide range of pressure, Appl. Therm. Eng. 145 (2018) 407–415.
[31] R.J. Benjamin, A.R. Balakrishnan, Nucleate pool boiling heat transfer of pure liquids at low to moderate heat fluxes, Int. J. Heat Mass Transf. 39 (12) (1996) 2495–2505.
[32] M.R. Abdollahi, M. Jafarian, M. Jamialahmadi, The rate of bubble growth in a superheated liquid in pool boiling, Heat Mass Transf. 53 (2017) 3433–3442.
[33] K.E. Forster, Growth of a vapour-filled cavity near a heating surface and some related questions, Phys. Fluids 4 (4) (1961) 448–455 April.
[34] F.J. Lesage, S. Siedel, J.S. Cotton, A.J. Robinson, A mathematical model for predicting bubble growth for low Bond and Jakob number nucleate boiling, Chem. Eng. Sci. 112 (2014) 35–46.
[35] H.J. Cho, E.N. Wang, Bubble nucleation, growth and departure: a new dynamic understanding, Int. J. Heat Mass Transf. 145 (2019) 118803.
[36] M.G. Cooper, A.J.P. Llyod, The microlayer in nucleate pool boiling, Int. J. Heat Mass Transf. 12 (1969) 895–913.
[37] Van Ouwerkerk, The rapid growth of a vapour bubble at a liquid-solid interface, Int. J. Heat Mass Transf. 14 (1971) 1415–1431.
[38] D.A. Labuntsov and V.V. Yagov, Tr. MEI, Issue 268, 3–15, 1975.
[39] Y.B. Zudin, Non-equilibrium Evaporation and Condensation Processes - Analytical Solutions, 3rd ed., Springer, 2021.
[40] R. Mei, W. Chen, J.F. Klausner, Vapour bubble growth in heterogenous boiling -I, Formulation, Int. J. Heat Mass Transf. 38 (5) (1995) 909–919.
[41] Yu.A. Buyevich, B.W. Webbon, Dynamics of vapour bubbles in nucleate boiling, Int. J. Heat Mass Transf. 39 (12) (1996) 2409–2426.
[42] H.W. Coleman, W.G. Steele, Experimentation, Validation, and Uncertainty Analysis For Engineers, 3rd ed., John Willey and Sons Inc., NJ, USA, 2009.
[43] T.L. Bergman, A.S. Lavine, F.P. Incropera, D.P. Dwitt, Fundamentals of Heat and Mass Transfer, 7th ed., John Willey and Sons Inc., NJ, USA, 2011.
[44] R.L. Mohanty, M.K. Das, A critical review on bubble dynamics parameters influencing boiling heat transfer, Renew. Sustain. Energy Rev. 78 (2017) 466–494.
[45] M. Saddy, G.J. Jameson, Prediction of departure diameter and bubble frequency in nucleate boiling in uniformly superheated liquids, Int. J. Heat Mass Transf. 14 (1971) 1771–1783.
[46] J.S. Saini, G.P. Gupta, S. Lal, Bubble departure diameter in nucleate pool boiling, Lett. Heat Mass Transf. 2 (1975) 41–48.
[47] W. Fritz, Berech des maximal volume von dampf blasen, Phys. Z. 36 (1935) 379–388.
[48] R. Ruckenstein, Recent trends in boiling heat and mass transfer, Appl. Mech. Rev. 17 (1964) 663–672.
[49] R. Cole, Bubble frequency and departure volumes at sub-atmospheric pressure, AIChE 13 (1967) 779–783.
[50] R. Cole, W.M. Rohsenow, Correlation of bubble departure diameters for boiling of saturated liquids, Chem. Eng. Prog. Symp. Ser. 65 (1969) 211–213.
[51] A.M. Kiper, Minimum bubble departure diameter in nucleate pool boiling, Int. J. Heat Mass Transf. 14 (7) (1971) 931–937.
[52] S.J.D. van Stralen, Fundamental developments in bubble dynamics, in: Proceedings of the 6th Int. Heat Transfer Conf., 6, 1978, pp. 429–450.
[53] K. Stephan, Saturated Pool Boiling and Sub-Cooled Flow Boiling of Mixtures, University of Auckland, Newzland, 1992 PhD thesis.
[54] S.S. Kutateladze, I.I. Gogonin, Growth rate and detachment diameter of a vapour bubble in free convection boiling of a saturated liquid, High Temp. 17 (1979) 667–671.
[55] M.K. Jensen, G.J. Memmel, Evaluation of bubble departure diameter correlations, in: Prog. 8th Int. Heat Transfer Conf, 4, 1986, pp. 1907–1912.
[56] I.Z. Zeng, J.F. Klausner, R. Mei, A unified model for the prediction of bubble detachment radius in boiling systems-I: pool boiling, Int. J. Heat Mass Transf. 36 (1993) 2261–2270.
[57] J. Kim, M.H. Kim, On the departure behaviours of bubble at nucleate pool boiling, Int. J. Multiph. Flow 32 (2006) 1269–1286.
[58] H.T. Phan, N. Caney, P. Marty, S. Colasson, J. Gavillet, Surface wettability control by nanocoating: the effects on pool boiling heat transfer and nucleation mechanism, Int. J. Heat Mass Transf. 52 (2009) 5459–5471.
[59] H.T. Phan, N. Caney, P. Marty, S. Colasson, J. Gavillet, A model to predict the effect of contact angle on the bubble departure radius during heterogeneous boiling, Int. Commun. Heat Mass Transf. 37 (2010) 964–969.
[60] Y. Nam, E. Aktinol, V.K. Dhir, Y.S. Ju, Single bubble dynamics on a superhydrophobic surface with artificial nucleation sites, Int. J. Heat Mass Transf. 54 (2011) 1572–1577.
[61] R. Cole, H.L. Shulman, Bubble departure radius at subatmospheric pressure, Chem. Eng. Progr. Symp. Ser. 62 (1966) 6–16.
[62] V.S. Golorin, B.A. Kol'chugin, E.A. Zhakharova, Investigation of the mechanism of nucleate boiling of ethyl alcohol and benzene by means of high-speed motion picture photography, Heat Transf. Sov. Res. 10 (1978) 79–98.
[63] T. Yabuki, O. Nakabeppu, Heat transfer mechanisms in isolated bubble boiling of water observed with MEMS sensor, Int. J. Heat Mass Transf. 76 (2014) 286–297.
[64] S.J.D. van Stralen, R. Cole, W.M. Sluyter, M.S. Sohal, Bubble growth rates in nucleate boiling of water at sub-atmospheric pressures, Int. J. Heat Mass Transf. 18 (1975) 655–669.
[65] S. Jung, H. Kim, An experimental method to simultaneously measure the dynamics and heat transfer associated with a single bubble during nucleate boiling on a horizontal surface, Int. J. Heat Mass Transf. 73 (2014) 365–375.